JAERI-M
85-025

EVALUATION REPORT ON CCTF CORE-II REFLOOD TEST SECOND SHAKEDOWN TEST C2-SH2 (RUN 54)

— EFFECT OF CORE SUPPLIED POWER ON REFLOOD PHENOMENA —

(Work done under Contract with the Government)

March 1985

Tadashi IGUCHI, Jun SUGIMOTO, Hajime AKIMOTO
Tsutomu OKUBO and Yoshio MURAO

日本原子力研究所
Japan Atomic Energy Research Institute

JAERI-M 85-025

Evaluation Report on CCTF Core-II Reflood Test
Second Shakedown Test, C2-SH2 (Run 54)
— Effect of core supplied power on reflood phenomena —

Tadashi IGUCHI, Jun SUGIMOTO, Hajime AKIMOTO
Tsutomu OKUBO and Yoshio MURAO

Department of Nuclear Safety Research,
Tokai Research Establishment, JAERI
(Received January 31, 1985)

A low power test (the initial averaged linear power density = 1.18 kW/m) and the base case test (1.4 kW/m) were performed with the Cylindrical Core Test Facility (CCTF) at Japan Atomic Energy Research Institute, in order to study the effect of the power on the reflood phenomena. The former linear power density corresponds nearly to the scaled linear power density based on the current safety evaluation criterio.

During the early period of the reflood (<100s), the heat transfer coefficient was identical between both tests in spite of the different power. Resultantly, the clad temperature and the turnaround temperature were lower in the low power test.

During the later period of the reflood (>200s) the heat transfer coefficient became higher and resultantly the quench front advanced faster in the low power test.

The core flooding rate was nearly identical between both tests, independently of the different power. The insensitiveness of the power to the core flooding rate was also observed in FLECHT-SET performed in the USA.

A significatn large differential pressure oscillation at ECC ports was experienced in the low power test, and it may be important for the long term core cooling although it has not been taken note on the previous studies.

Keywords: Reactor Safety, LOCA, Reflood, Two-phase Flow, Heat Transfer, Hydrodynamics

---

The work was performed under the contract with the Atomic Energy Bureau of Science and Technology Agency of Japan.

大型再冠水円筒第二次炉心機能試験 C2-SH2（RUN54）評価報告書 -炉心出力の効果-

日本原子力研究所東海研究所安全工学部
井口 正・杉本 純・秋本 肇
大久保努・村尾良夫

（1985年1月31日受理）

ＣＣＴＦにより低出力試験（平均初期線出力1.18 kW/m ）および基準試験（1.4 kW/m ）を行い，炉心出力の再冠水現象におよぼす影響を調べた。低出力試験における線出力は，現行の安全評価で用いられている手法による評価値より約７％高い。

再冠水過程初期（＜１００ｓ）には，炉心出力が異っていても熱伝達率はほぼ等しく，その結果低炉心出力条件で被覆管温度およびターンアラウンド温度は低下した。

再冠水過程中期以降（＞２００ｓ）では，低出力条件で熱伝達率は大きくなり，クエンチ点は急速に進行した。炉心冷却を支配する主要因子と考えられる炉心冠水速度は，両試験でほぼ等しかった。炉心冠水速度に及ぼす炉心出力の影響が小さい傾向は，米国のＦＬＥＣＨＴ－ＳＥＴ試験でもみられた。

極端に炉心出力を低めたところ，冷却水注入ポートで蒸気は完全凝縮し激しい圧力振動が生じた。本振動については従来の研究では充分な注意が払われていないが，長期的炉心冷却の維持の観点から重要である可能性がある。

本報告書は，電源開発促進対策特別会計法に基づき，科学技術庁からの受託によって行った研究の成果である。

Contents

目　　次

Table List

Figure List

1. Introduction

The present report describes the effect of the core supplied power on the reflood phenomena observed in the Cylindrical Core Test Facility (CCTF) Core-II at Japan Atomic Energy Research Institute (JAERI).

The large scale reflood test program[1] had been conducted at JAERI in order to demonstrate the effectiveness of the emergency core cooling (ECC) system, to verify the best-estimate analysis codes and to supply information for the improved thermo-hydrodynamic models during the reflood phase of a hypothetical loss-of-coolant accident (LOCA) of a PWR. For that purpose the CCTF and the Slab Core Test Facility (SCTF) have been constructed. The CCTF is a 1/20 scale integral test facility with a cylindrical core, 4-loop primary systems, and active steam generators. Whereas the SCTF is designed to simulate the two-dimensional flows in the core with an eight heater rod bundles arranged in a slab geometry.

In the previous safety evaluation, the decay heat by fission product was determined based on old ANS standard with 20 % margin. Recent re-evaluation of decay heat data allows us to use new ANS standard with 2σ as more realistic decay heat criterio. This change of the decay heat criterio leads to about 16 % reduction of the decay heat at 30S after scram. Thus, the decay heat level at the reflood initiation depends on the assumed criterio. Another factor which governs the decay heat level is the reflood initiation time. Most safety evaluations show that the reflood initiation time is 30 s to 40 s after scram. Since the decay heat level depends on the assumed criterio, it is necessary to study the effect of the decay heat on the reflood phenomena.

In the previous CCTF tests[2], the core power was determined based on the old decay heat criterio used in previous safety evaluation and set to 9.35 MW (the initial averaged linear power density = 1.40 kW/m) at the reflood initiation. Beside the tests, a test was conducted, in which the core supplied power was set to 7.78 MW (the initial averaged linear power density = 1.18 kW/m) simulating the decay heat used in the new safety evaluation. This test is designated as a low power test. By comparing the results of both tests, the effect of the core supplied power on reflood phenomena is studied. The study of the power effect was made in FLECHT-SET in the range of 1.69 ~ 2.1 kW/m of the initial averaged linear power density. By comparing the results of both facilities, the general effect of the core supplied power is expected to be derived.

2. Test description

2.1 Test facility

The CCTF Core-II was designed in consideration of the following objectives and criteria:

a. Design objectives

(1) The facility should provide the capability to reasonably simulate the flow conditions in the primary system of a PWR during the refill and reflood phases of a LOCA.

(2) The downcomer design should provide ECC flow behavior throughout the test which is reasonably representative of that of the PWR downcomer.

b. Design criteria

(1) The reference reactors are the Trojan reactor in USA and certain aspects of the Ohi reactor in Japan.

(2) The vertical dimensions and locations of system components are kept as close to those of the reference reactors as possible.

(3) The flow areas of the system components are scaled down in proportion to the scaling factor of core flow area.

(4) The facility is equipped with four loops which are composed of three intact loops and a broken loop.

(5) A cold leg break is simulated.

(6) The ECCS consists of an accumulator (Acc) and a low pressure coolant injection (LPCI) system, and the injection locations are the upper plenum and the downcomer as well as the lower plenum and the cold legs.

(7) The maximum allowable pressure of the facility is 588 kPa (6 kg/cm^2 absolute).

(8) The maximum allowable temperature of the simulated fuel rods is 1173 K (900°C).

(9) The maximum allowable temperature of the components in the primary system except the simulated fuel rod assembly is 623 K (350°C).

(10) The reactor vessel contains approximately 2,000 electrically heated rods simulating the fuel rods.

(11) The design of upper plenum internals is based on that of a new 17×17 type fuel assembly.

(12) The flow resistance of each loop is adjusted by an orifice in the pump simulator.

(13) The containment system consists of two tanks.

A bird's-eye view and a schematic diagram of the CCTF are shown in Figs. 2.1 and 2.2, respectively. The scaled dimensions of the components are given in Tables 2.1 and 2.2.

The differences in the design of the Core-II facility from the Core-I are:

(1) Axial peaking factor of heater rods.

(2) Local peaking factor of heater rods in a bundle.

(3) Core structure (Grid spacers)

(4) Upper plenum structures (upper plenum internals, plugging devices in top nozzle region and a upper ring).

(5) Vent valves.

(6) Alternative ECCS (downcomer injection and upper plenum injection).

(7) Instruments.

2.1.1 Pressure vessel and internals

The pressure vessel is of a cylindrical type as shown in Fig. 2.3. The height is the same as the reference reactor pressure vessel. The radial direction is scaled down in proportion to the core flow area scaling, that is, 1/21.44. The upper ring was newly installed for the installation of the upper plenum ECC water injection lines and the instruments. Four vent valves and two downcomer ECC water injection nozzles, which are called Core Flooding Nozzle (CFN), are also newly equipped in the Core-II facility as shown in Figs. 2.3 and 2.4. Vent valves and CFNs are for the simulation of a Babcock & Wilcox (B & W) type PWR. The vent valves and CFNs are forcedly closed in this test.

The cross section of the pressure vessel is shown in Fig. 2.4 and the dimensions are given in Fig. 2.5. The core consists of thirty-two 8×8 electrically heated rod bundles arranged in a cylindrical configuration and simulates Westinghouse 15×15 type fuel assemblies.

The downcomer is an annulus of 61.5 mm gap. In determining the gap size, the flow area of the core baffle region was added to that of the downcomer region. Thus, the core baffle flow area is included in the downcomer simulation and is not simulated separately in this vessel.

The vessel wall is constructed of carbon steel which is cladded with stainless steel lining. The wall is 90 mm thick and simulates the stored energy as reasonably as possible during ECC water injection.

The design of upper plenum internals is based on that of the new Westinghouse 17×17 type fuel assemblies instead of the old type simulated in the Core-I facility. The internals consists of ten control rod guide tubes, ten support columns and twelve open holes as shown in Fig. 2.6. The radius of each internals is scaled down by factor of 8/15 from that of an actual reactor. They are illustrated in Fig. 2.7. Flow resistance baffles are inserted into the guide tubes. The baffles consist of kinds of baffle plates and a shaft. The baffle plates are shown in Fig. 2.8.

The end box and the upper core support plate (UCSP) are installed between the core and the upper plenum. The structure for one heater rod bundle is shown in Fig. 2.9. The tie plate is a 10 mm thick perforated plate with round flow holes. Plugging devices are installed newly in the Core-II facility as shown in Figs. 2.9 and 2.10 to simulate the flow resistance more correctly. The UCSP is a 60 mm thick perforated plate. The geometry of the perforation is analogous to that of an actual reactor.

2.1.2 Heater rod assembly

The heater rod assembly simulating the fuel assembly consists of thirty-two 8×8 array rod bundles. Each bundle consists of fifty-seven electrically heated rods and seven non-heated rods as shown in Fig. 2.11. The core is usually subdivided into three regions to achieve a desired radial power distribution. This is shown in Fig. 2.5. The high, medium and low power regions are named as A, B and C regions, respectively. The local peaking factor of heated rods in a bundle is unity, that is, all heated rods in a bundle have the same power density in the Core-II facility.

A heater rod consists of a nichrome heating element, magnesium oxide (MgO) and boron nitride (BN) insulators, and Inconel-600 sheath. BN is used for only central part of the heated region and MgO for the other part as shown in Fig. 2.12. The heated length and the outer diameter of the heater rods are 3.66 m and 10.7 mm, respectively, which are identical to the corresponding dimensions of actual PWR fuel rods. The sheath wall thickness is 1.0 mm and is thicker than the actual fuel cladding, because of the requirements for thermocouple installation. The heating element

is a helical coil with a varying pitch to generate a 17 steps chopped consine axial power profile as shown in Fig. 2.13. The peaking factor is 1.40, instead of 1.489 for a Core-I rod.

Non-heated rods are either stainless steel pipes or solid bars of 13.8 mm O.D. All the pipes are utilized for installation of instruments such as steam superheat probes and thermocouples. All the bars are used for carrying the assembly loads.

The heater rods and non-heated rods are held in radial position by grid spacers which are located at six elevations along the axial length as shown in Fig. 2.13. A grid spacer is a lattice structure composed of stainless steel plates of 0.4 mm and 0.8 mm thick and 40 mm high. The top and the bottom edges of the stainless steel plates are sharpened in CCTF Core-II. The rod pitch is 14.3 mm which is same as that of the reference PWR.

The heater rods penetrate through the bottom plate of the vessel to facilitate lead out of the power cables from the bottom of the vessel. The outer diameter of the rods in the lower plenum is reduced to 8.6 mm. Three phase electric current is used for heating the heater rods and the electrical neutral point is at the top of the rods where they are interconnected to each other.

2.1.3 Primary loops and ECCS

Primary loop consists of three intact loops and a broken loop. Each loop consists of hot leg and cold leg pipings, a steam generator simulator and a pump simulator. The cold leg break is simulated for the broken loop. The broken cold leg is connected to two containment tanks through blowdown valves. The primary loop arrangement is shown in Figs. 2.14 and 2.15.

The inner diameter of the pipings is scaled down in proportion to the core flow area scaling. The length of each piping section is almost the same as the corresponding sections of the reference PWR.

The steam generator simulators are of U-tube and shell type as shown in Fig. 2.16. The tube length is about 5 m shorter than the reference PWR. The vertical height of the steam generator simulators is also about 5 m lower than the reference PWR. The primary coolant passes through the tube side and the secondary coolant is stagnant in the shell side. The steam generator simulators of two loops are housed in a single shell assembly which has two sets of separated inlet and outlet headers for

two loops. The wall thickness of the U-tube is 2.9 mm instead of 1.27 mm for the reference PWR, because of a higher pressure difference between the primary and secondary sides in the steam generator simulator.

The pump simulator consists of the casing and vane simulators and an orifice plate as shown in Fig. 2.17. The each loop resistance is simulated wth the orifice plate. Each orifice plate has a hole with diameter and thickness of 95 mm and 10 mm, respectively.

ECC water can be injected into each cold leg, lower plenum and upper plenum, as shown in Fig. 2.14.

Figure 2.18 shows the upper plenum injection devices. ECC water from Alternative tank 1 flows into a header installed in upper ring. The header has two water injection pipes, which inside diameters are 49.5 mm. Each water injection pipe has a flow hole of 3 mm diameter at the elevation of the hot leg center line. The ECC water is injected horizontally into upper plenum through the flow holes. In order to keep the same flow rates between the flow holes, orifices with 33 mm diameter are installed between the header and the water injection pipes.

The radial location of the water injecion pipes is shown in Fig. 2.19. The arrows in the figure show the injection direction of the ECC water.

2.1.4 Instrumentation

The instrumentation is divided into two groups. One of them is JAERI-supplied instruments measuring the temperatures, absolute pressures, differential pressures, water levels and flow rates. Thermocouples measure the temperatures of the rod surface, fluid and structure. The absolute pressures are measured in the upper and lower plena, steam generator plena and containment tanks. The differential pressure measurements are carried out at many locations covering the whole system almost completely. In the ECC water supply tanks and the containment tank 1, the liquid levels are measured. The flow meters measure the ECC water flow rate. Furthermore, flow rates in the downcomer, loop seal pipings and vent line from the containment tank 2 to the atmosphere are measured with the drag disk flow meter, pitot tubes and ventulli tube, respectively. The total number of the JAERI-supplied instruments are 1316 channels and the signals from these instruments are recorded on magnetic tapes.

The other group of the instrumentation is the USNRC-supplied instruments. They are the advanced instrumentation for the two-phase flow measurement. The names and quantities of those are tabulated in Table 2.3. The total number is 536 channels.

Table 2.1 CCTF Component scaled dimensions

Component		PWR	JAERI	Ratio
Pressure vessel				
Vessel inside diameter	(mm)	4394 (173")	1084	
Vessel thickness	(mm)	216 (8 1/2")	90	
Core barrel outside diameter	(mm)	3874	961	
Core barrel inside diameter	(mm)	3760	929	
Thermal shield outside diameter	(mm)	4170		
Thermal shield inside diameter	(mm)	4030		
Downcomer length	(mm)	4849	4849	1/1
Downcomer gap	(mm)	114.3	61.5	
Downcomer flow area	(m^2)	4.23	0.197	1/21.44
Lower plenum volume	(m^3)	29.6	1.38	1/21.44
Upper plenum volume	(m^3)	43.6	2.76	1/15.8
Fuel (heater rod) assembly				
Number of bundles	(—)	193	32	
Rod array	(—)	15×15	8×8	
Rod heated length	(mm)	3660	3660	1/1
Rod pitch	(mm)	14.3	14.3	1/1
Fuel rod outside diameter	(mm)	10.72	10.7	1/1
Thimble tube diameter	(mm)	13.87	13.8	1/1
Instrument tube diameter	(mm)	13.87	13.8	1/1
Number of heater rods	(—)	39372	1824	1/21.58
Number of non-heated rods	(—)	4053	244	1/18.09
Core flow area	(m^2)	5.29	0.25	1/21.2
Core fluid volume	(m^3)	17.95	0.915	1/19.6
Primary loop				
Hot leg inside diameter	(mm)	736.6 (29")	155.2	1/4.75
Hot leg flow area	(m^2)	0.426	0.019	1/22.54
Hot leg length	(mm)	3940	3940	1/1
Pump suction inside diameter	(mm)	787.4 (31")	155.2	1/5.07
Pump suction flow area	(m^2)	0.487	0.019	1/25.77
Pump suction length	(mm)	9750	7950	1/1

Table 2.1 (cont'd)

Component		PWR	JAERI	Ratio
Cold leg inside diameter	(mm)	698.5 (27.5")	155.2	1/4.50
Cold leg flow area	(m^2)	0.383	0.019	1/20.26
Cold leg length	(mm)	5600	5600	1/1
Steam generator simulator				
Number of tubes/loop	(—)	3388	158	1/21.44
Tube length (average)	(m)	20.5	15.2	1/1.35
Tube outside diameter	(mm)	22.225 (0.875")	25.4	
Tube inside diameter	(mm)	19.7 (0.05")	19.6	1/1
Tube wall thickness	(mm)	1.27	2.9	
Heat transfer area/loop	(m^3)	4784 (51500 ft^2)	192	1/24.92
Tube flow area/loop	(m^2)	1.03	0.048	1/21.44
Inlet plenum volume/loop	(m^3)	4.25	0.198	1/21.44
Outlet plenum volume/loop	(m^3)	4.25	0.198	1/21.44
Primary side volume/loop	(m^3)	30.50 (1077 ft^3)	1.2	1/25.4
Secondary side volume/loop	(m^3)	157.33 (5556 ft^3)	2.5	1/62.9
Containment tank 1	(m^3)		30	
Containment tank 2	(m^3)		50	
Storage tank	(m^3)		25	
Acc. tank	(m^3)		5	
Saturated water tank	(m^3)		3.5	

Table 2.2 Component elevations of Cylindrical Core Test Facility

COMPONENT		PWR	CCTF	DISCREPANCY
BOTTOM OF HEATED REGION IN CORE	(mm)	0	0	0
TOP OF HEATED REGION IN CORE	(mm)	3660	3660	0
TOP OF DOWNCOMER	(mm)	4849	4849	0
BOTTOM OF DOWNCOMER	(mm)	0	0	0
CENTERLINE OF COLD LEG	(mm)	5198	4927	-271
BOTTOM OF COLD LEG (INSIDE)	(mm)	4849	4849	0
CENTERLINE OF LOOP SEAL LOWER END	(mm)	2056	2047	- 9
BOTTOM OF LOOP SEAL LOWER END	(mm)	1662	1959	+297
CENTER OF HOT LEG	(mm)	5198	4927	-271
BOTTOM OF HOT LEG (INSIDE)	(mm)	4830	4849	+ 19
BOTTOM OF UPPER CORE PLATE	(mm)	3957	3957	0
TOP OF LOWER CORE PLATE	(mm)	- 108	- 50	+ 58
BOTTOM OF TUBE SHEET OF STEAM GENERATOR SIMULATOR	(mm)	7308	7307	- 1
LOWER END OF STEAM GENERATOR SIMULATOR PLENUM	(mm)	5713	5712	- 1
TOP OF TUBES OF STEAM GENERATOR SIMULATOR (avg)	(mm)	17952.7	14820	

Table 2.3 Instruments provided by USNRC

Instrument	Number of sets	Number of sensors
DC FDG	18	162
DC VOP	1	1
DC drag disk	4	4
Core velocimeter	4	4
Core impedance probe	12	24
Core LLD	6	96
LP LLD	3	15
End box turbine meter	8	8
UP turbine meter	4	4
UP FDG	11	110
UP film probe	2	4
UP prong probe	2	4
UP VOP	1	1
VV turbine meter	2	2
VV string probe	2	2
HL film probe	2	4
HL VOP	1	1
Reference probe	1	1
Spool piece	8	89
Total	92	536

Note :

DC : Downcomer, FDG: Fluid distribution grid,
VOP: Video optical probe, LLD: Liquid level detector,
LP : Lower plenum, UP : Upper plenum,
VV : Vent valve

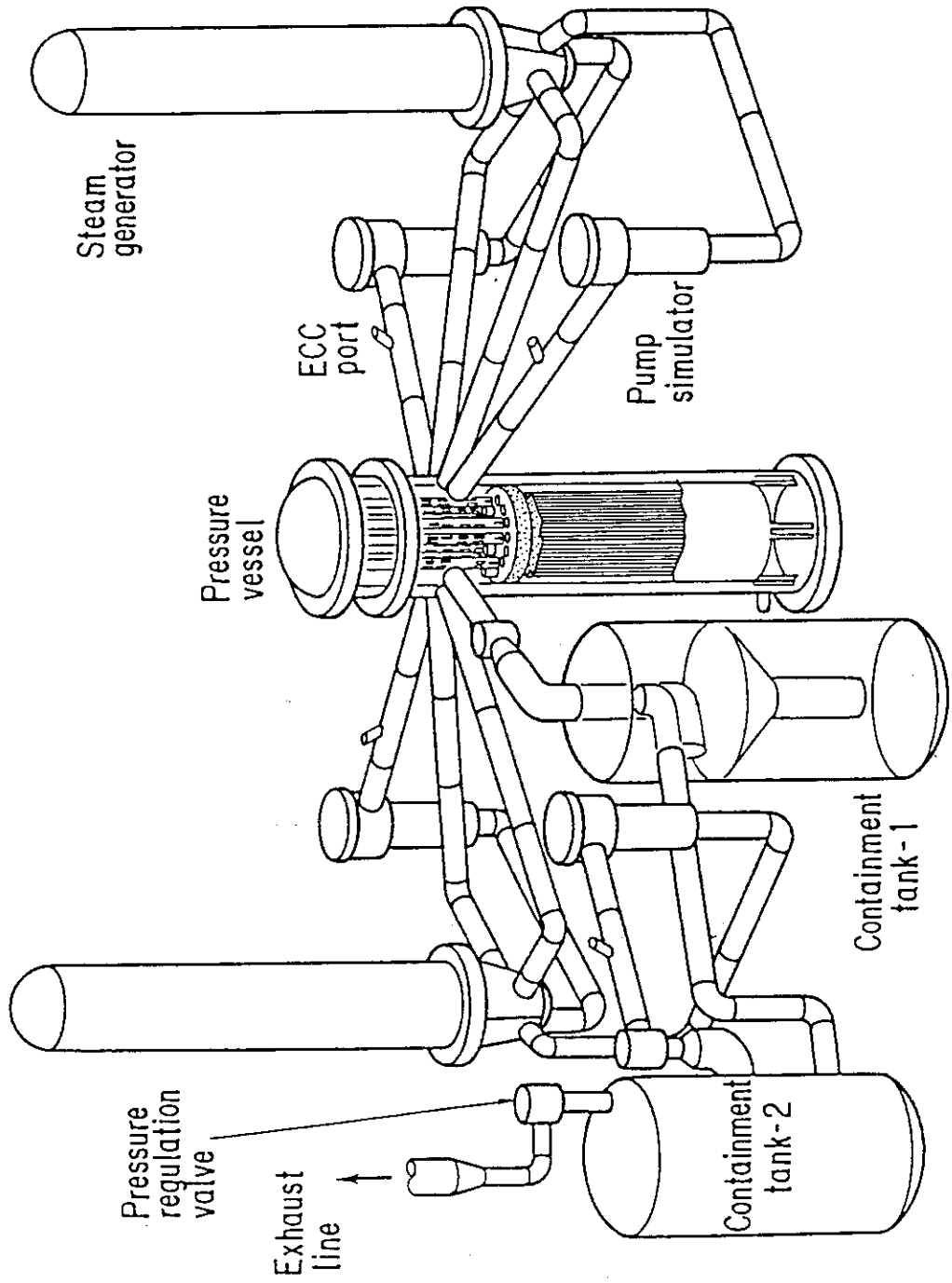

Fig. 2.1 Bird's-eye view of CCTF

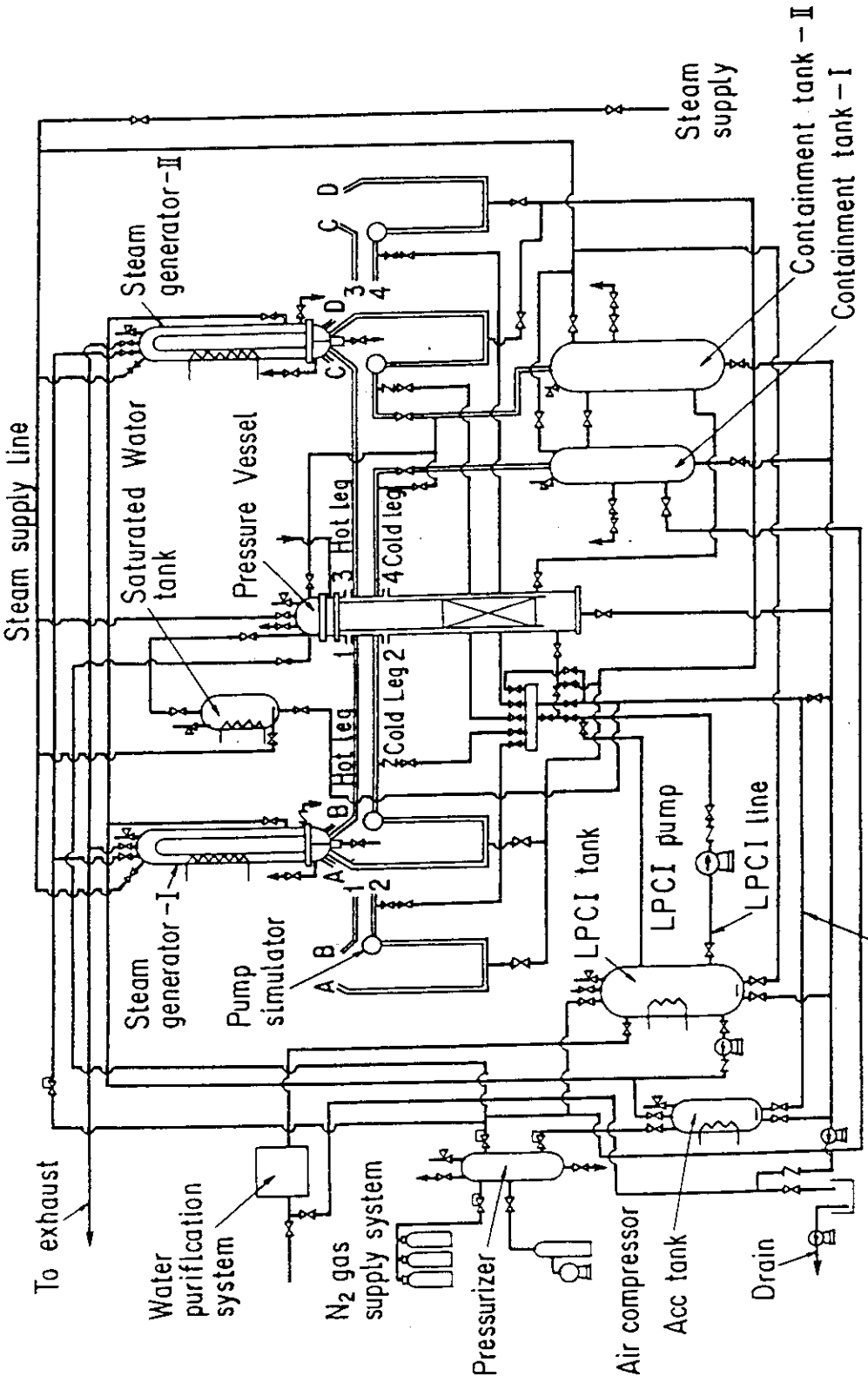

Fig. 2.2 Schematic diagram of CCTF

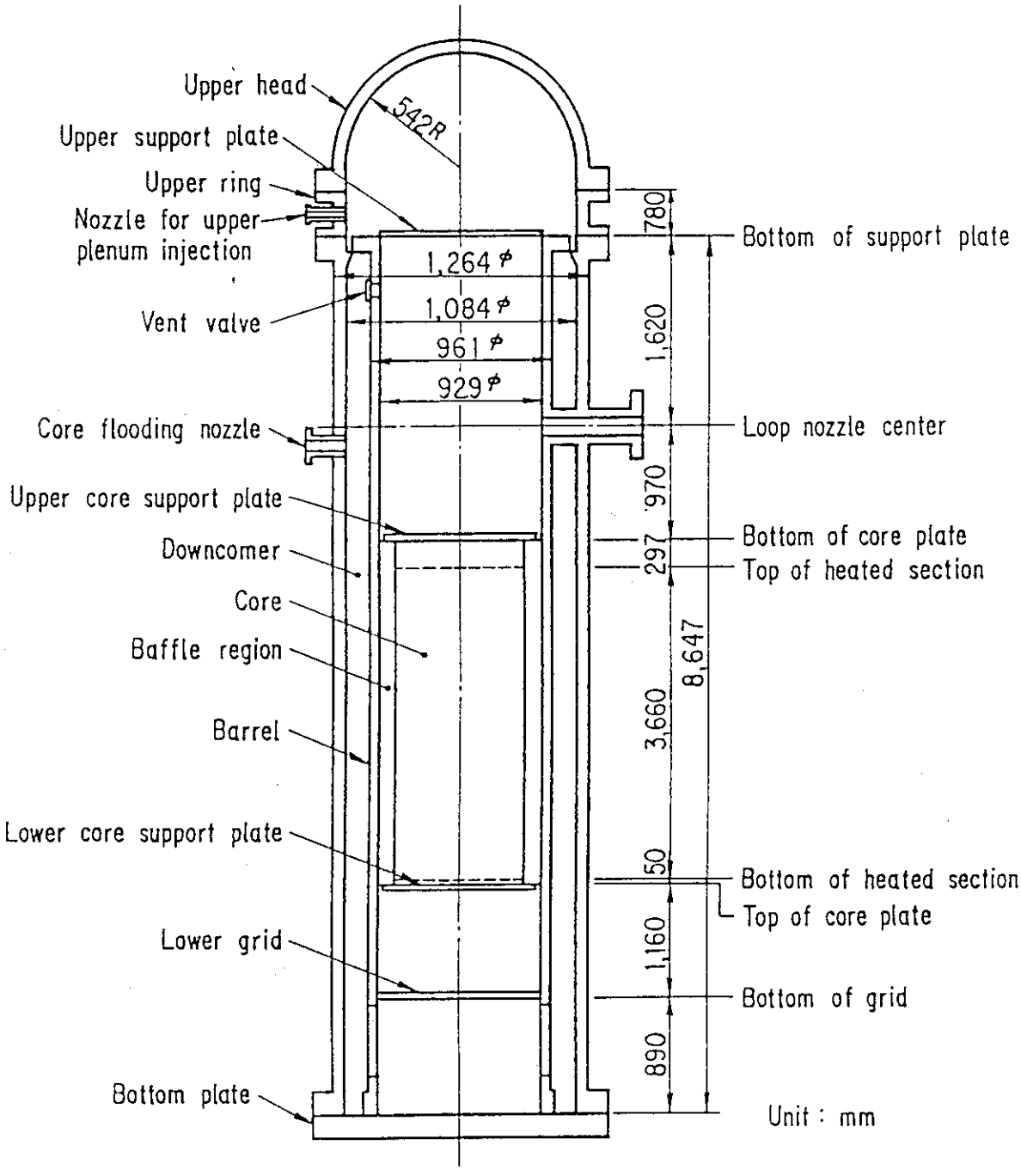

Fig. 2.3 CCTF Core-II pressure vessel

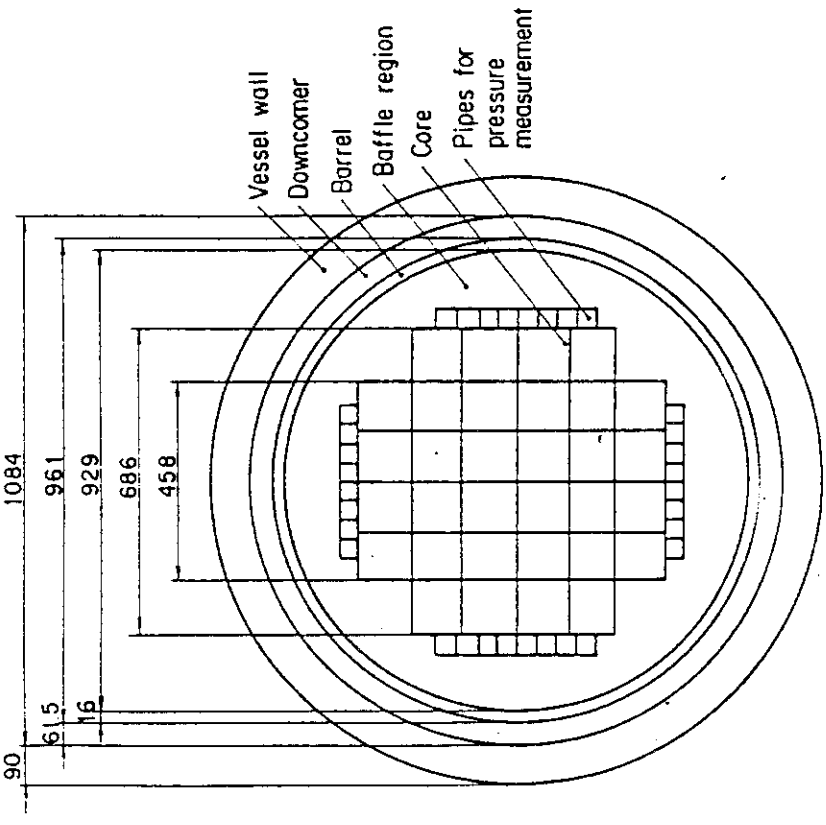

Fig. 2.5 Dimension of CCTF Core-II pressure vessel cross section

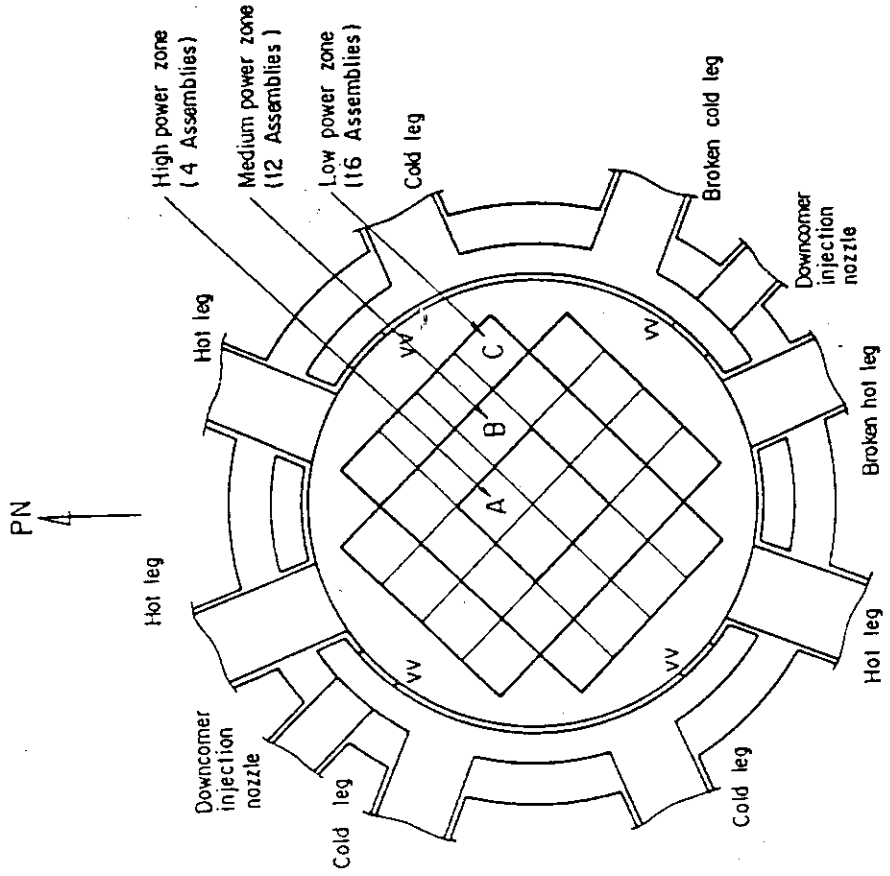

Fig. 2.4 Cross section of CCTF Core-II

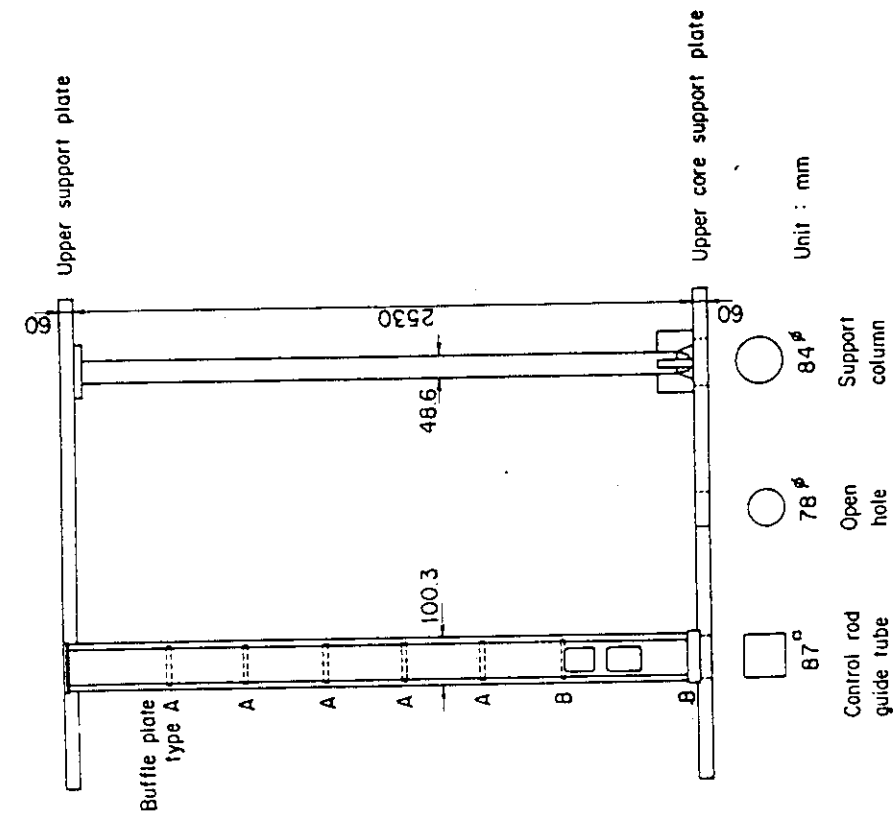

Fig. 2.7 Upper plenum internals

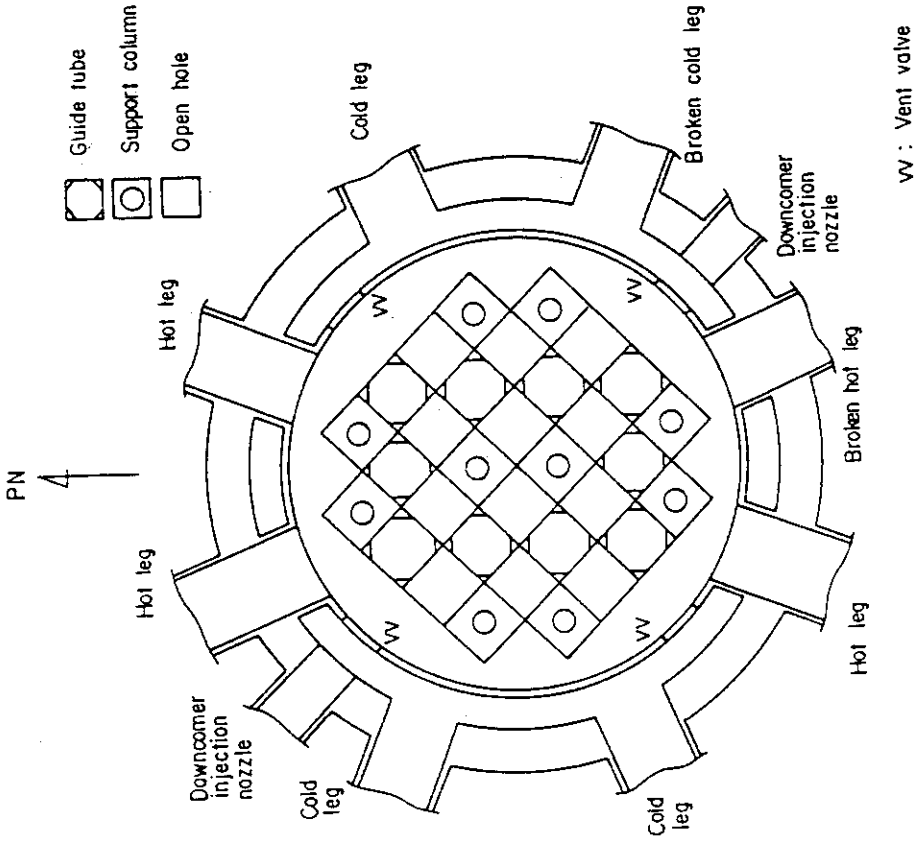

Fig. 2.6 Arrangement of upper plenum internals

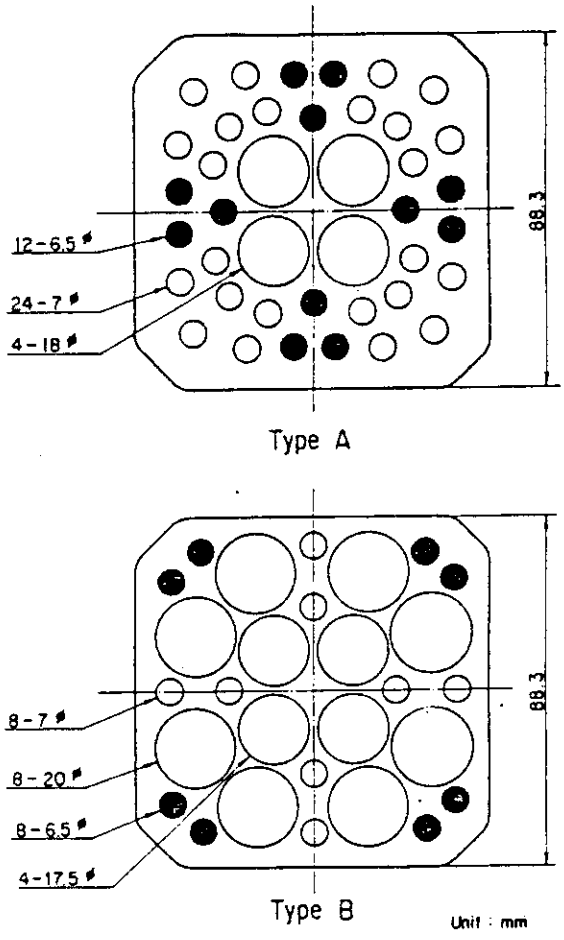

Fig. 2.8 Buffle plates in control rod guide tube

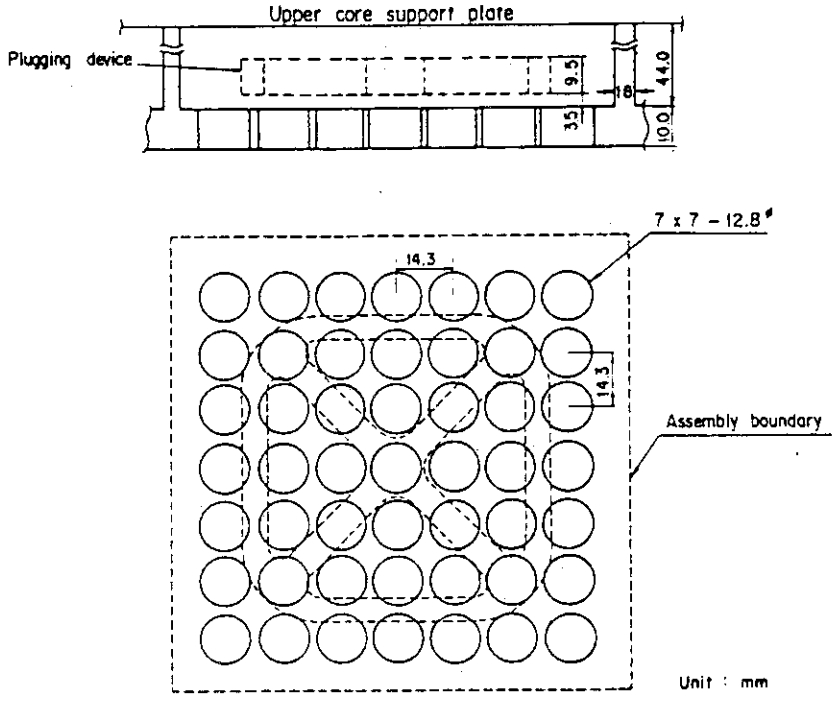

Fig. 2.9 Dimensions of holes of end box tie plate

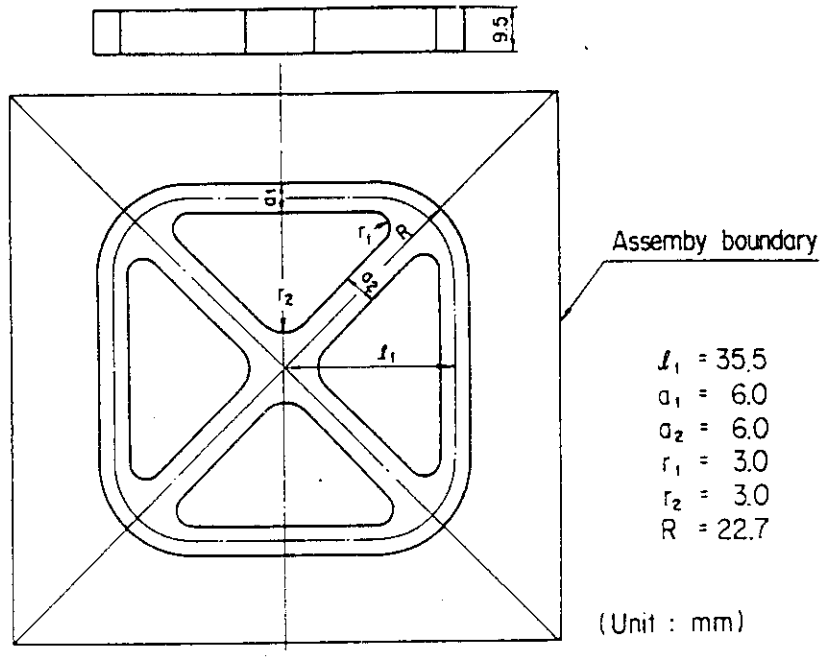

Fig. 2.10 Dimensions of plugging device

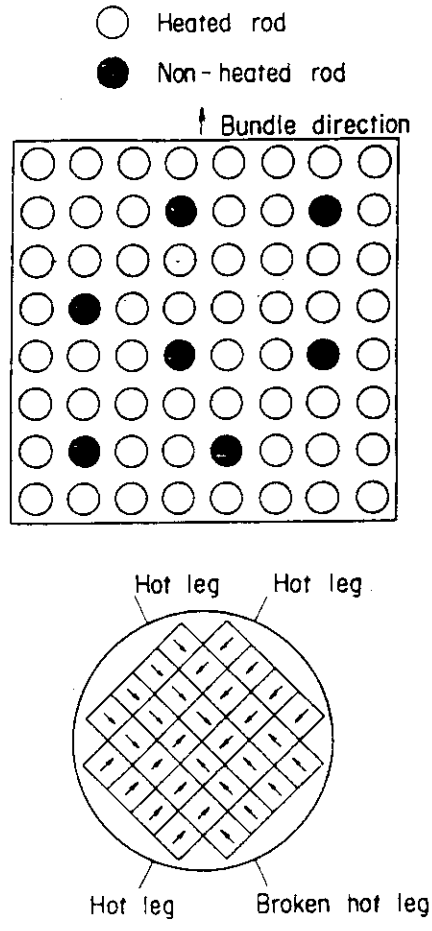

Fig. 2.11 Arrangement of non-heated rods bundle direction

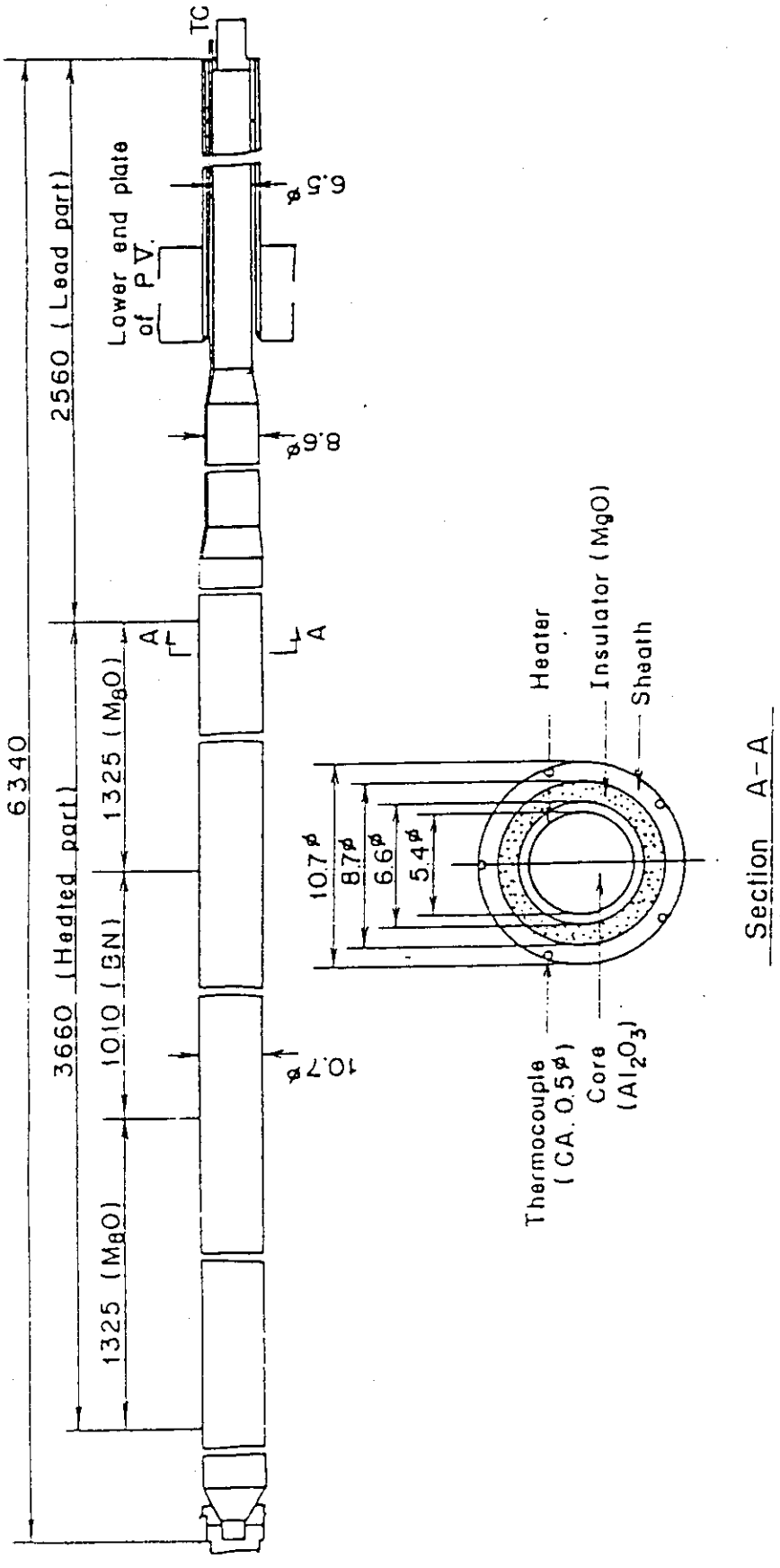

Fig. 2.12 Heater rod

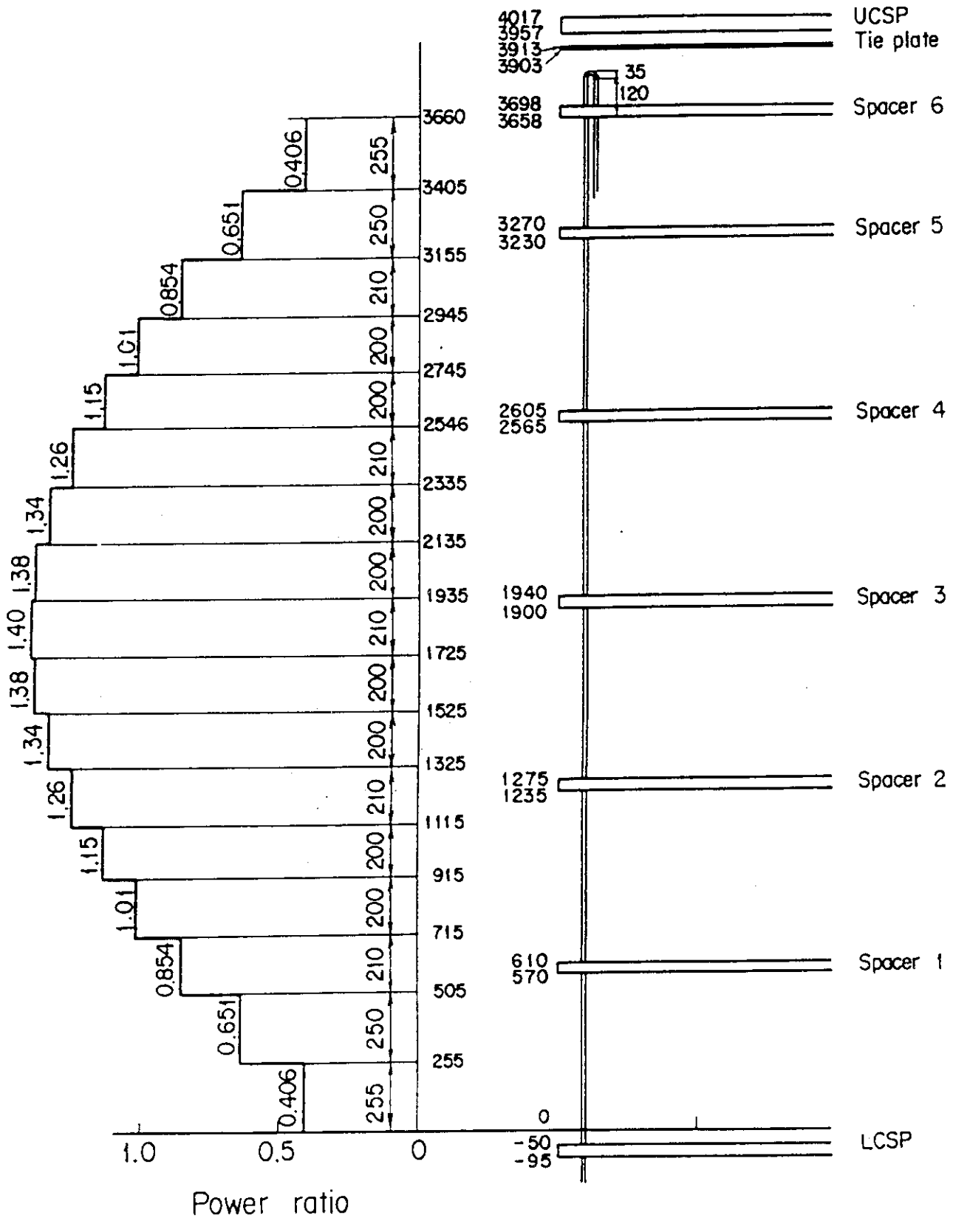

Fig. 2.13 Axial power profile of CCTF Core-II heater rod

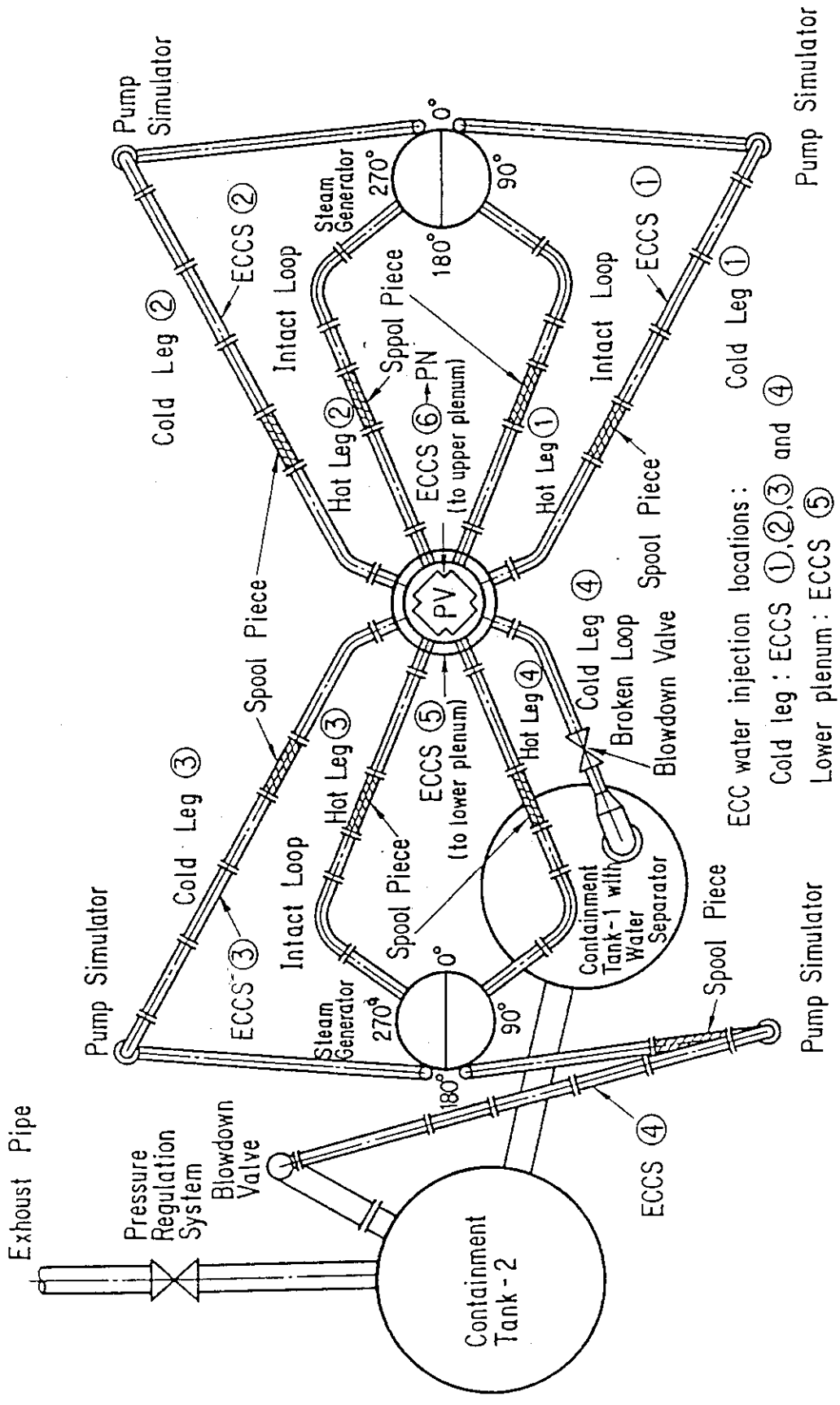

Fig. 2.14 Top view of primary loop pipings

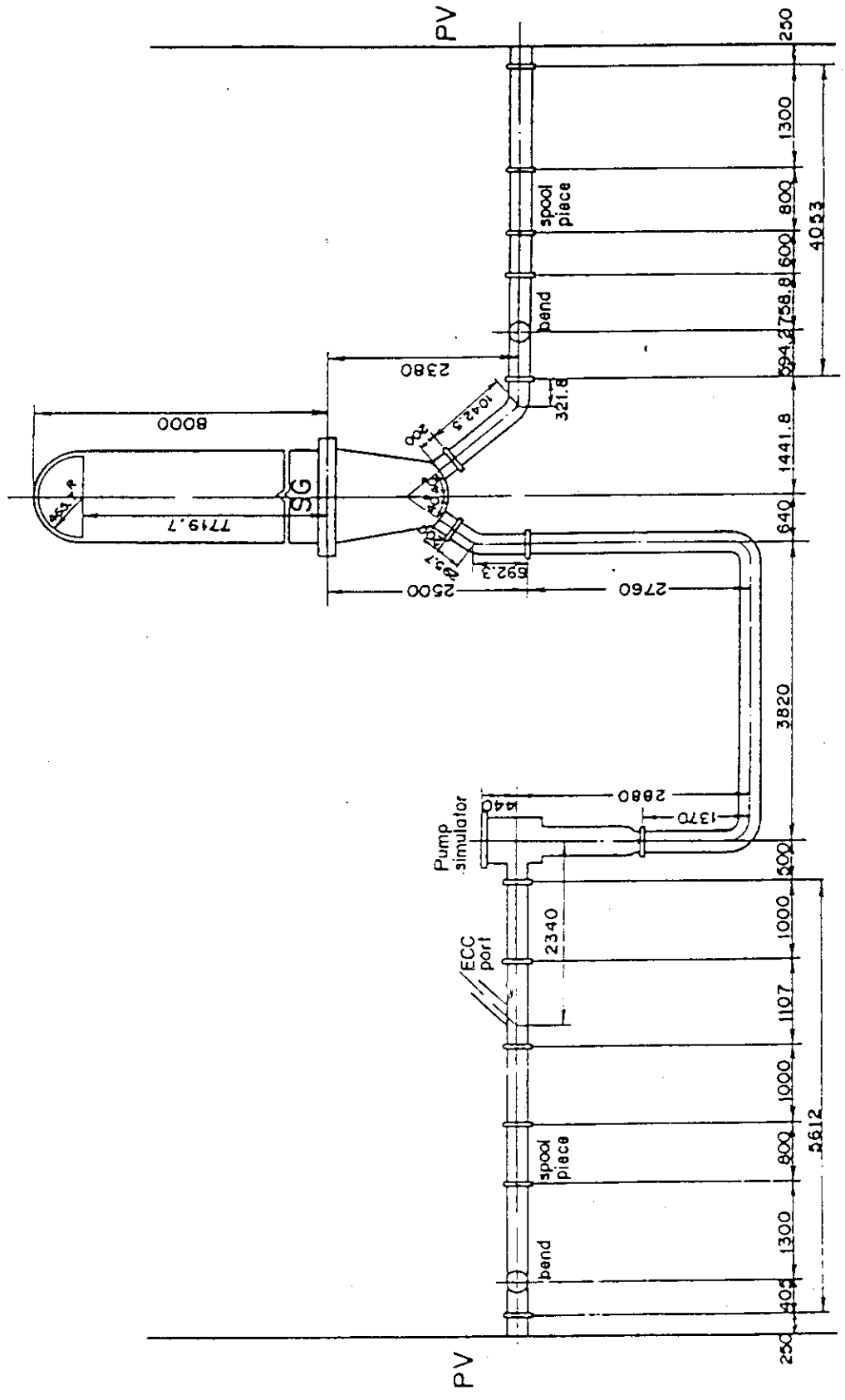

Fig. 2.15 Dimensions of primary loop

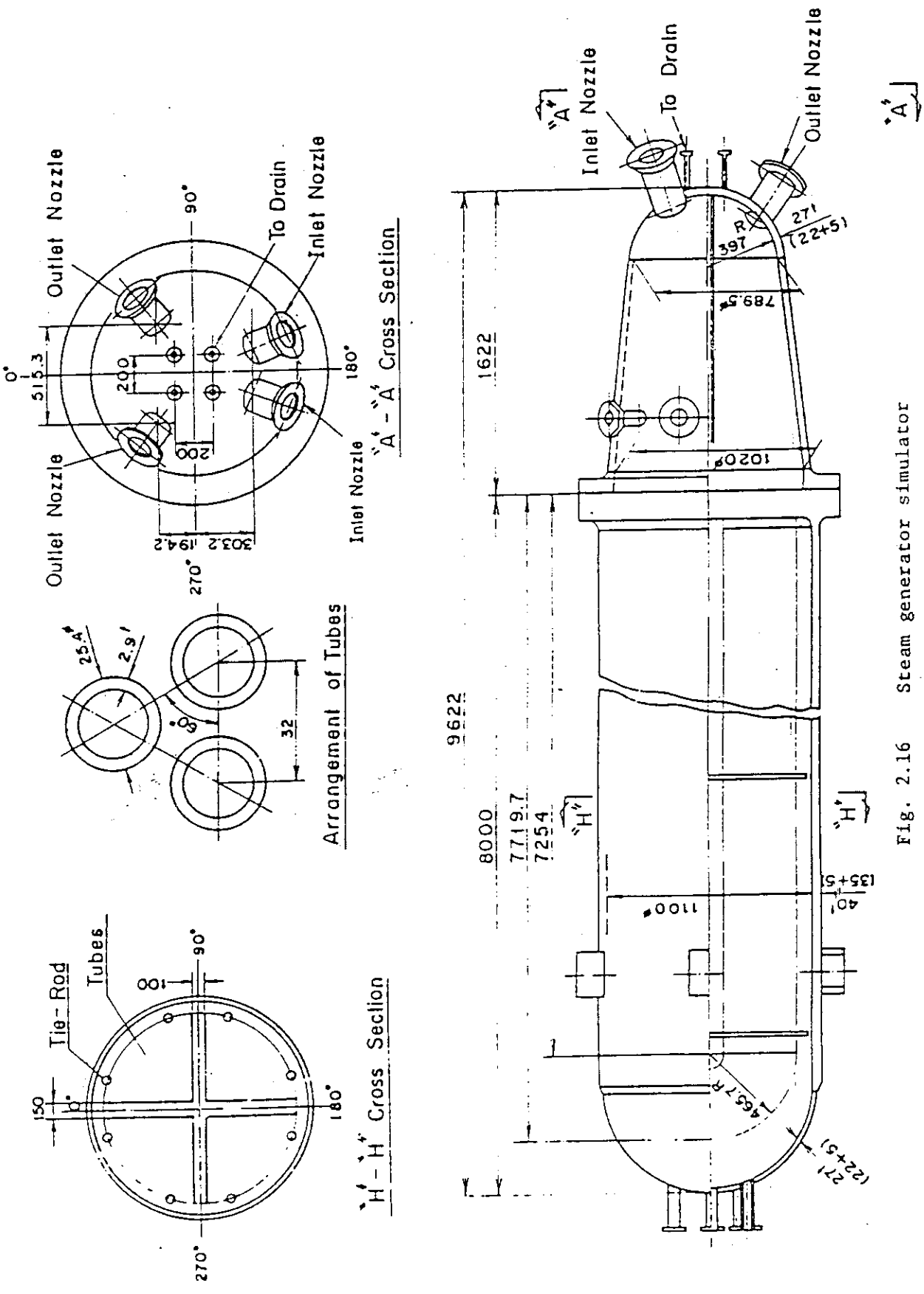

Fig. 2.16 Steam generator simulator

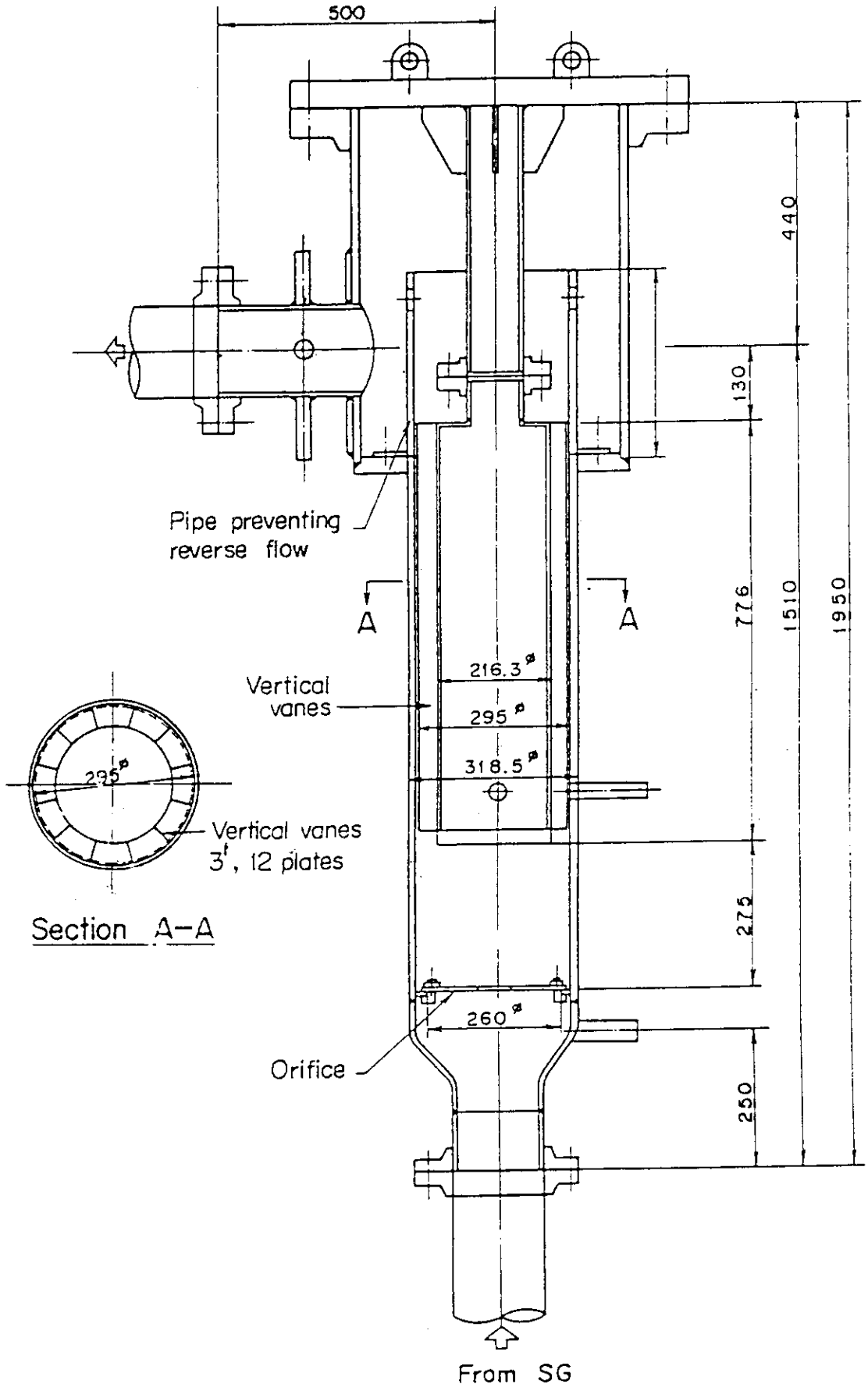

Fig. 2.17 Pump simulator

3. Test Procedure and Test Conditions

3.1 Test Procedure

After establishing the initial conditions of the test, the electric power for preheating was turned off and the lower plenum was filled to a specified level (about 0.9 m) directly from the saturated water tank. When the water level in the lower plenum reached the specified level and other initial conditions of the test stabilized at the allowable tolerance, electric power was applied to the heater rods in the core and the data recording was started. The temperature rises of the rods were monitored by using a computer. When a specified initial clad temperature (1003 K) was reached, direct injection (0.104 m^3/s) of the Acc water into the lower plenum was initiated. The system pressure was maintained at the specified initial pressure (0.2 MPa) throughout the test by controlling the outlet valve of containment tank-II. Decay of power input to the rods was programmed to begin when the water reached the bottom of the heated region of the core. The speficied initial clad temperature (995 K) of the heater rods for initiation of coolant injection was predetermined by interpolation between the clad temperature (394 K) after preheating and the clad temperature (1073 K) assumed for the time of core bottom recovery. The specified power decay was obtained by normalizing the decay curve of the ANS standard $\times 1.0 + {}^{238}U$ capture decay at 30 s after shutdown.

When the assumed water level reached the specified level (0.5 m) from the bottom of th heated region of the core, the injection port was changed from the lower plenum to the three intact cold leg ECC ports. This water level was assumed to be the level at which considerable steam generation occurs in the core to minimize the untypical oscillatory behavior due to the condensation at the ECC ports. The accumulator injection flow rate was then reduced to 0.088 m^3/s in the cold leg injection period. At a specified time (16.5 s) after the time of core bottom recovery, the valves in the Acc lines and LPCI circulation lines were closed and the valves in LPCI injection line were opened. These actions transferred the ECC injection from Acc injection mode to LPCI mode. A specified LPCI flow rate (0.011 m^3/s) was maintained constantly until the ECC injection was turned off.

The generated steam and the entrained water flowed via broken and intact loops to the containment tanks. The steam was then vented to the atmosphere to maintain a constant pressure in the containment tanks. After all thermocouples on the surface of the heater rods indicated quenching of the rods, the power supply to the heater rods was decreased linearly.

This linear power decay was performed in order to study any particular reflood phenomena under very low power supply. The linear power decay was initiated at 690.5 s and the power was turned off at 898 s. After the ECC injection was turned off, the recording system was stopped, thus terminating the test.

3.2 Test conditions

The test conditions of the present low power test are shown in Table 3.1. The specified test conditions were similar to those of the Core-II base case test[3], except for the power supply to the heater rods. In the low power test, the power was set 16 % lower than that of the core II base case test. The test conditions of the core II base case test are shown in Table 3.2.

(1) Decay heat in PWRs

In the previous safety evaluation, the decay heat during the reflood phase was assumed as

$$1.02 \times (\text{Old ANS} \times 1.2 + \text{Actinide}).$$

In 1981 it was approved to use the following equation for the above one.

$$1.02 \times (\text{New ANS} + 2\sigma + \text{Actinide})$$

The above equations lead to 8.8 MW and 7.4 MW of the initial total power by the CCTF scaling (1/21.4) respectively, assuming the initiation of the reflood phase at 30 s after scram.

(2) Determination of the core supplied power

In the previous CCTF tests, the power was determined as

$$1.02 \times (\text{Old ANS} \times 1.2 + \text{Actinide}) \times F_{ex} \text{ (Experimental margin)}$$

Assuming (i) $F_{ex} = 1.07$ and (ii) the initiation of the reflood phase at 30 s after scram, the power was set to 9.4 MW, which was 7 % higher than the scaled one based on the old decay heat criterio. In order to study the effect of the power on the reflood phase, the power in the low power test was determined as

$$1.02 \times (\text{Old ANS} + \text{Actinide}) \times F_{ex}$$

Assuming (i) and (ii), the power is set to 7.9 MW, which is 7 % higher than the scaled one based on the new decay heat criterio.

Figure 3.1 shows the comparison of the supplied power between base case test and the present low power test. In low power test the supplied power was decreased instantaneously by 16 % at the time = 90.5 s and was decreased linearly after the time = 690.5 s.

The sequence of events that occurred during the tests are listed in Table 3.3 and 3.4.

Table 3.1 Summary of measured test conditions (I)

1. Test type: Low power test
2. Test No. : Shakedown test 2 (Run 54)
3. Test data: March 30, 1982
4. Power : Total; 7.87 MW, Linear; 1.18 kW/m
5. Radial power distribution:

A	B	C
1.37	1.20	0.76

6. Pressure (MPa):
   Containment ; 0.2
   Steam generator secondary; 5.3
7. Temperature (K):
   Downcomer wall ; 468 K
   Vessel internals ; 423 K
   Primary piping ; 406 K
   Lower plenum liquid; 394 K
   ECC liquid ; 310 K
   Steam generator secondary side; 539 K
8. ECC injection type : Lower plenum and cold leg injection
9. Pump K-factor : 15
10. ECC injection rates, durations and injection locations:
    Acc ; 0.104 m^3/s from 81.0 s to 94.0 s into lower plenum
    0.088 m^3/s from 94.0 s to 107.0 s into cold legs
    LPCI; 0.011 m^3/s from 107.0 s to 979.0 s into cold legs
11. Initial water level:
    In lower plenum ; 0.86 m
    In steam generator secondary side; 7.4 m
12. Power decay:
    Constant ; from 0 s to 90.5 s
    ANS×1.0+Actinide (30 s after scram); from 90.5 s to 690.5 s
    Linear decay ; from 690.5 s to 898.0 s
13. Reflood initiation time: 90.5 s
14. Peak clad temperature at reflood initiation: 1074 K at TE31Y17

* Note: Time in this table is defined as time after test initiation.

Table 3.2 Summary of measured test conditions (II)

1. Test type: Base case test
2. Test No. : Shakedown test 1 (Run 53)
3. Test data: March 18, 1982
4. Power : Total; 9.35 MW, Linear; 1.40 kW/m
5. Radial power distribution:

   A : B : C

   1.37 : 1.20 : 0.76
6. Pressure (MPa):

   Containment ; 0.2

   Steam generator secondary; 5.2
7. Temperature (K):

   Downcomer wall ; 470 K

   Vessel internals ; 393 K

   Primary piping ; 393 K

   Lower plenum liquid; 360 K

   ECC liquid ; 308 K

   Steam generator secondary side; 540 K
8. ECC injection type : Lower plenum and cold leg injection
9. Pump K-factor : 15
10. ECC injection rates, durations and injection locations:

    Acc ; 0.105 m^3/s from 81.0 s to 94.5 s into lower plenum

    0.089 m^3/s from 94.5 s to 105.0 s into cold legs

    LPCI; 0.011 m^3/s from 105.0 s to 948.0 s into cold legs
11. Initial water level:

    In lower plenum ; 0.95 m

    In steam generator secondary side; 7.4 m
12. Power decay:

    Constant ; from 0 s to 89.5 s

    ANS×1.2+Actinide (30 s after scram); from 89.5 s
13. Reflood initiation time: 89.5 s
14. Peak clad temperature at reflood initiation: 1064 K at TE31Y17

* Note: Time in this table is defined as time after test initiation.

Table 3.3 Chronology of Events for Test C2-SH2 (Run 54) (I)

Event	Time after test initiation (s)	Time after reflood initiation (s)
Test Initiated (Heater Rods Power on) (Data Recording Initiated)	0(15.51.39)	-90.5
Accumulator Injection Initiated	81.0	-9.5
Power Decay Initiated (Bottom of Core Recovery) (Reflood Initiation)	90.5	0.0
Accumulator Injection Switched from Lower Plenum to Cold Leg	94.0	3.5
Accumulator Injection Ended and LPCI Injection Initiated	107.0	16.5
Maximum Turnaround	123.0	32.5
All Heater Rods Quenched	552.5	462.0
Linear Power Decay Initiated	690.5	600.0
Power Off	898.0	807.5
LPCI Injection Ended	979.0	888.5
Test Ended (Data Recording Ended)	1032.0	941.5

Table 3.4 Chronology of Events (II)

Event	Time after test initiation (s)	Time after reflood initiation (s)
Test Initiated (Heater Rods Power on) (Data Recording Initiated)	0	-90.5
Accumulator Injection Initiated	81.0	-9.5
Power Decay Initiated (Bottom of Core Recovery) (Reflood Initiation)	89.5	0.0
Accumulator Injection Switched from Lower Plenum to Cold Leg	94.5	3.5
Accumulator Injection Ended and LPCI Injection Initiated	105.0	16.5
Maximum Turnaround	141.0	32.5
All Heater Rods Quenched	665.0	575.5
LPCI Injection Ended	948.0	888.5
Test Ended (Data Recording Ended)	1029.0	941.5

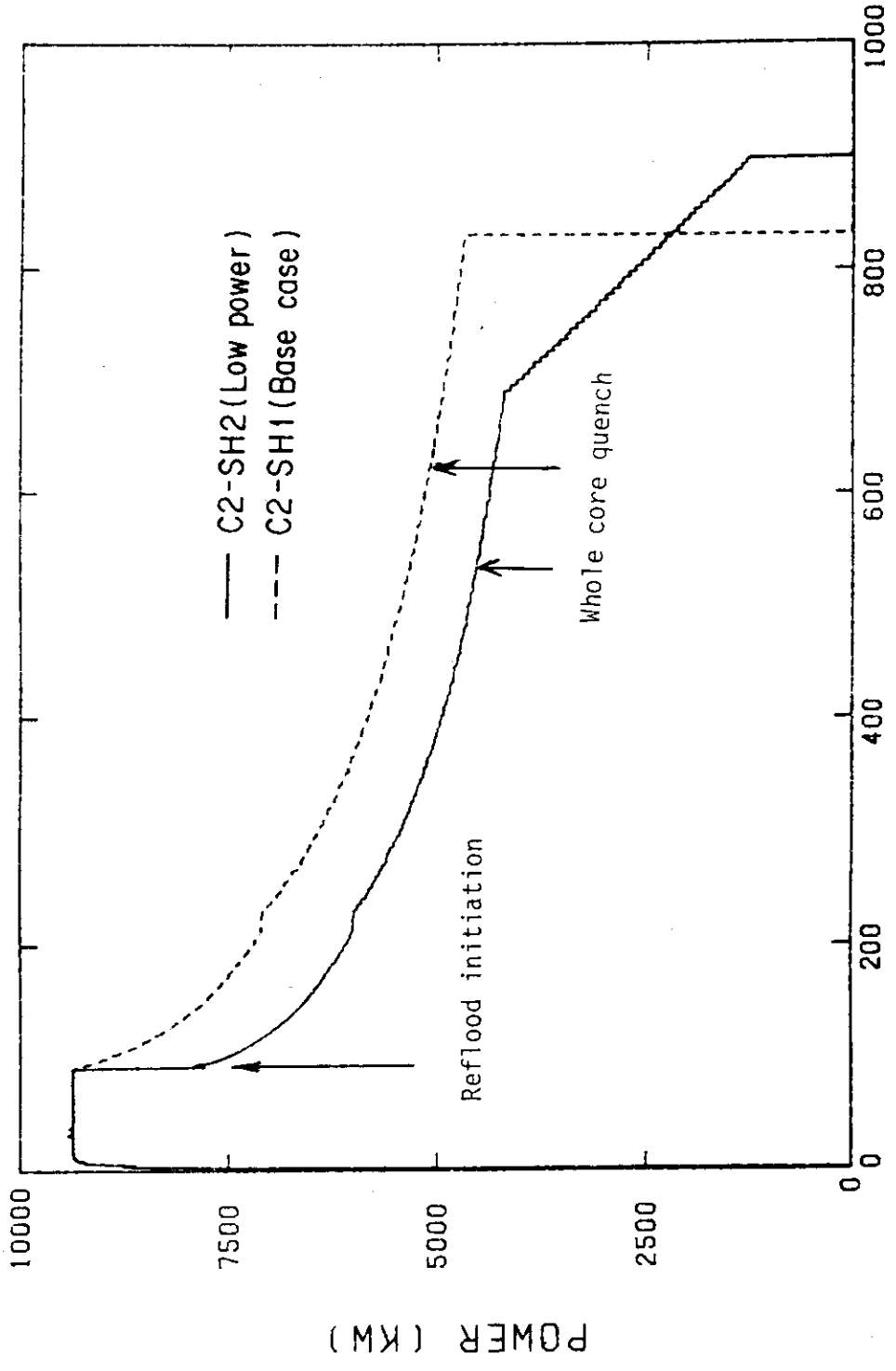

Fig. 3.1 Supplied power

4. Results and discussion

4.1 System behavior

The experimental result of the present low power test C2-SH2 (Initial average linear power density = 1.18 kW/m) was compared with that of the CCTF Core II base case test C2-SH1 (1.40 kW/m) in order to study the effect of the power on the reflood phenomena.

(1) Steam generation rate in the core

Figure 4.1 shows the transient of the evaluated steam generation rate in the core in the low power test and the Core-II base case test. The evaluated steam generation rate was obtained by the heat balance calculation in the core, using the measured clad temperature of the heater rods[6].

The evaluated steam generation rate is identical in two tests during the early stage (upto 100 s after reflood initiation) in spite of the different power. After 200 s, the evaluated steam generation rate is lower in the low power test. The reason why the effect of the power on the steam generation rate is little during the early stage is considered to be due to the fact that the heat release from the heater rods mainly depends on the stored heat in the heater rods. This fact is consistant with the result of the initial clad temperature tests[4], in which the initial stored energy was a main factor controlling the reflood phenomena during the early stage of the reflood transient.

The lower steam generation rate during the later period (> 200 s) for the low power test is due to the lower clad temperature resulted from the lower power supply.

(2) Water accumulation in pressure vessel

Figure 4.2 shows the core differential pressure. The core differential pressure increases after reflood initiation. The increasing rate of the core differential pressure becomes generally smaller with time. This trend of the core differential pressure is commonly observed in two tests. The core differential pressure in the low power test is nearly equal to that in the Core-II base case test until 200 s after reflood initiation. After 200 s, the core differential pressure in the low power test is larger than that in the Core-II base case test. The larger core differential pressure, i.e. the larger water accumulation in the core, in low

power test during the later period is due to the smaller steam generation in the core, as shown in Fig. 4.1, causing the lower void fraction. The FLECHT-SET test[5] shows that the core differential pressure in low power test (Initial peak linear power: 0.84 kW/m) is the same as that in high power test (Initial peak linear power: 1.05 kW/m) for the initial period of the reflood (30 s after reflood initiation) and afterwards the core differential pressure in low power test is larger (+20 %) than in high power test. This trend is common between CCTF and FLECHT-SET data although the time scale is larger in CCTF than FLECHT-SET.

Figure 4.3 shows the upper plenum differential pressure. The upper plenum differential pressure is nearly zero upto 200 s after reflood initiation in the low power test and the Core-II base case test. This time is corresponding to the times when the core differential pressure initiates to increase again as shown in Fig. 4.2 and roughly when the steam generation in the core initiate to decrease again as shown in Fig. 4.1. After 200 s, the upper plenum differential pressure in the low power test is larger than that in the Core-II base case test. The larger upper plenum differential pressure in the low power test during the later period can be attributed to the smaller steam flow rate into the upper plenum, which is caused by the smaller steam generation in the core.

Figure 4.4(1) shows the downcomer differential pressure. The downcomer differential pressure rapidly increases after reflood initiation, and reaches the maximum value (about 0.065 MPa). Then, it decreases gradually. After it reaches the minimum value, it increases gradually again and eventually becomes constant. This trend of the downcomer differential pressure is commonly observed in the low power test and the Core-II base case test.

During the period between 20 s and 200 s after reflood initiation, the downcomer differential pressure is smaller in the low power test. This is probably due to the lower effective downcomer water head caused by the higher fluid temperature in the downcomer, as shown in Fig. 4.4(2), which is resulted by the higher initial fluid temperature in the lower plenum, as shown in Fig. 4.4(3) and Fig. 4.4(4). The fact why the higher initial fluid temperature in the lower plenum results in the higher fluid temperature in the downcomer is related to the test procedure adopted for both the low power and the base case tests, in which the Acc water was injected directly to the lower plenum for the first transient, so that the fluid was transfered from the lower plenum to the downcomer for the first

period.

Figure 4.5(1) shows the loop differential pressure. The intact loop differential pressure increases after reflood initiation, and reaches the maximum value at about 20 s after reflood initiation, and then decreases gradually. After it reaches the minimum value, it increases gradually again and eventually becomes constant at 300 s. This trend of the intact loop differential pressure is commonly observed in the low power test and the core II base case test, and it is very similar to the trend of the downcomer differential pressure as shown in Fig. 4.4(1). The broken loop differential pressure increases after reflood initiation, and reaches the maximum value, and then shows the trend of decreasing with a long term oscillation.

The intact and the broken loop differential pressures in the low power test are smaller than those in the core II base case test. This is due to the smaller steam flow rate through loops in the low power test, as shown in Figs. 4.5(2) and (3). The smaller intact and broken loop differential pressures with the lower power are also observed in the FLECHT-SET data.

Figure 4.6 shows the integrated mass of the overflowing water from the downcomer to containment tank I. The rapid increasing of the overflowing water at the termination of Acc injection is observed in the low power test and the core II base case test. After 30 s until 180 s, almost constant overflowing water flow rate (9.5 kg/s) is observed. After that, constant but smaller overflowing water flow rate (7.3 kg/s) is observed. The above trend is very similer to that in the core II base case test. Thus, the effect of the power on the overflowing water flow rate from the downcomer to containment tank I is slight.

4.2 Core inlet flow conditions

Figure 4.7 shows the core flooding flow rate, pressure in the upper plenum and the fluid temperature at the core inlet. The core flooding flow rate and the pressure are almost identical in the low power test and the base case test. The fluid temperature at the core inlet is approximately 10 K higher in the low power test than in the base case test. The higher fluid temperature in the low power test is the result of the higher initial fluid temperature in the lower plenum. The higher fluid

temperature, and then the lower subcooling, in the low power test resulted in the smaller static water heat due to the lower boiling point elevation in the lower core (0 m ~ 0.61 m), as shown in Fig. 4.9. Since the difference of the subcooling is smaller, the steam generation rate is not affected by the different subcooling, and hence it is considered that the core cooling is not affected by the different subcooling except for the bottom part of the core.

Figure 4.8 shows the integrated mass of the water flooding into the core. The effluent mass through loops and the stored mass in the core are also shown in the figure. The flooding masses into the core in the low power test and the core II base case test are nearly identical with each other in spite of the different power. Upto 200 s after reflood initiation, the effluent masses through loops and the stored masses in the core in both tests are also identical with each other. These are due to that the initial stored energy is a dominant factor for the steam generation in the core for the first transient. After the time, the effluent mass through loops is smaller and the stored mass in the core is larger in the low power test than in the core II base case test. Since the smaller effluent mass through loops and the larger stored mass in the core compensated with each other, the flooding mass into the core in the low power test became identical to that in the core II base case test. This suggests that the power which was supplied into the core affects little the water flooding rate into the core. The FLECHT-SET data also showed that the core flooding rate was nearly identical even under the different power, as shown in 4.8(2).

4.3 Core thermo-hydraulic behavior

(1) Sectional core differential pressure

Figures 4.9 and 4.10 show the sectional core differential pressure. It was measured by dividing the core axially into 6 sections. Figure 4.9 shows the sectional core differential pressure of the lower core section, which elevation is from 0 m to 1.83 m from the bottom of the core. Figure 4.10 shows the sectional core differential pressure of the upper core section, which elevation is from 1.83 m to 3.66 m from the bottom of the core. The data upto 150 s after reflood initiation is not certain due to wrong zero shift, which is caused by the incomplete preconditioning of water filling in pressure taps. Since the measured differential pressure

at the no void condition (after the power-off) agreed with the static heat of the solid water, it is considered that the measured one is reliable after 150 s.

The sectional core differential pressures in the lower part of the core (0 m ~ 0.61 m and 0.61 m ~ 1.22 m) are smaller upto 200 s after reflood initiation in the low power test than in the core II base case test. This is due to the higher fluid temperature at core inlet, as show in Fig. 4.7., resulting in the lower boiling initiation point. After 200 s, on the contrary, they are larger in the low power test than in the core II base case test. This is due to the lower power supply, resulting in the lower steam flow rate and hence the lower void fraction.

(2) Clad temperature

Figures 4.11 and 4.12 show the clad temperatures of the heated rods in the core. Since the supplied power is equal in the low power test and the core II base test upto reflood initiation, the clad temperatures at the reflood initiation are equal between both tests. Since the supplied power is decreased at reflood initiation in the low power test, the clad temperature is lower in the low power test after reflood initiation. It is noticed from the figure that the turnaround time and quench time are earlier and the turnaround temperature is lower in the low power test than in the core II base case test, as shown in the following.

	C2-SH2 (Low power)	C2-SH1 (Base case)
Turnaround time	32.5 s	141 s
Turnaround temperature	1113 K	1148 K
Quench time	462 s	576.5 s

The earlier turnaround time, the lower turnaround temperature and the earlier quench time with the lower power are also observed in FLECHT-SET data.

(3) Heat transfer coefficient

Figure 4.13 shows the heat transfer coefficient at the average power rod in the medium power zone (Bundle 22). The heat transfer coefficient at each elevation (0.38, 1.02, 1.83, 2.44 and 3.05 m) in the low power test is nearly identical to that in the core II base case test upto 200 s after

reflood initiation. The effect of the power on the heat transfer coefficient is very small during the early stage. After that, the heat transfer coefficient in the low power test is higher than in the core II base case test. This is dependent partly on the earlier quench time (Fig. 4.15(1)) and partly on the lower void fraction (Figs. 4.9 and 10) in the low power test.

(4) Turnaround time and quench time

Figure 4.14(1) and (2) show the turnaround time along the elevation. The solid line in Fig. 4.14(1) is an average turnaround time in the high power region (A region) for the low power test and the chain line is that for base case test. The earlier turnaround for the low power test than the base case test is observed, especially in the upper part of the core.

Figures 4.15(1) and (2) show the quench time along the elevation. The solid and chain lines in Fig. 4.15(1) are average quench times in the high power region for the low power test and base case test, respectively. Similarly to the case of the turnaround time, the earlier quench for the low power test than the base case test is observed, especially in the upper part of the core.

The earlier turnaround and quench times in a low power test have the similar trend in forced feed tests, and are consistent with FLECHT-SET data[5]. The above result can be attributed to direct result of the above item(3).

(5) Turnaround temperature, temperature rise and quench temperature

Figures 4.16(1) and (2) show the turnaround temperature along the elevation. The solid and chain lines in Fig. 4.16(1) are average turnaround temperatures in the high power region for the low power test and base case test, respectively. The lower turnaround temperature for the low power test than the base case test is observed in the upper core.

Figures 4.17(1) and (2) show the temperature rise along the elevation. The solid and chain lines in Fig. 4.17(1) are average temperature rises in the high power region for the low power test and base case test, respecitively. The lower temperature rise for the low power test than the base case test is observed.

Figures 4.18(1) and (2) show the quench time along the elevation. The solid and chain lines in Fig. 4.18(1) are average quench time in the high power region for the low power test and base case test, respectively.

The lower quench time for the low power test than the base case test is observed.

The lower turnaround temperature in a low power test is the similar trend in forced feed tests, and are consistent with FLECHT-SET data[5]. The above result can be attributed to direct result of the above item(3).

4.4 Oscillation phenomena

The following oscillations are observed in the low power test.

(1) Oscillation of loop differential pressure with long period

This type of oscillation is shown in Fig. 4.19. The $\Delta P_{\text{Loop broken}}$ is defined as the differential pressure across the broken loop, and is measured ΔP between the upper plenum and the location downstream the break point. The $\Delta P_{\text{Loop intact}}$ is defined as the differential pressure across the intact loop, and is measured ΔP between the upper plenum and the exit of the intact cold leg. The $\Delta P_{\text{Broken nozzle}}$ is defined as the differential pressure across the nozzle of the broken cold leg of the downcomer side, and is measured ΔP between the exit of the intact cold leg and the location downstream the break point. The oscillation with long period (200 s ~ 400 s) is clearly noticed in the broken loop differential pressure, the broken nozzle differential pressure and the mass flow rate through the broken nozzle. The intact loop differential pressure and the pressure in the upper plenum also show the weak oscillatory behavior. All these oscillations are synchronous with each other. The period of the oscillation is shorter for the low power test. This is found by comparing $\Delta P_{\text{Loop broken}}$ in the low power and that in base case test in the figure shown below. The further investigation on the mechanism of the above oscillation is necessary.

(2) Significant pressure oscillation induced by the complete condensation at the ECC port

As shown in Fig. 4.20, significant differential pressure oscillation between ECC port and the upper plenum is observed after 700 s. The initiation time of the oscillation corresponds to the time when the differential pressure across the broken cold leg nozzle becomes zero, or the steam flow through the broken cold leg becomes zero. Figure 4.21 shows the fluid temperature around the ECC port. The fluid around the ECC port

is subcooled after the initiation of the oscillation. These suggest that the complete steam condensation and the stagnant subcooled water at the ECC port are the causes of this type of the oscillation.

The complete steam condensation occurred in the present test when the supplied power into the core decrease upto 1.7 MW.

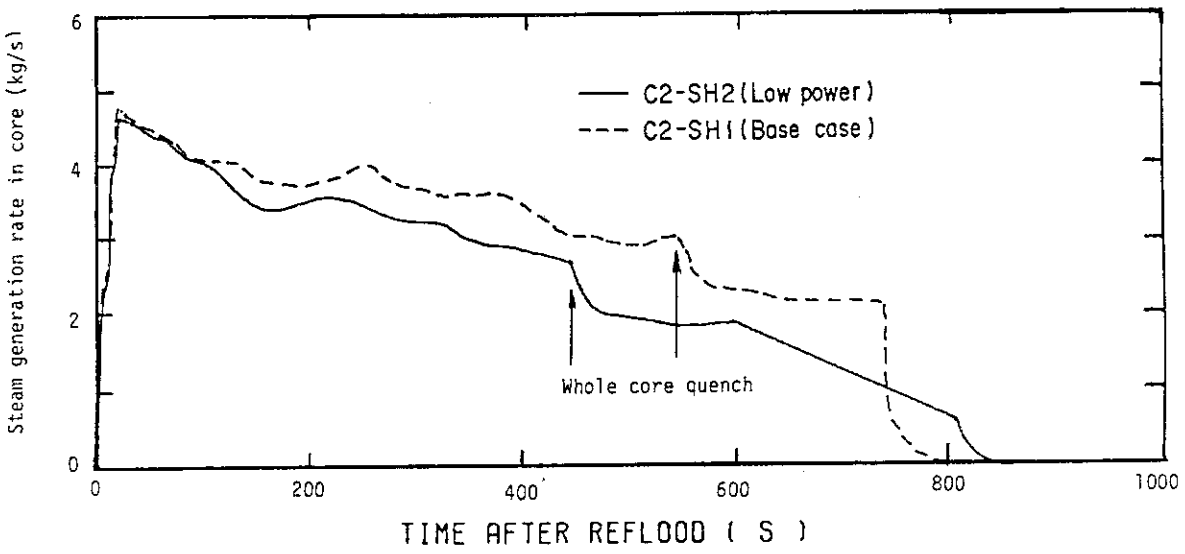

Fig. 4.1 Comparison of steam generation rate

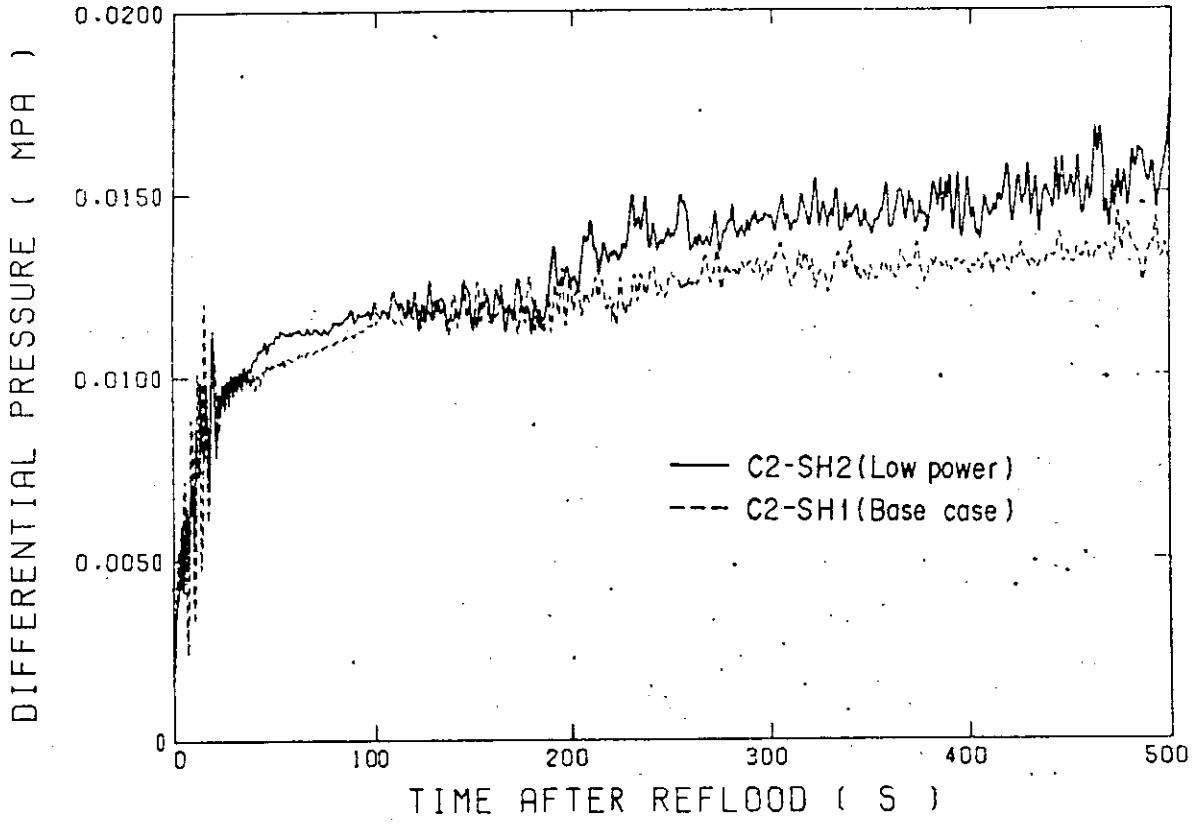

Fig. 4.2 Comparison of core differential pressure

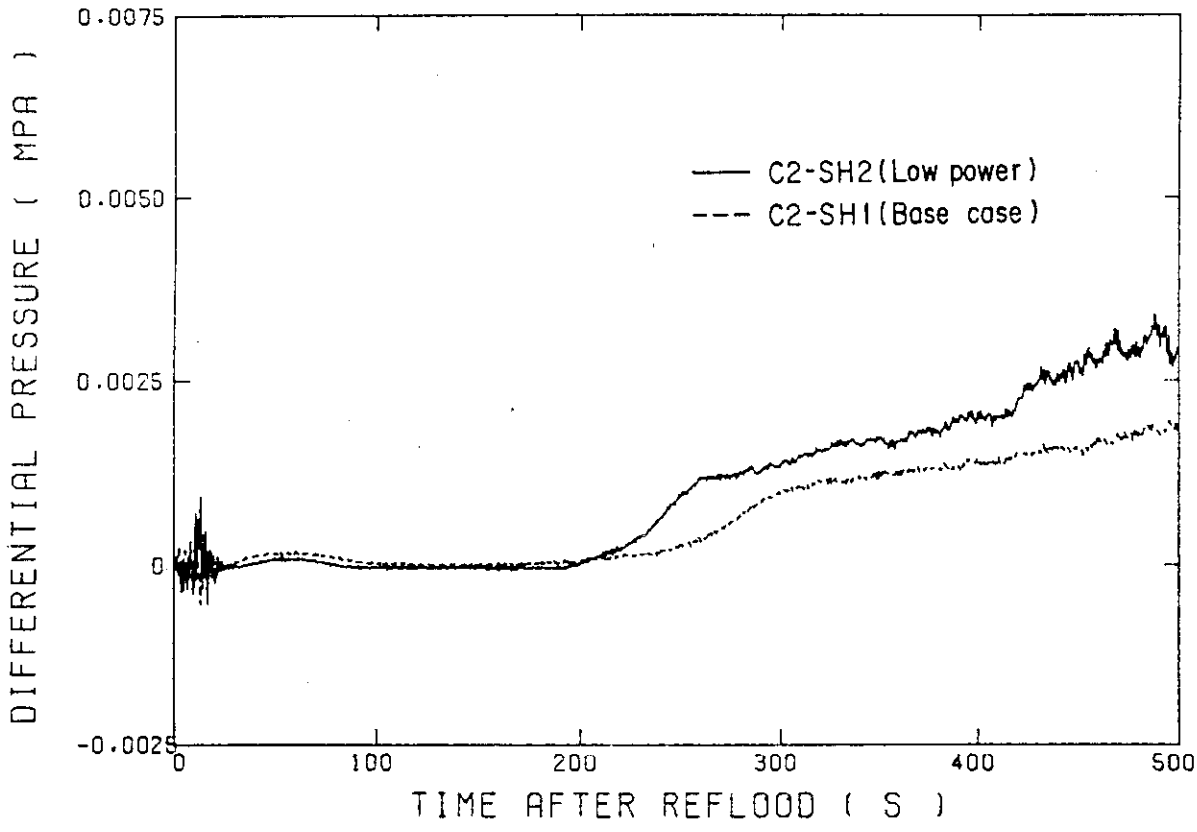

Fig. 4.3 Comparison of upper plenum differential pressure

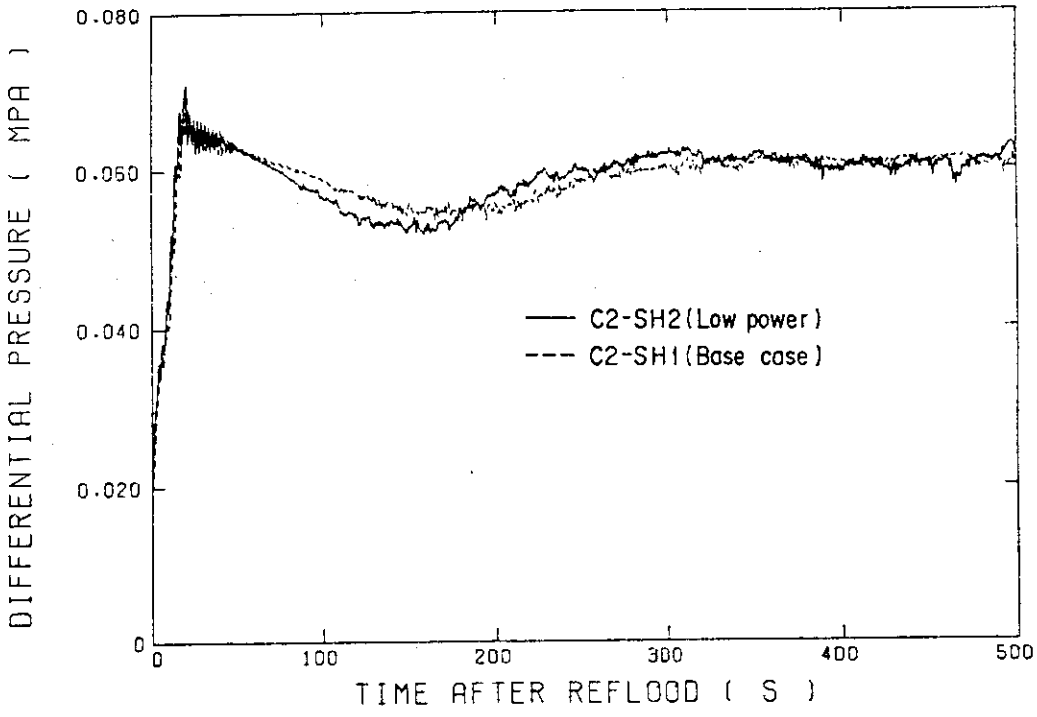

Fig. 4.4(1) Comparison of downcomer differential rpessure

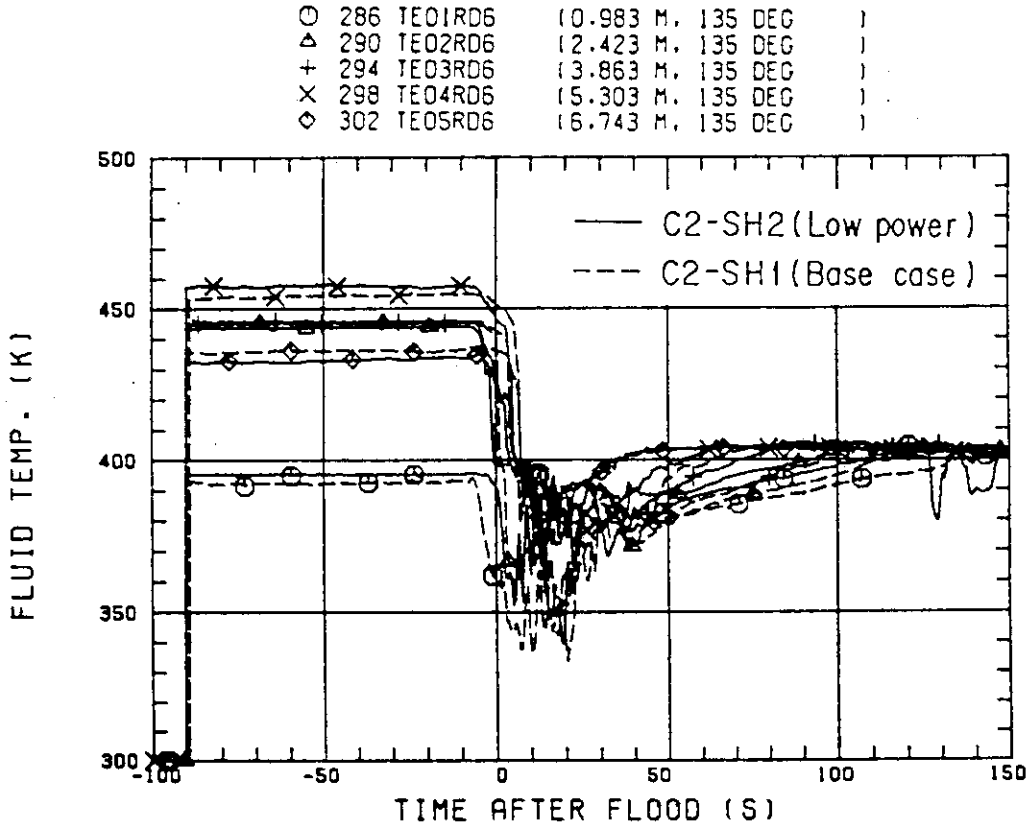

Fig. 4.4(2) Comparison of fluid temperature in downcomer

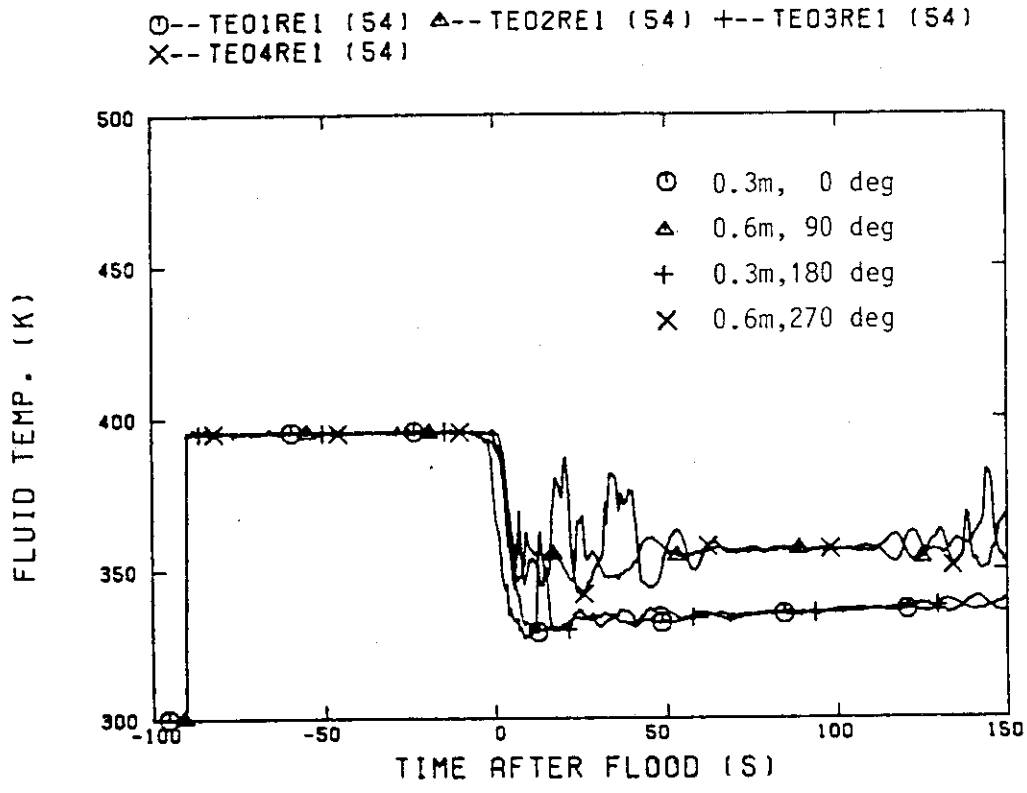

Fig. 4.4(3) Fluid temperature in lower plenum for the low power test

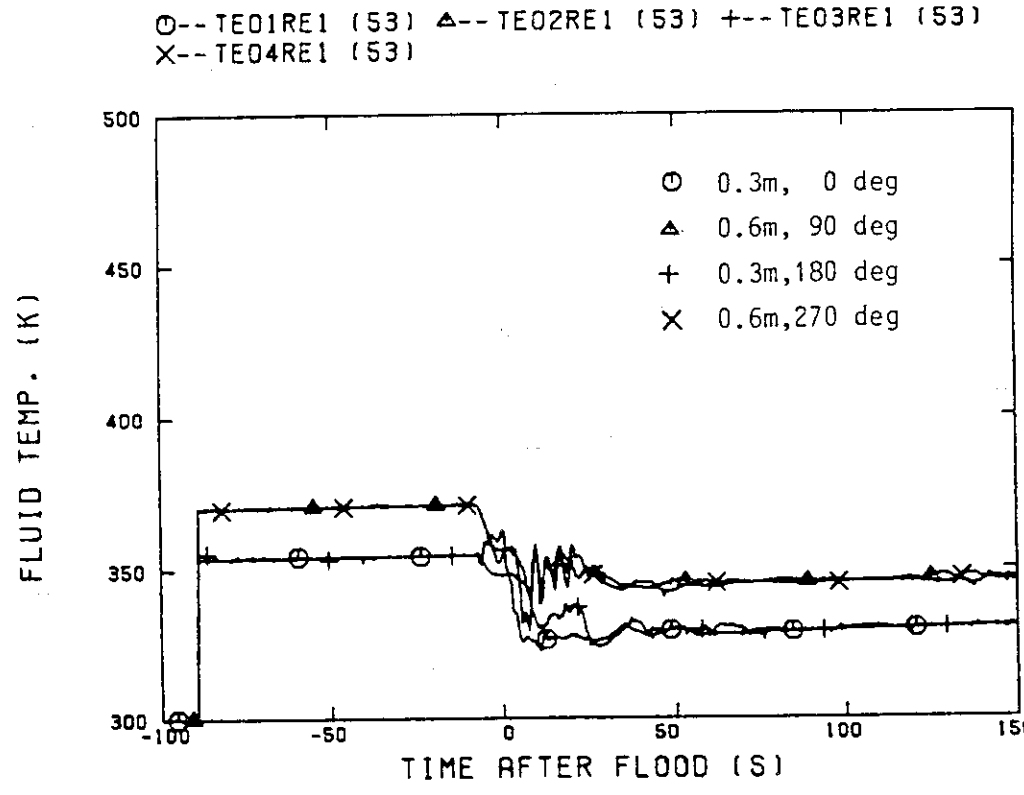

Fig. 4.4(4) Fluid temperature in lower plenum for base case test

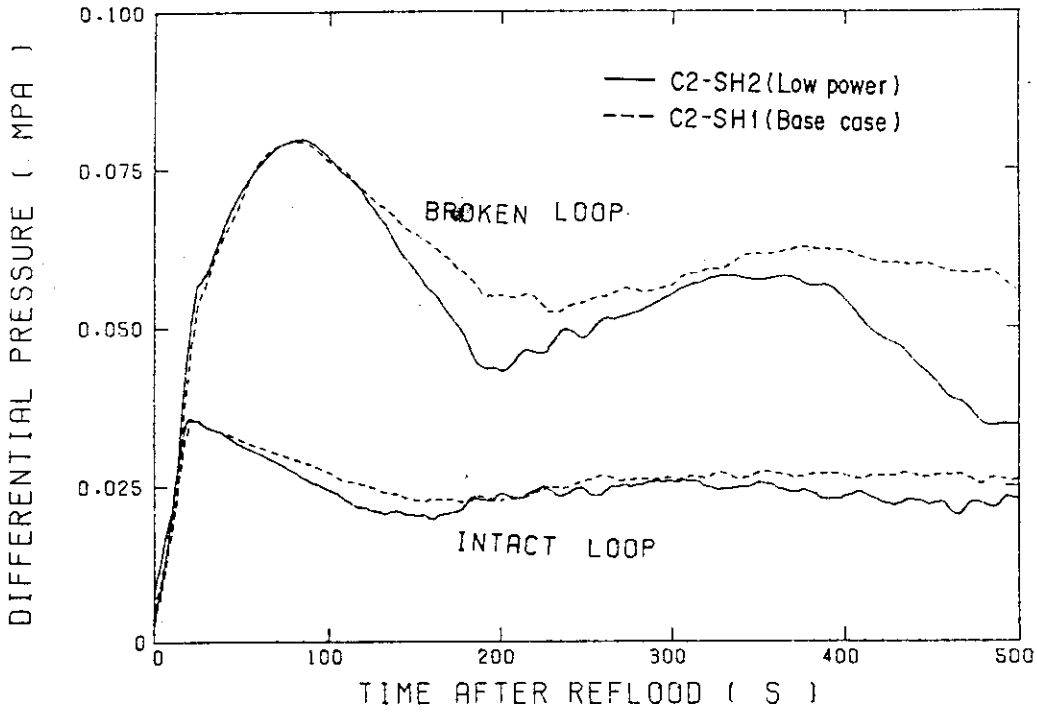

Fig. 4.5(1) Comparison of loop differential pressure

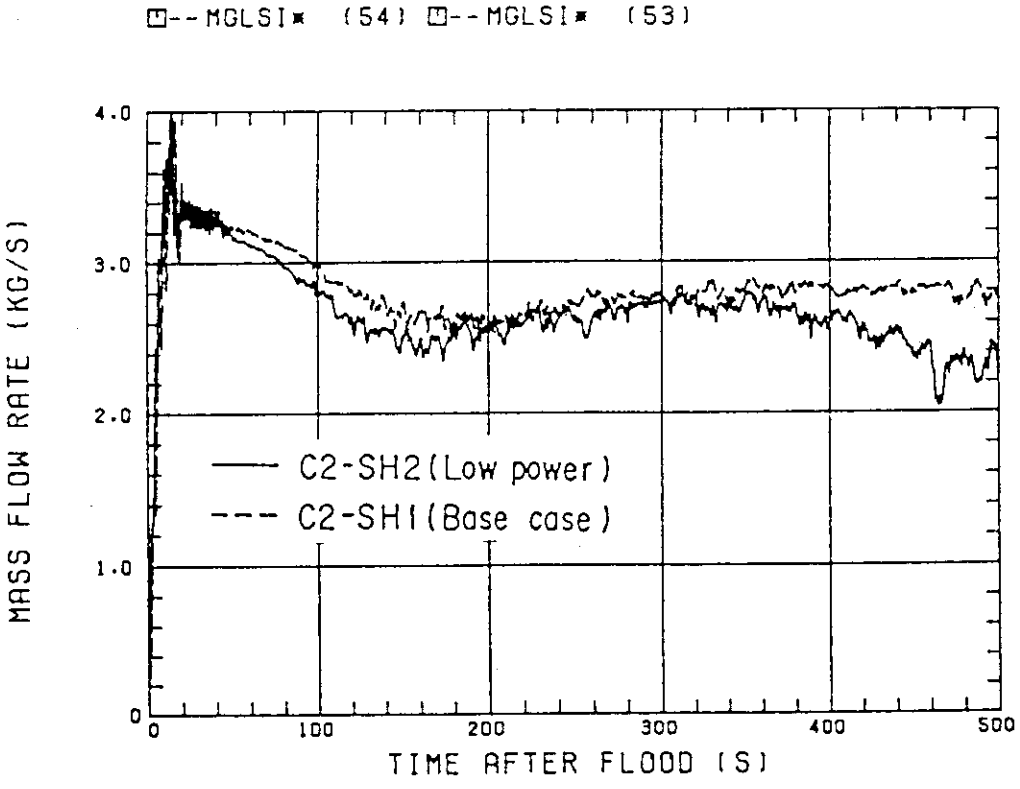

Fig. 4.5(2) Comparsion of intact loops mass flow rate

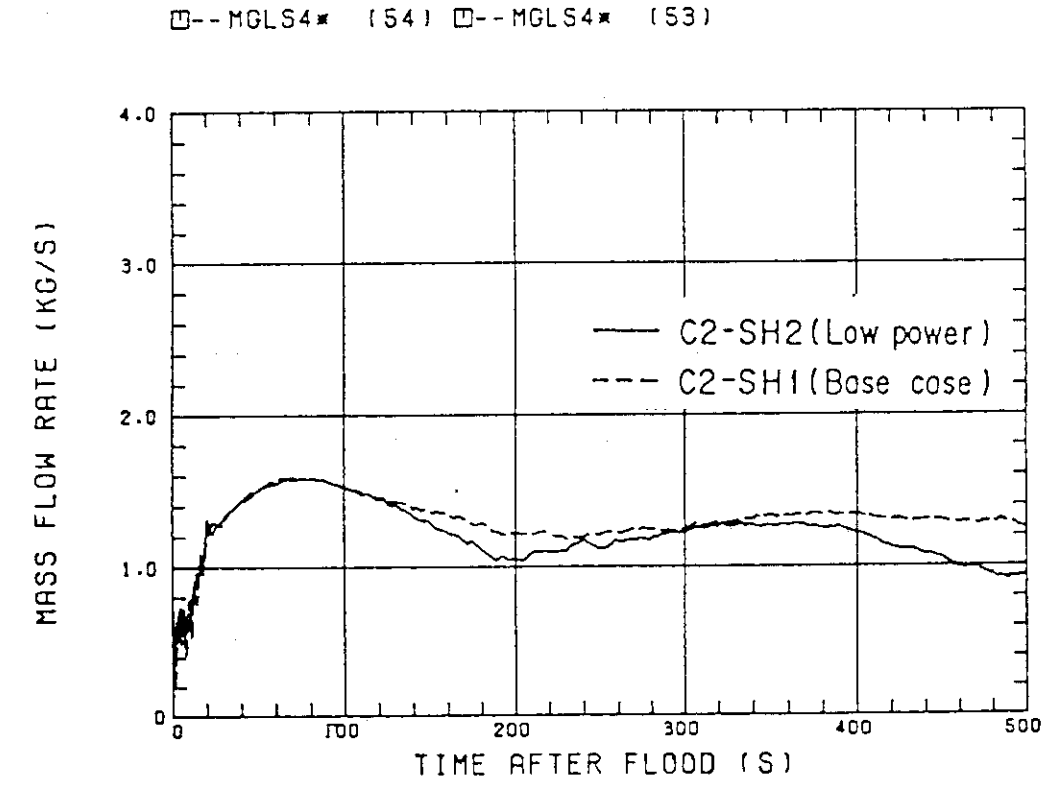

Fig. 4.5(3) Comparison of broken loop mass flow rate

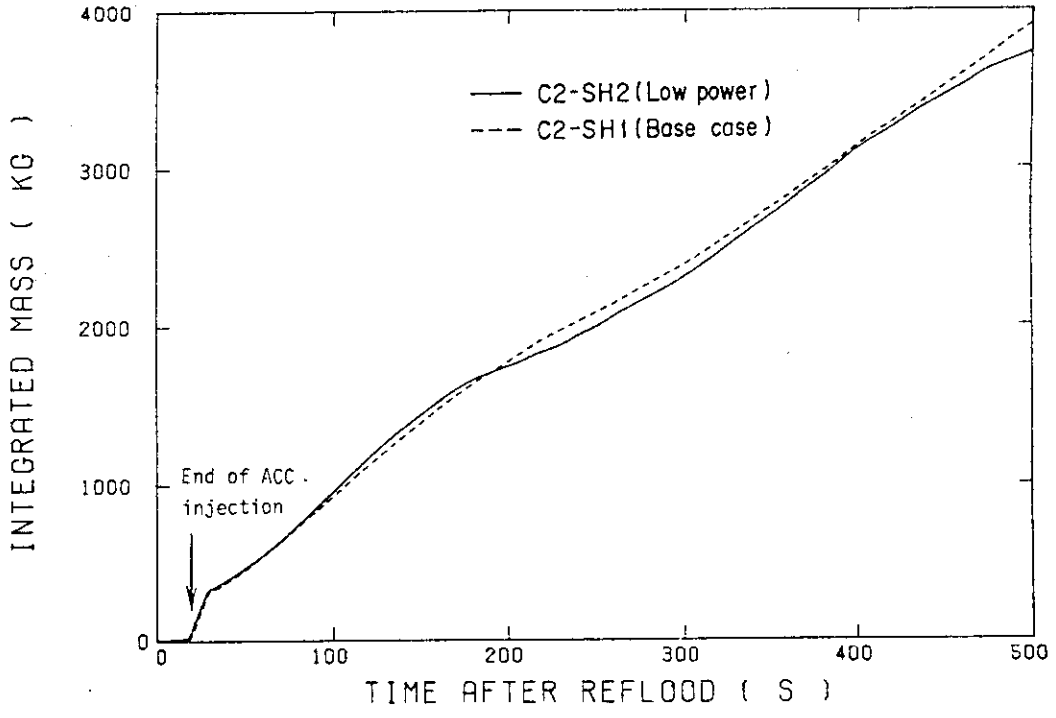

Fig. 4.6 Comparison of overflowing water from downcomer to containment tank 1

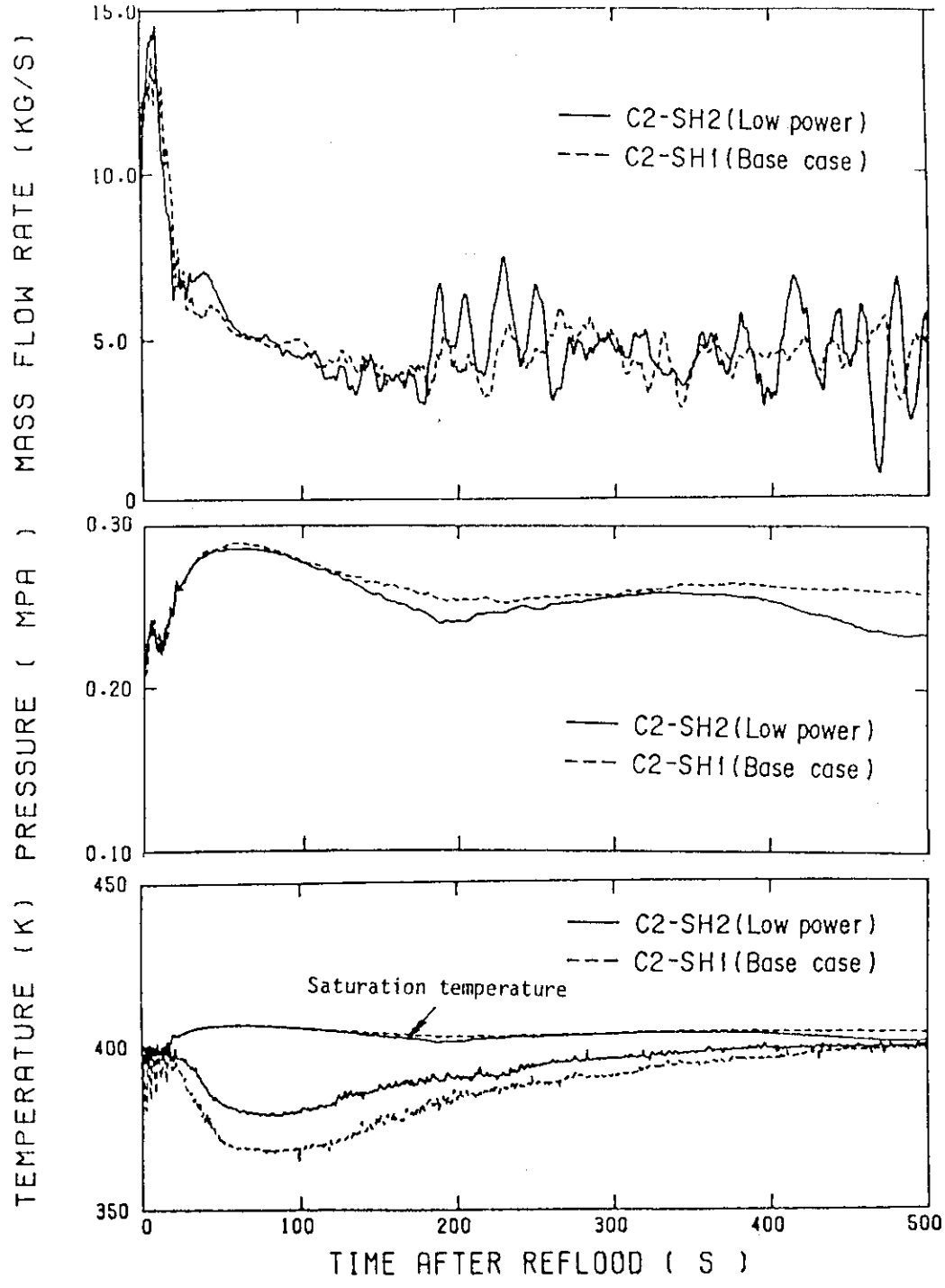

Fig. 4.7 Comparison of core inlet mass flow rate, pressure in upper plenum and the fluid temperature at core inlet

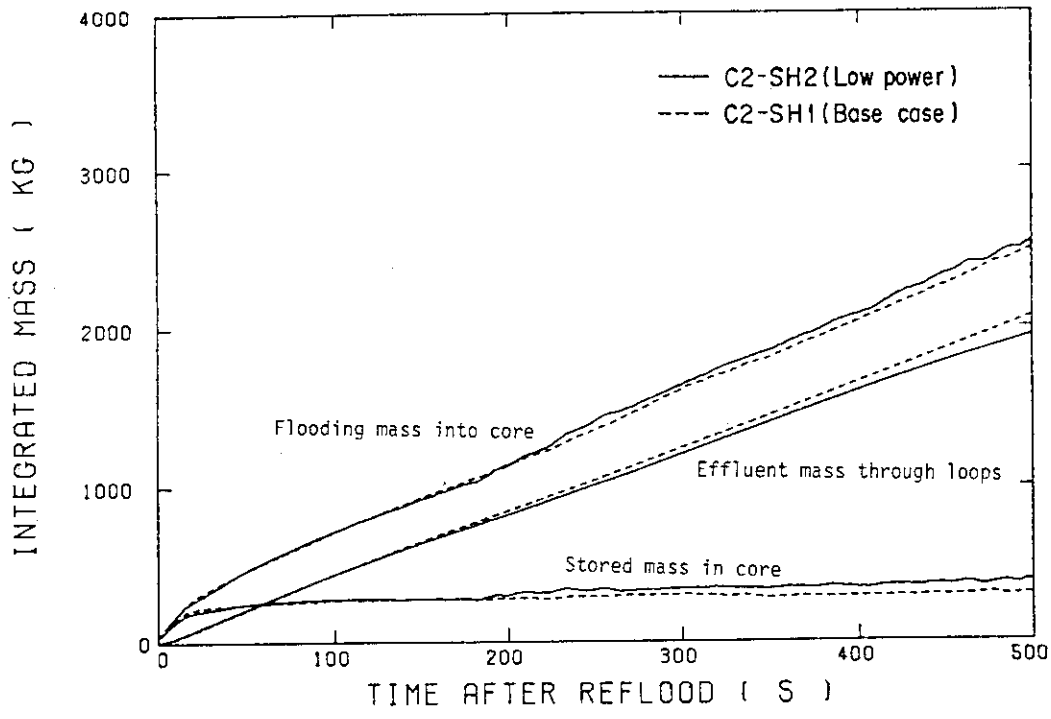

Fig. 4.8(1) Comparison of stored and effluent mass

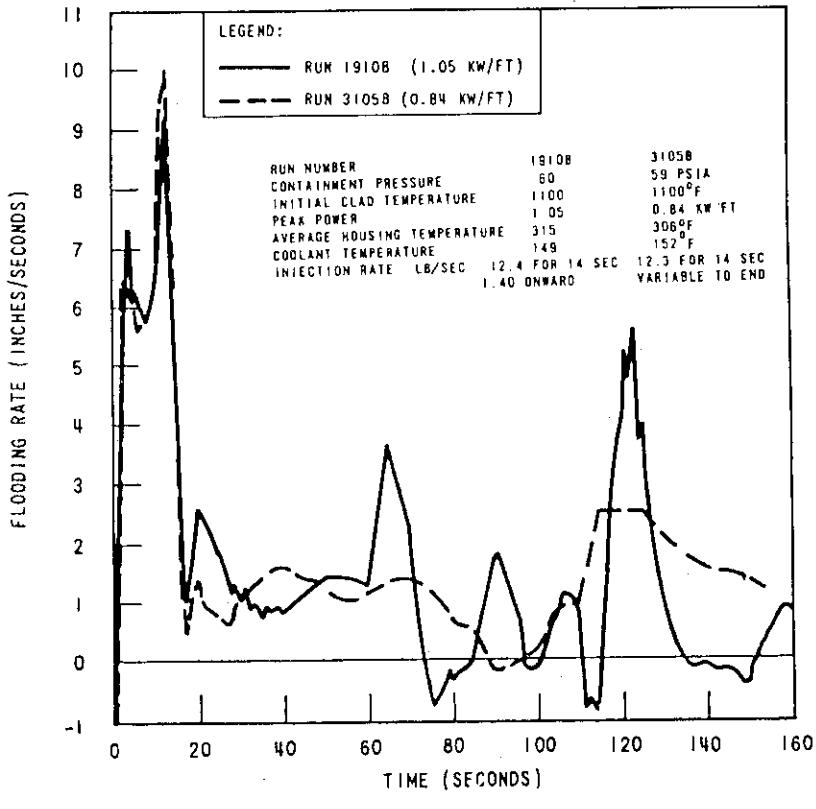

Fig. 4.8(2) Effect of rod power on flooding rate[7]

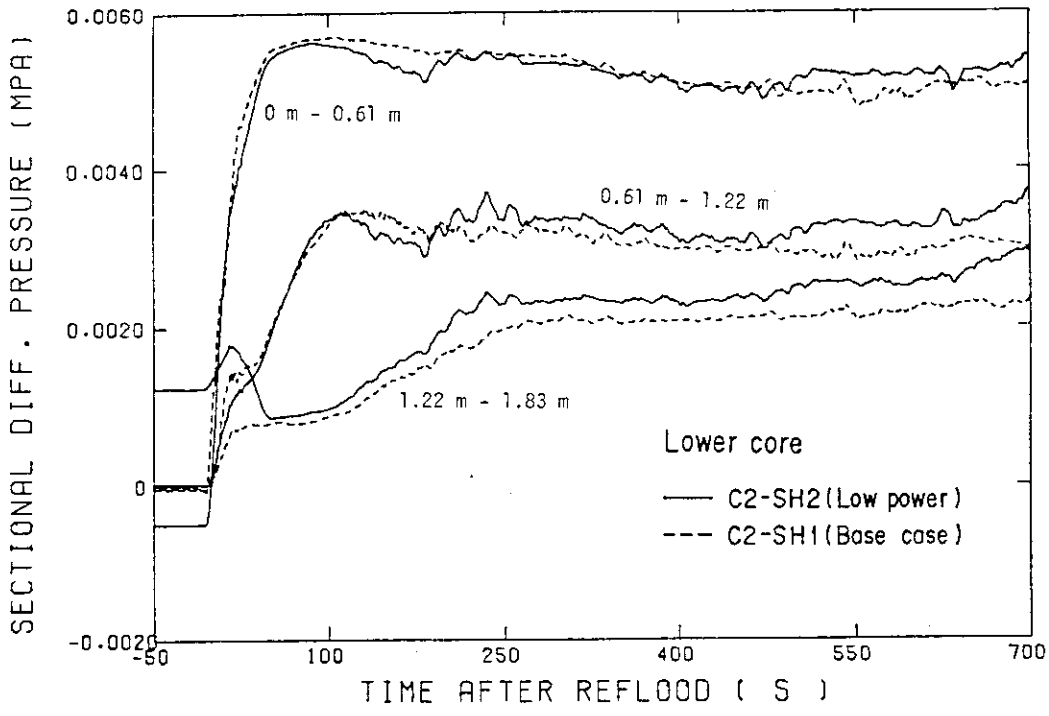

Fig. 4.9 Comparison of sectional differential pressure in lower core

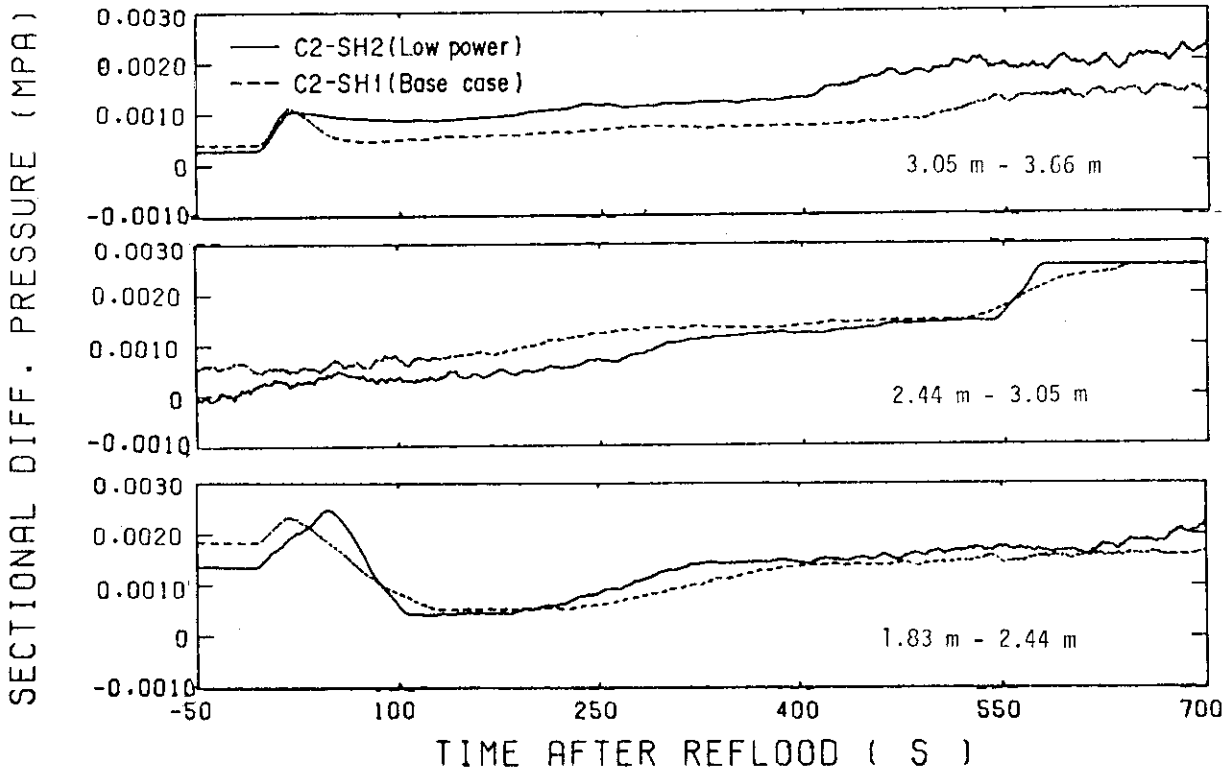

Fig. 4.10 Comparison of sectional differential pressure in upper core

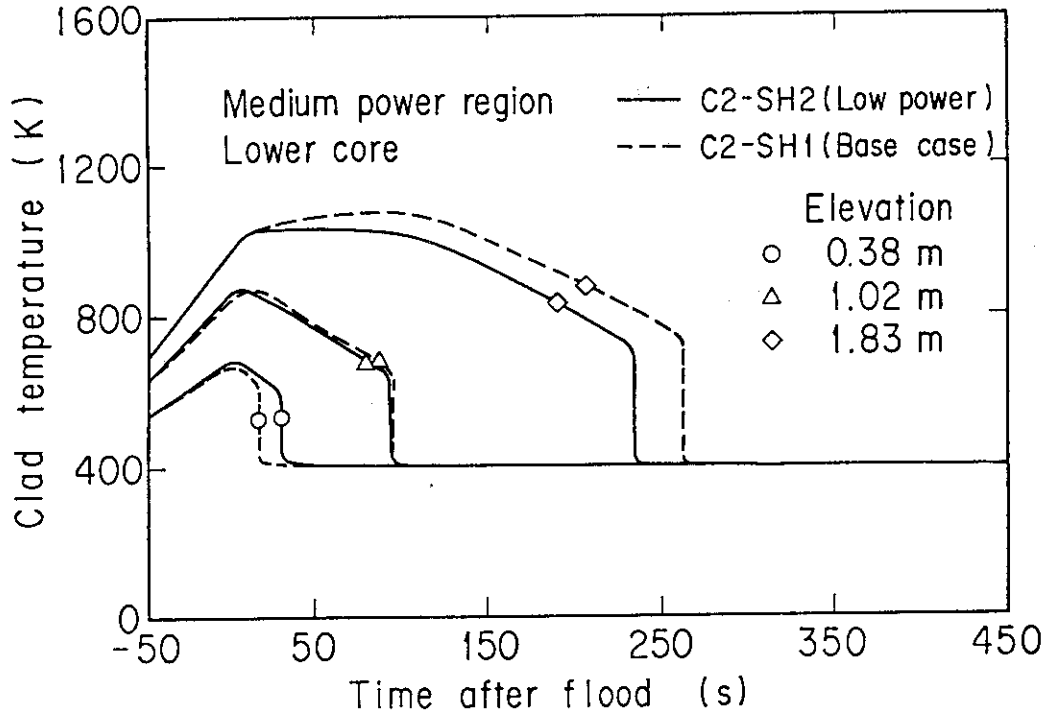

Fig. 4.11 Comparison of clad temperature in lower core

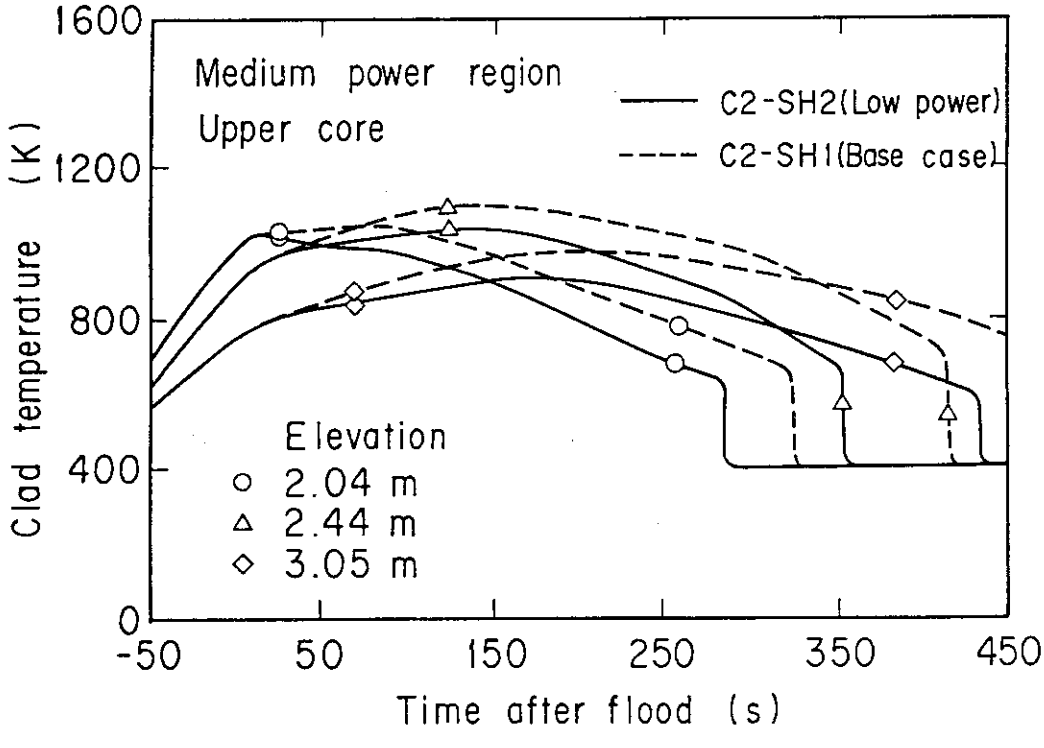

Fig. 4.12 Comparison of clad temperature in upper core

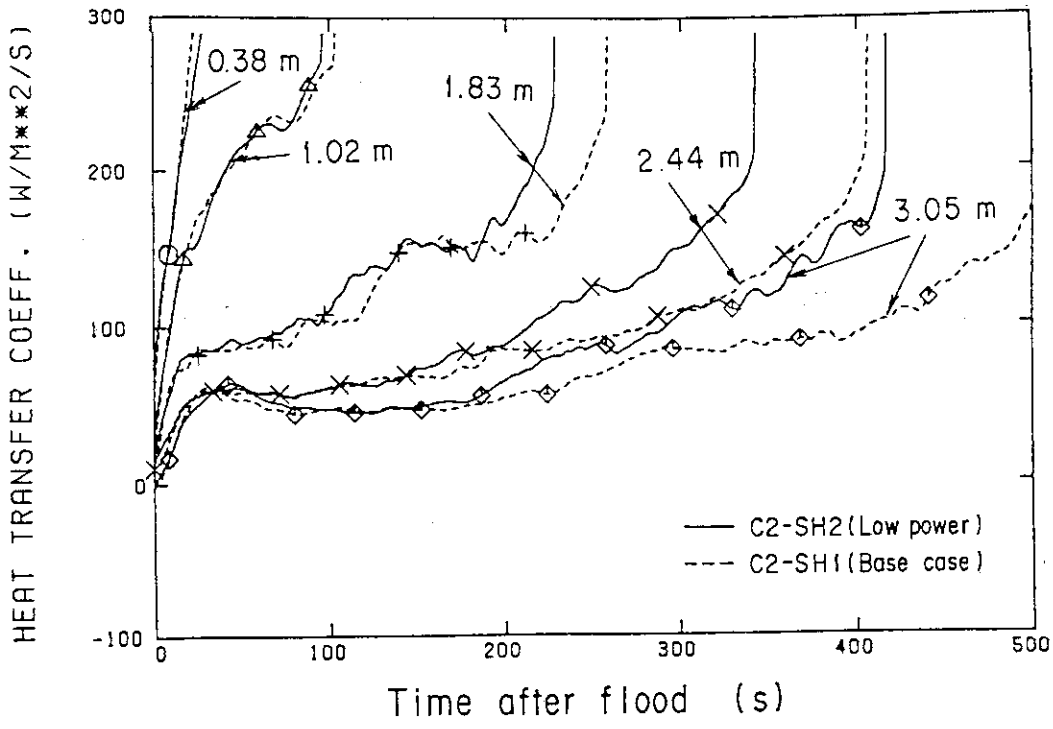

Fig. 4.13 Comaprison of heat transfer coefficient

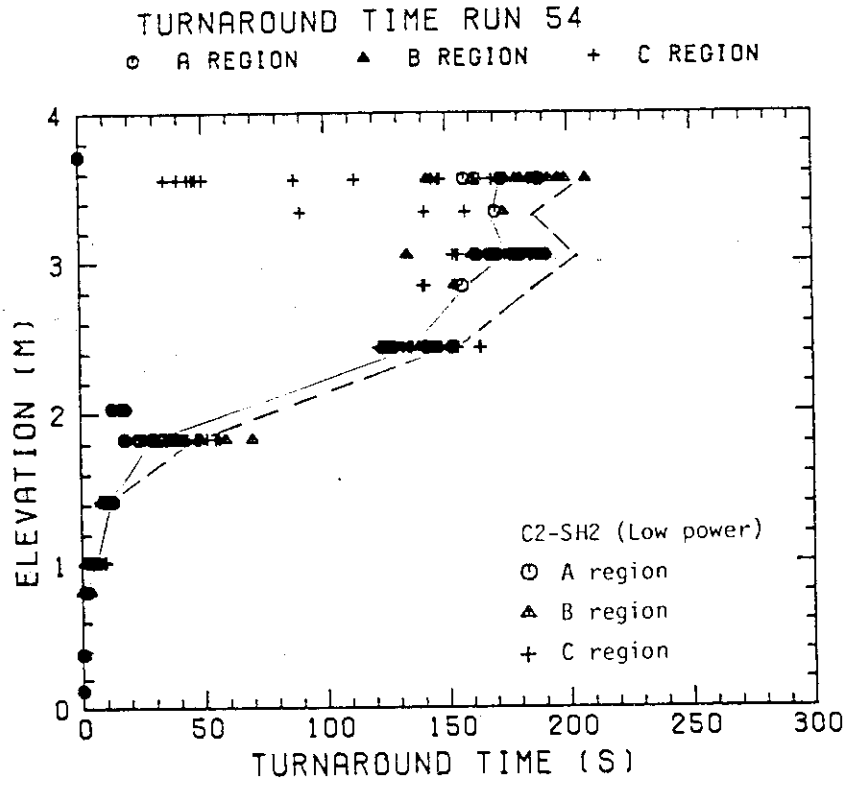

Fig. 4.14(1) Turnaround time along the elevation for the low power test for base case test

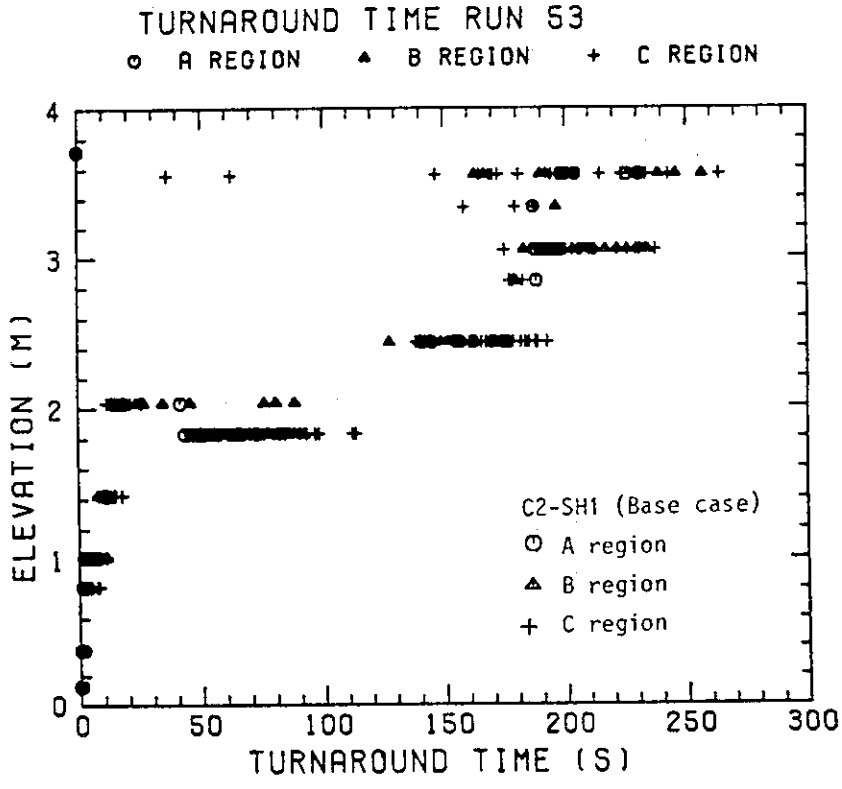

Fig. 4.14(2) Turnaround time along the elevation for base case test

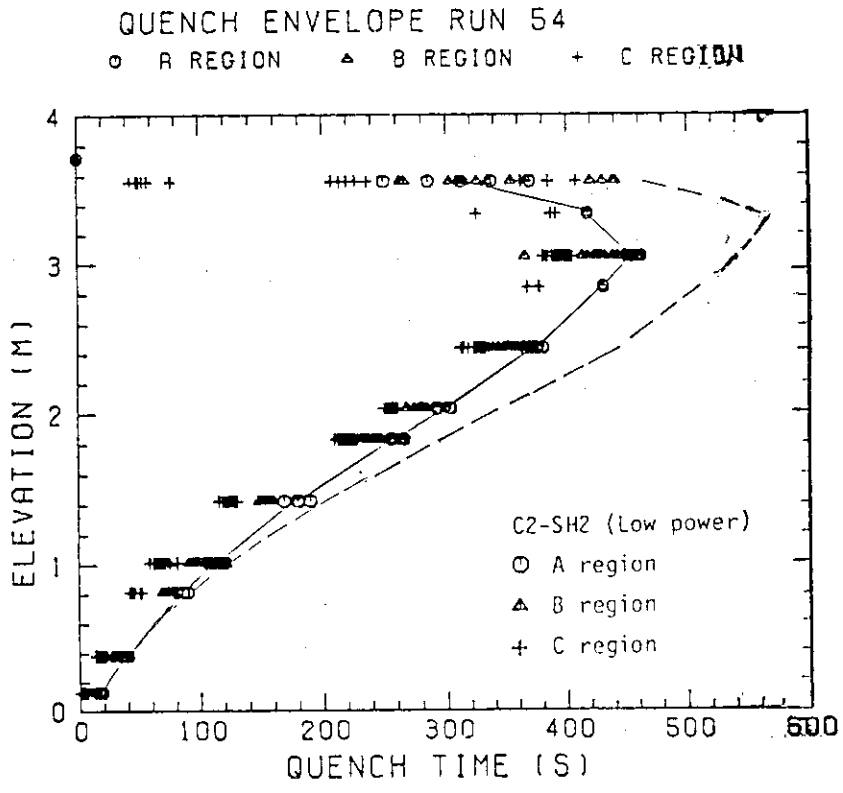

Fig. 4.15(1) Quench time along the elevation for the low power test for base case test

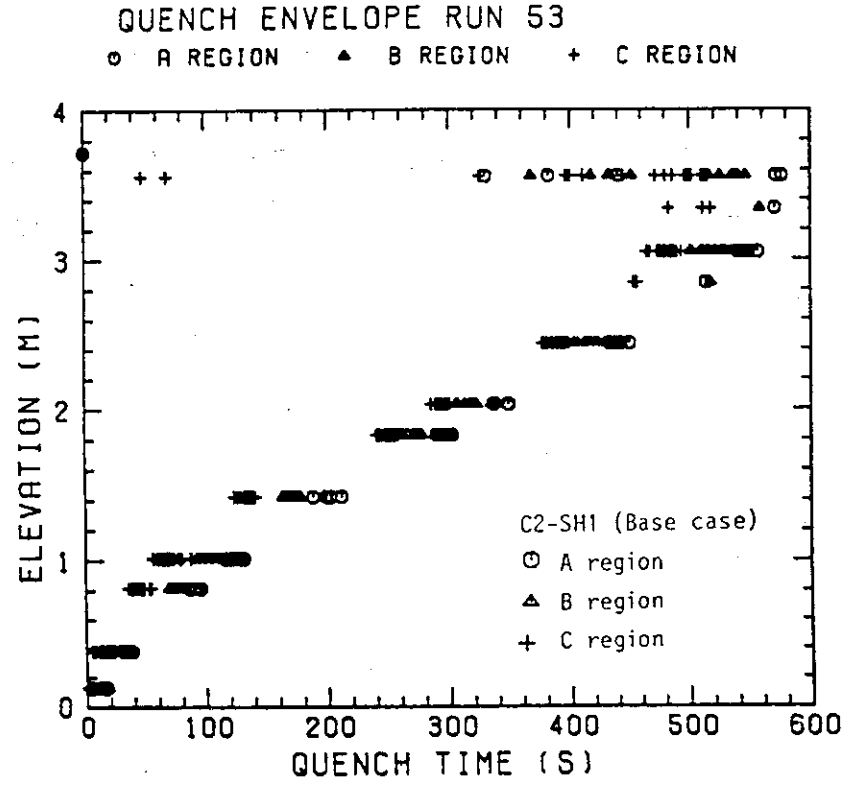

Fig. 4.15(2) Quench time along the elevation for base case test

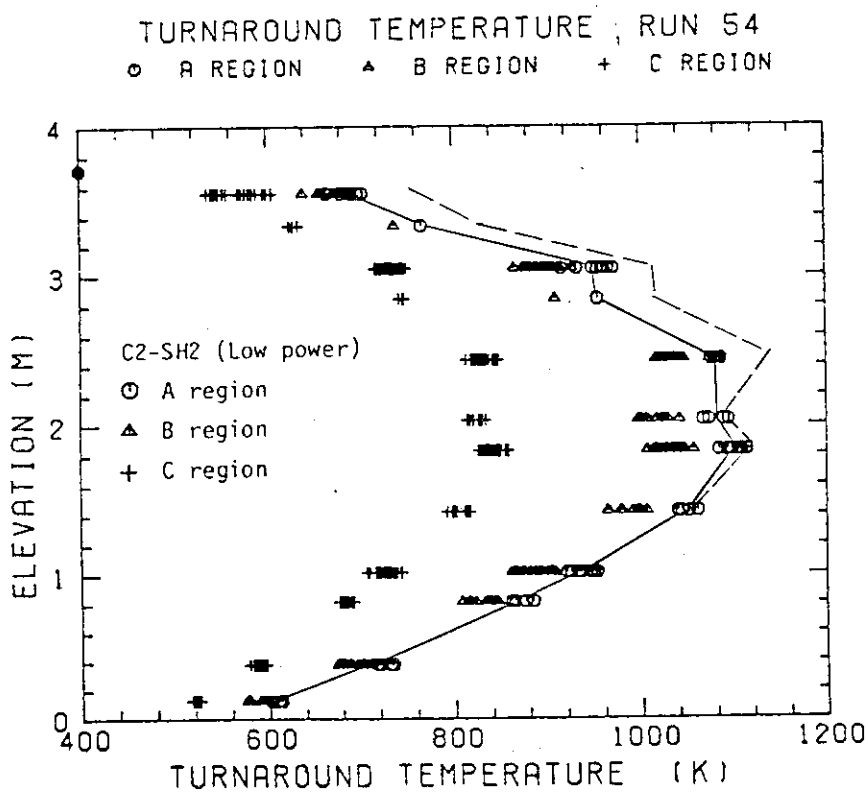

Fig. 4.16(1) Turnaround temperature along the elevation for the low power test

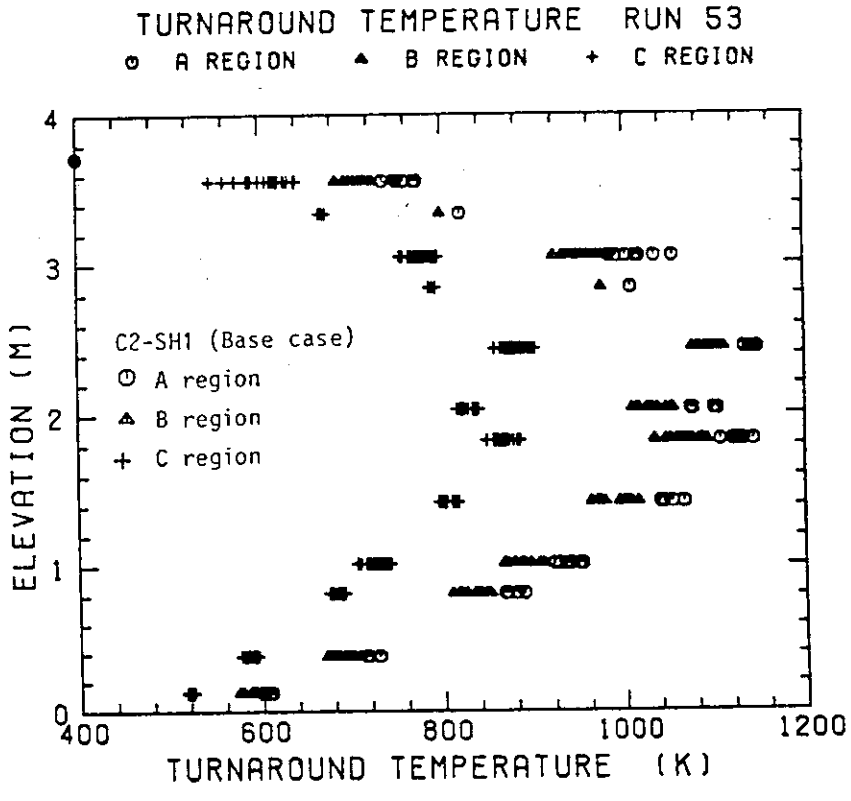

Fig. 4.16(2) Turnaround temperature along the eleration for base case test

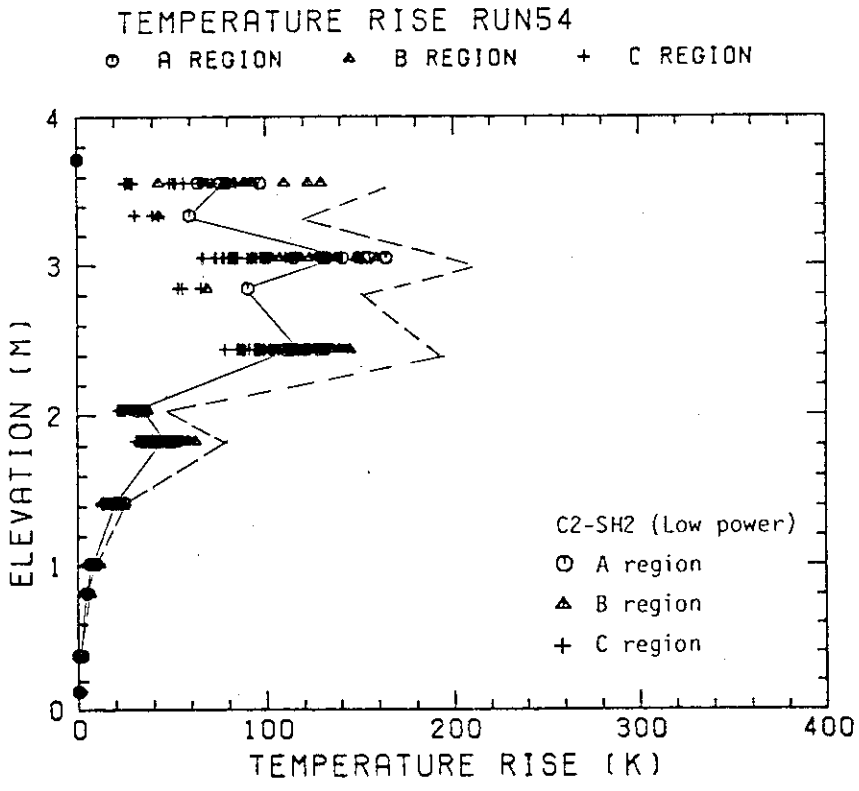

Fig. 4.17(1) Temperature rise along the elevation for the low power test

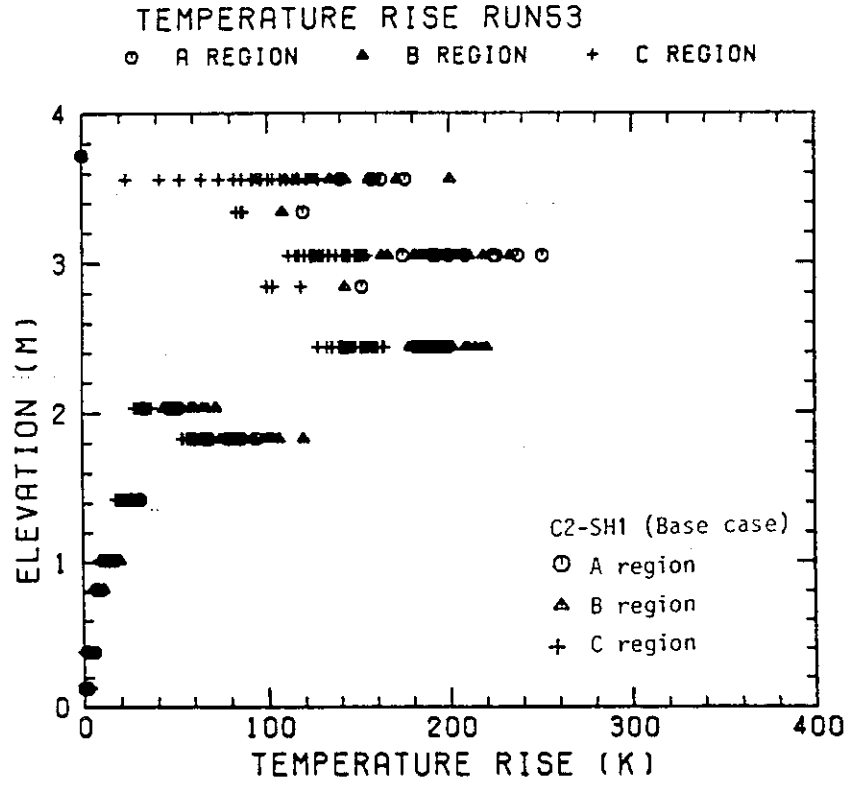

Fig. 4.17(2) Temperature rise along the elevation for base case test

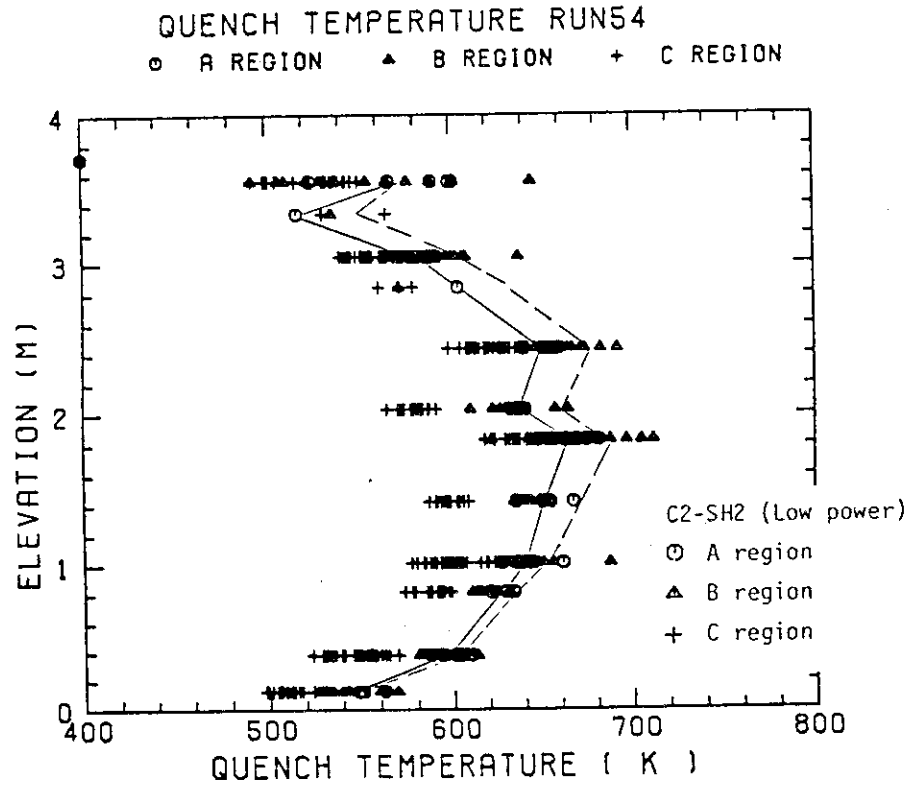

Fig. 4.18(1) Quench temperature along the elevation for the low power test

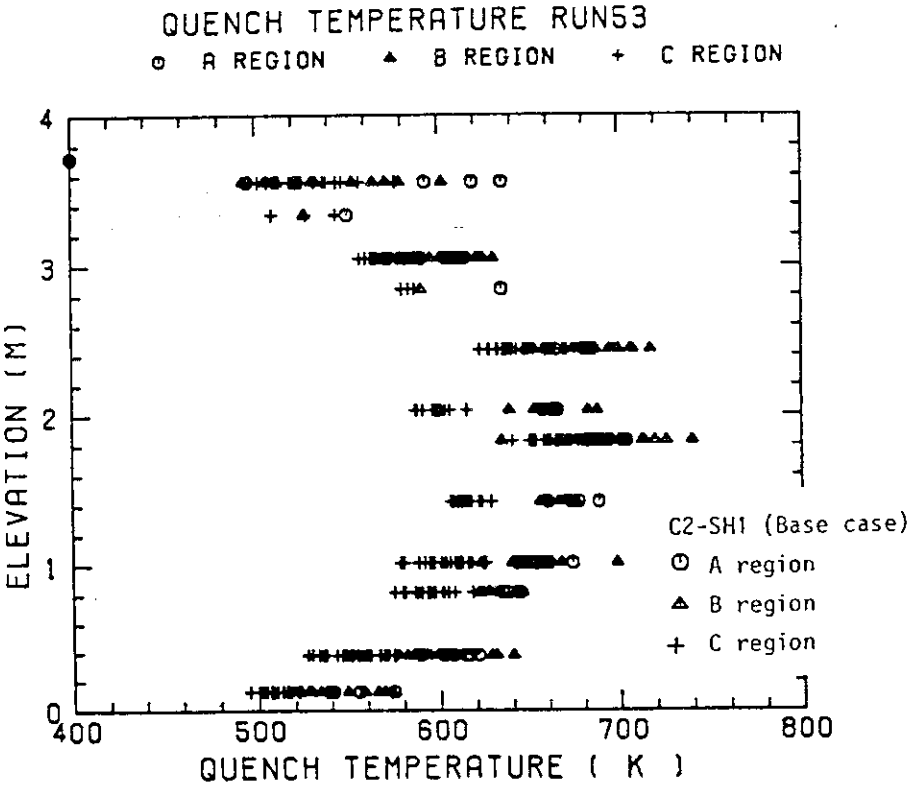

Fig. 4.18(2) Quench temperature along the elevation for base case test

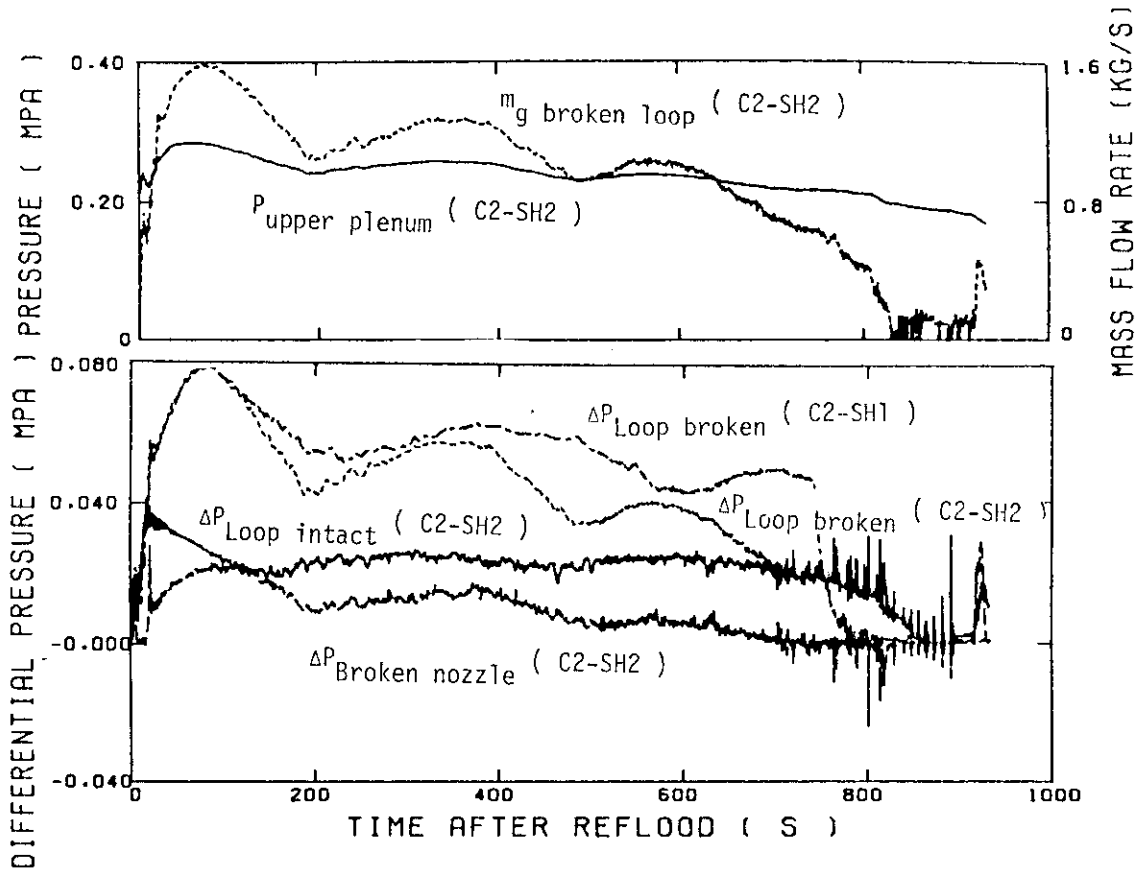

Fig. 4.19 Oscillation observed in loop mass flow rate

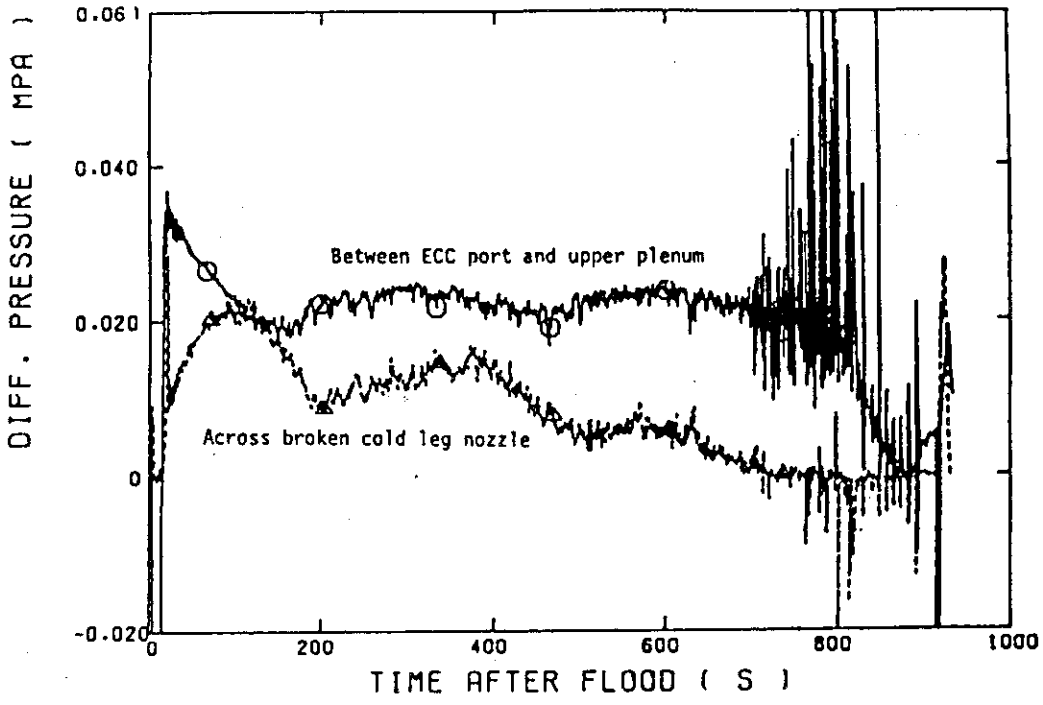

Fig. 4.20 Oscillation observed around cold leg ECC injection port

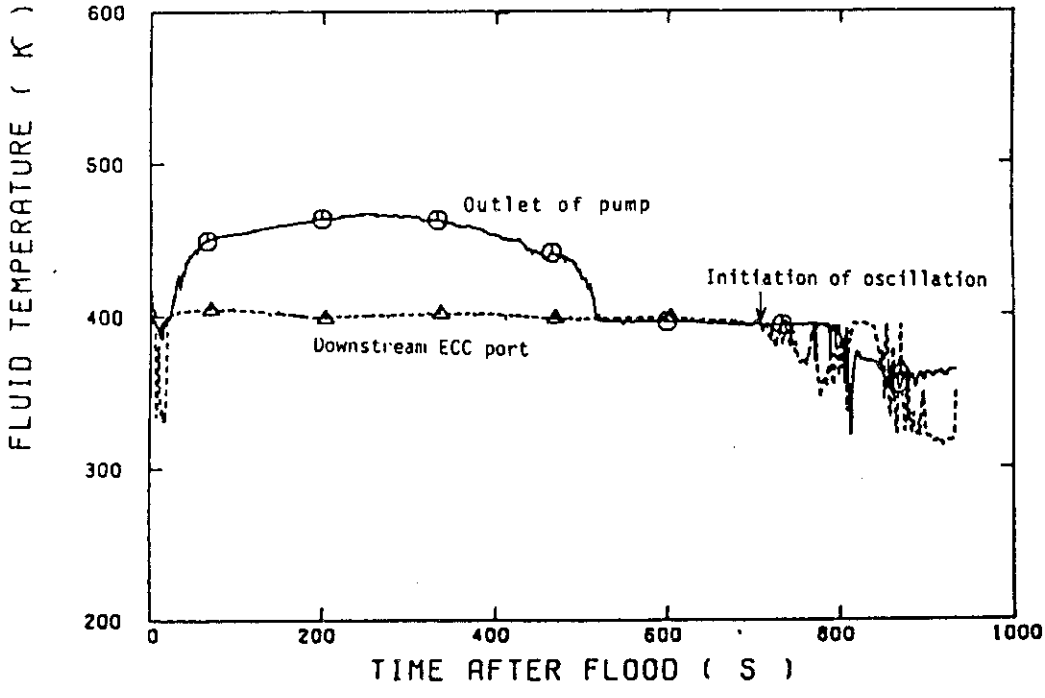

Fig. 4.21 Fluid temperature around cold leg ECC injection port

5. Conclusions

A low power test (the initial averaged linear power density is 1.18 kW/m) was performed with CCTF. The result of the test was compared with the result of the base case test (1.40 kW/m). The following conclusions were obtained.

(1) During the early period of the reflood (<100 s), the steam generation rate in the core was nearly identical in both tests in spite of the different power. During the later period (>200 s), the steam generation rate in the low power test was smaller. This is due to that the release of the initial stored energy mostly contributed to the steam generation rate rather than the power supplied to the core during the early period, and the power supplied to the core mostly contributed to the steam generation rate rather than the initial stored energy during the later period.

(2) During the early period of the reflood (nearly upto 200 s), the water accumulation in the core, the water accumulation in the upper plenum and the broken loop differential pressure were identical in both two tests. During the later period (>200 s), the higher water accumulation in the core, the higher water accumulation in the upper plenum and the lower differential pressure in the intact and broken loops were observed in the low power test. This is probably due to the same steam generation rate during the early period and the smaller steam generation rate in the core during the later period.

(3) The core flooding mass flow rate was identical in both tests in spite of the different power during both the early and later periods. The identical core flooding mass flow rate during the later period is the result of the compensation of the increased water accumulation in the core with the decreased mass flow rate through loops in the low power test.

(4) The heat transfer coefficient at the same time and location was identical in both tests during the early stage. It was higher in the low power test after 200 s. This is probably due to the higher water accumulation in the core and the faster quench front propagation with the lower power.

(5) The earlier turnaround and quench times and the lower turnaround temperature in the low power test were observed, as similar to the trend in forced feed test. This can be attributed to direct result of item (4).

(6) The same trends described in items (2) ~ (5) were observed in FLECHT-SET data. The insensitiveness of the core supplied power to the core flooding mass flow rate was observed in the range of 1.18 kW/m ~ 2.1 kW/m of the initial averaged linear power density.

(7) The significantly large oscillation of the differential pressure was observed around the ECC ports in cold legs when the differential pressure through broken cold leg was zero. This suggests that the complete steam condensation at the ECC port causes the differential pressure oscillation. This situation occurred at 1.7 MW of the power in the low power test. This oscillation may be important in term of long term core cooling, although it has not been taken note on the previous studies.

Acknowledgements

The authors are much indebted to Dr. M. Nozawa, Deputy Director General of Tokai Establishment, Dr. M. Katsurage, Deputy Director General of Tokai Estalishment, Dr. M. Hirata, Director of Nuclear Safety Research Center, and Dr. K. Hirano, Deputy Director of Department of Nuclear Safety Research, respectively, for their guidance and encouragement for this study. We would like to express our appreciation to the members of our analysis group, especially Messrs. H. Adachi, M. Sobajima, T. Iwamura, A. Ohnuki and Y. Abe for valuable discussions. We also would like to express our thanks to the 2D/3D project members of the USA and FRG for valuable discussions.

References

(1) Hirano, K. and Murao, Y., "Large scale reflood test", J. At. Energy Soc. Japan, (in Japanese), 22[10], p681 (1980)

(2) For instance: Murao, Y. et al., "Findings in CCTF Core-I Test", NUREG/CP-0041, Vol. 1, 275 (1983).

(3) Sudoh, T., et al., "Quick Look Report on CCTF Core-II Reflood Test C2-SH1 (Run 53)", Private communication.

(4) Sugimoto, J., et al., "Evaluation Report on CCTF Core-I Reflood Test C1-5 (Run 14), C1-7 (Run 16) and C1-14 (Run 23) - Effects of Initial Clad Temperature -", JAERI-M 83-026, February (1983).

(5) Waring, J. P., et al., "PWR FLECHT-SET Phase B1 Evaluation Report", WCAP-8583, August (1975).

(6) Iguchi, T. and Murao, Y., "Water Accumulation Phenomena in Upper Plenum during Reflood Phase of PWR-LOCA by Using CCTF Data", J. Nucl. Sci. and Technol., 20[6], pp453 (1983)

Acknowledgements

The authors are much indebted to Dr. M. Nozawa, Deputy Director General of Tokai Establishment, Dr. M. Katsurage, Deputy Director General of Tokai Estalishment, Dr. M. Hirata, Director of Nuclear Safety Research Center, and Dr. K. Hirano, Deputy Director of Department of Nuclear Safety Research, respectively, for their guidance and encouragement for this study. We would like to express our appreciation to the members of our analysis group, especially Messrs. H. Adachi, M. Sobajima, T. Iwamura, A. Ohnuki and Y. Abe for valuable discussions. We also would like to express our thanks to the 2D/3D project members of the USA and FRG for valuable discussions.

References

(1) Hirano, K. and Murao, Y., "Large scale reflood test", J. At. Energy Soc. Japan, (in Japanese), 22[10], p681 (1980)

(2) For instance: Murao, Y. et al., "Findings in CCTF Core-I Test", NUREG/CP-0041, Vol. 1, 275 (1983).

(3) Sudoh, T., et al., "Quick Look Report on CCTF Core-II Reflood Test C2-SH1 (Run 53)", Private communication.

(4) Sugimoto, J., et al., "Evaluation Report on CCTF Core-I Reflood Test C1-5 (Run 14), C1-7 (Run 16) and C1-14 (Run 23) - Effects of Initial Clad Temperature -", JAERI-M 83-026, February (1983).

(5) Waring, J. P., et al., "PWR FLECHT-SET Phase B1 Evaluation Report", WCAP-8583, August (1975).

(6) Iguchi, T. and Murao, Y., "Water Accumulation Phenomena in Upper Plenum during Reflood Phase of PWR-LOCA by Using CCTF Data", J. Nucl. Sci. and Technol., 20[6], pp453 (1983)

Appendix A

Definitions of Tag IDs

Figure List

1. Definition of Tag. ID for clad surface temperatures and heat fransfer coefficients

Notation : TEnnYlm (temperature)

HTEmmYlm (heat transfer coefficient)

nn : Bundle number (see Fig. A-1)

m : Elevation number

	Elevation (m)	Axial power factor
3	0.38	0.651
5	1.015	1.147
7	1.83	1.40
9	2.44	1.256
A	3.05	0.854

2. Definition of power zone and boundle number

See Fig. A-1

3. Definition of Tag. ID for void fraction

See Fig. A-2

4. Definition of Tag. ID for average linear power of heater rod in each power unit zone

See Fig. A-3

5. Definition of Tag. ID for differential pressure through downcomer, upper plenum, core and lower plenum

See Fig. A-4

6. Definition of Tag. ID for differential pressure through intact and broken loop and broken cold leg nozzle

See Fig. A-5

7. Definition of Tag. ID for fluid temperature in inlet and outlet plenum and secondary side of steam generator

See Fig. A-6

8. Definition of Tag. ID for ECC water injection rate, ECC water temperature and vented steam flow rate

   See Fig. A-7

9. Definition of initial temperature, turnaround temperature quench temperature, temperature rise, turnaround time and quench time. (See Fig. A-8)

   T_i : Initial temperature (Clad surface temperature at reflood initiation)

   T_t : Turnaround temperature (Maximum clad surface temperature in each temperature history)

   ΔT_r : Temperature rise ($= T_t - T_i$)

   T_q : Quench temperature (Clad surface temperature at quenching)

10. Definition of quenching

    See Fig. A-8

Quench time t_t is determined as

$$t_t = i \times \Delta t - \text{(reflood initiation time)}$$

In above equation, i is determined by the following criteria.

(1) Clad surface temperature is high, compared with the saturation temperature.

$$T_i > T_{sat} + \Delta T_1$$

(2) Decreasing rate of clad surface temperature is large.

$$\frac{T_{i+1} - T_i}{\Delta t} < - C_{st}$$

(3) Clad surface temperature falls around the saturation temperature.

$$T_{i + k_1} \leq T_{sat} + \Delta T_1$$

(4) If the determined i is inadequate, the value i is manually re-determined.

Δt : Data sampling period (s)

T_i : Clad surface temperature (K)

T_{sat} : Saturation temperature at the pressure in upper plenum (K)

ΔT_1 : Temperature discrepancy (K)
Default value = 50.0

C_{st} : Decreasing rate of clad surface temperature (K/S)
Default value = 25.0

k_1 : Number of referred data (-)
Default value = 6

11. Definition of Tag. ID for core inlet mass flow rate, time-integral core inlet mass flow rate and carry-over rate fraction

(1) Core inlet mass flow rate : $\dot{m}_F$
Notation : MLCRI□ (□ = N, 1 or 11)

(2) Time-intefral core inlet mass flow rate : $\int \dot{m}_F dt$
Notation : IMLCRI□ (□ = N, 1 or 11)

(3) Carry-over rate fraction : $(\dot{m}_F - \dot{m}_{CR})/\dot{m}_F$
Natation : CRF□ (□ = N, 1 or 11)

where $\dot{m}_F$: Core inlet mass flow rate (See item 12)

$\dot{m}_{CR}$: Water accumulation rate in core

Suffix	$\dot{m}_F$ base on
N	Eq.(A.2)
1	Eq.(A.1) with K=15
11	Eq.(A.1) with K=20

12. Evaluation of core inlet mass flow rate

The reflood phenomena is a relatively slow transient and a steady state condition can be applied. In a steady state condition, based on the mass balance relations of the system, the core flooding mass flow rates $\dot{m}_F$s can be written as follows:

By using the data measured at the downstream of the core inlet, $\dot{m}_F$ is derived as,

$$\dot{m}_F = \dot{m}_C + \dot{m}_U + \dot{m}_B + \Sigma \dot{m}_I \quad , \qquad (A.1)$$

where $\dot{m}_C$ and $\dot{m}_U$ are the mass accumulation rates in the core and the upper plenum respectively. The $\dot{m}_B$ and $\dot{m}_I$ are the mass flow rates in the broken loop and the intact loop, respectively.

By using the data measured at the upstream of the core inlet, $\dot{m}_F$ is derived as,

$$\dot{m}_F = \Sigma \dot{m}_{DL} - \dot{m}_D - \dot{m}_O + \dot{m}_{ECC/LP} \quad , \tag{A.2}$$

where $\dot{m}_{DL}$ and $\dot{m}_O$ are the mass flow rates of the water flowing into and overflowing from the downcomer, $\dot{m}_{ECC/LP}$ and $\dot{m}_D$ are the mass flow rate of the ECC water injected into the lower plenum and the water accumulation rate in the dowmcomer respectively.

The $\dot{m}_I$s and $\dot{m}_B$ can be obtained from the pressure drops at the pump simulators with orifices by assuming the K-factor of the orifice is constant. The values of $\dot{m}_C$, $\dot{m}_D$ and $\dot{m}_U$ can be evaluated with the differential pressure ΔP_C, ΔP_D and ΔP_U, respectively, as follows:

$$\dot{m}_n = d(\Delta P_n S_n/g)/dt \quad (n : C, D, U) \quad , \tag{A.3}$$

where g is the gravitational acceleration and S_n is the cross sectional area. The value of $\dot{m}_O$ can be obtained from the liquid level X in the Containment tank 1 as,

$$\dot{m}_O = d(X\rho_\ell S_o)/dt \quad , \tag{A.4}$$

where ρ_ℓ is the liquid density and S_o is the cross sectional area of the containment tank 1.

The value of $\dot{m}_{DL}$, $\dot{m}_{DV}$ and h, which are liquid flow rate, steam flow rate and enthalpy of two phase mixture downstream each ECC port respectively, are obtained from the following mass and energy balance relations at each ECC port under the assumption of thermal equilibrium:

$$\dot{m}_{DV} + \dot{m}_{DL} = \dot{m}_{ECC} + \dot{m}_I \quad , \tag{A.5}$$

$$(\dot{m}_{DV} + \dot{m}_{DL})i = \dot{m}_{ECC}h_{ECC} + \dot{m}_I h_I \quad , \tag{A.6}$$

$$\begin{aligned} &\text{if} \quad h_g \geq h \geq h_\ell \ , \ (\dot{m}_{DV} + \dot{m}_{DL})h = \dot{m}_{DV}h_g + \dot{m}_{DL}h_\ell \\ &\text{if} \quad h \geq h_g \quad , \ \dot{m}_{DL} = 0 \quad , \\ &\text{if} \quad h \geq h_\ell \quad , \ \dot{m}_{DV} = 0 \end{aligned} \tag{A.7}$$

where h is enthalpy of fluid and h_ℓ and h_g are enthalpies of liquid and steam at the saturation temperature, respectively.

The fluid temperatures can be measured with thermocouples immersed in the fluid and the enthalpies h_I and h_{ECC} can be estimated.

Mass balance calculations were performed with Eqs. (A.1) and (A.2). The K-factor of the orifice in the pump simulator was evaluated in the following two ways.

The K-factor of 20 was obtained with the steam and water single phase calibration tests using the flow meter and spool piece data. The K-factor of 15 was obtained with the Pitot tube measurement in a typical reflood condition assuming the flat velocity profile in the pipings. In the differentiation, higher frequency components of the data tends to be amplified more. Therefore, in the differentiation of the differential pressure data, the smoothing procedure was used to suppress the high frequency components of the data.

In the Acc injection period, the calculated $\dot{m}_F$s with Eqs. (A.1) and (A.2) are significantly different from each other. This discrepancy may be caused by inaccuracy of the mass flow rate injected into the system and by the unaccounting of the storage of water in the cold leg pipe. The former might be introduced from the slow time response of the flow meter (time constant 1 second) and the change of the gas volume in the injection line. In this period, especially before the steam generation from the core becomes noticeable, the mass flow rate, $\dot{m}_F$, calculated with Eq. (A.1) is probably reasonable, since the calculation uses the increasing rates of the masses in the core and the upper plenum and their accuracy is good enough for our estimation.

In the LPCI injection period, the calculated $\dot{m}_F$s are slightly different from each other. Judging from the time-integral values of both $\dot{m}_F$s, their average values are nearly proportional. The discrepancy was inferred to be caused by the disregard of the bypass of steam and liquid from the upper plenum without going through the hot legs in the calculation with Eq. (A.1). And additionally the discrepancy was caused by the disregard of the steam generation in the downcomer due to the hot wall of the pressure vessel in the calculation with Eq. (A.2). It was estimated that the disregard of the downcomer steam generation causes the error of 0.25 kg/s on predicted $\dot{m}_F$. The estimation was made by comparing the results of the tests with hot and cold downcomer conditions.

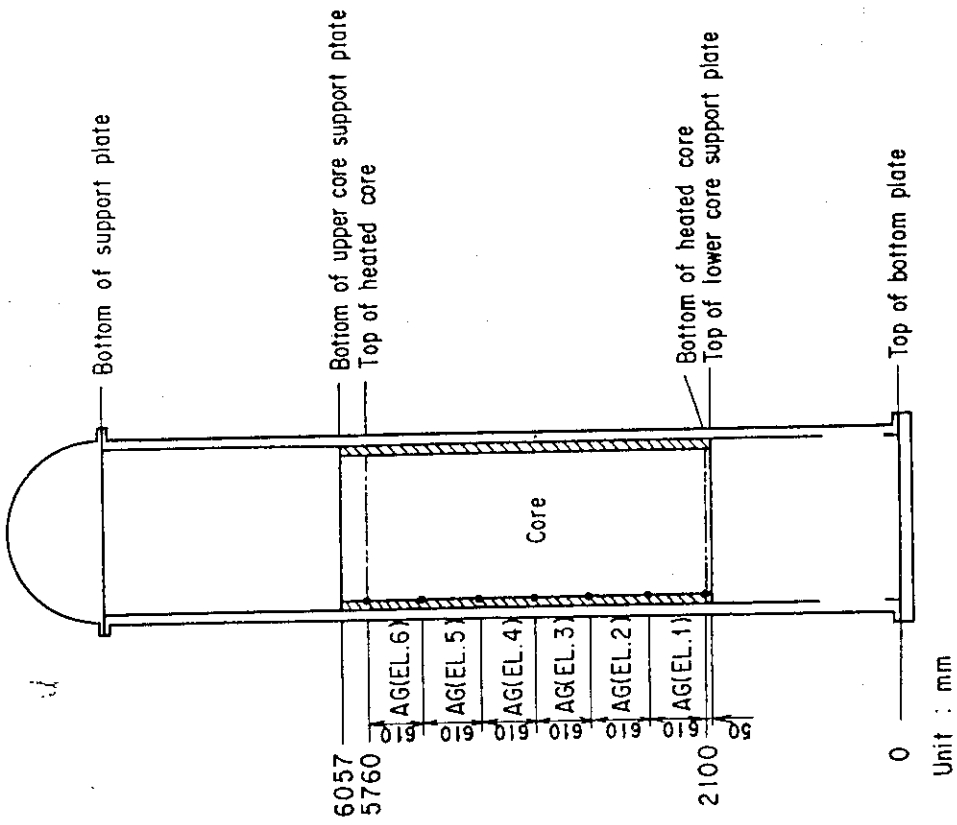

Fig. A-2 Definition of Tag.ID for void fraction (AG(EL.1) ~ AG(EL.6))

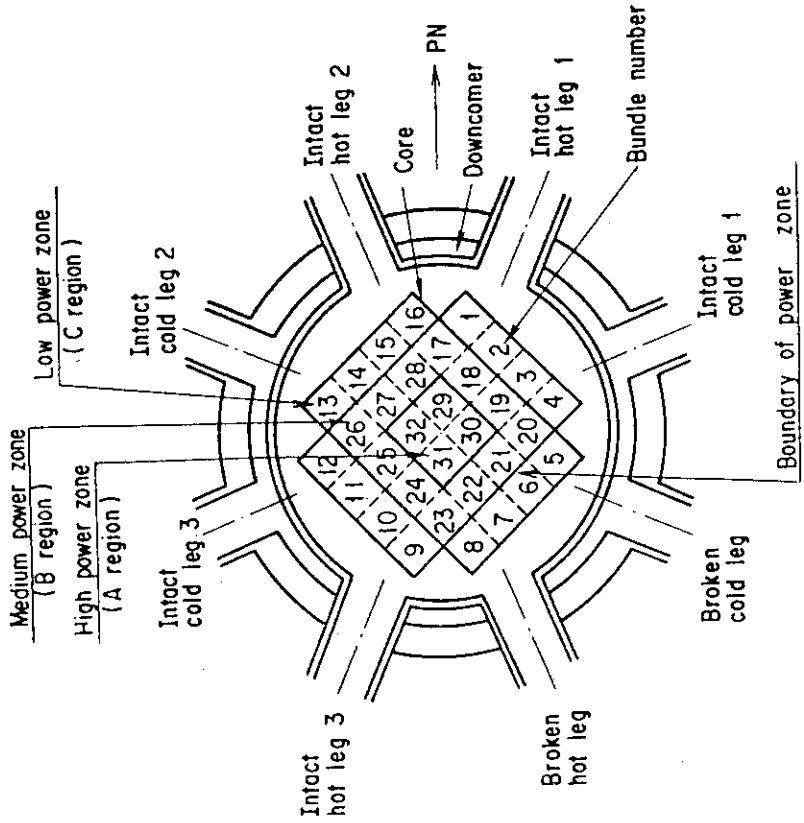

Fig. A-1 Definition of power zones and bundle numbers

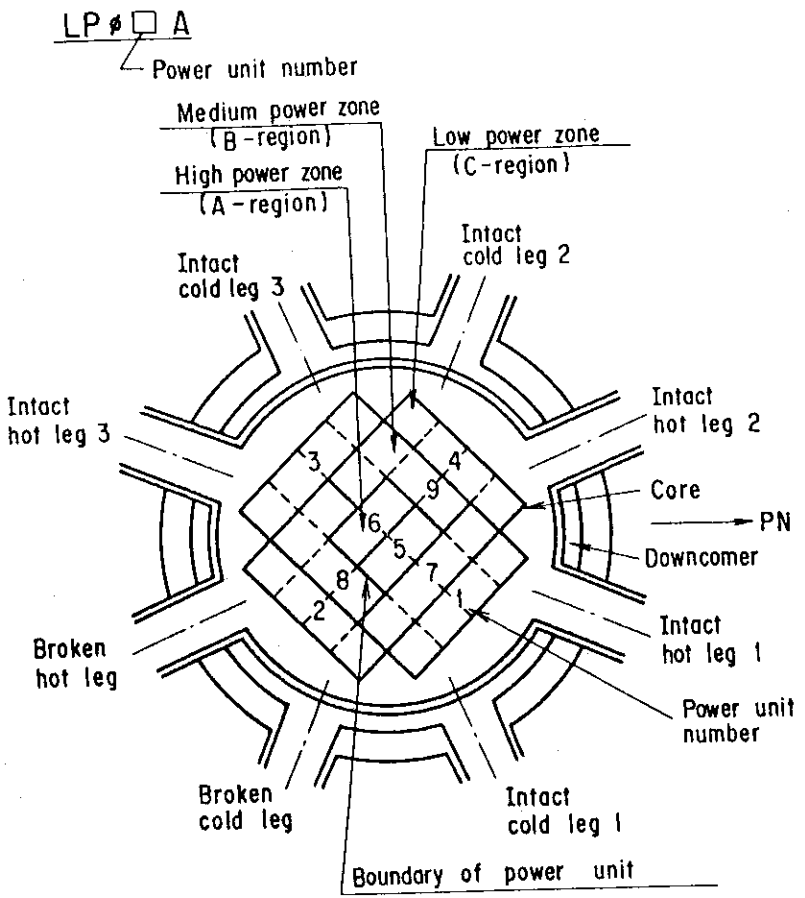

Fig. A-3 Definition of Tag. ID for average linear power of heater rod in each power unit zone
(LP01A ~ LP09A)

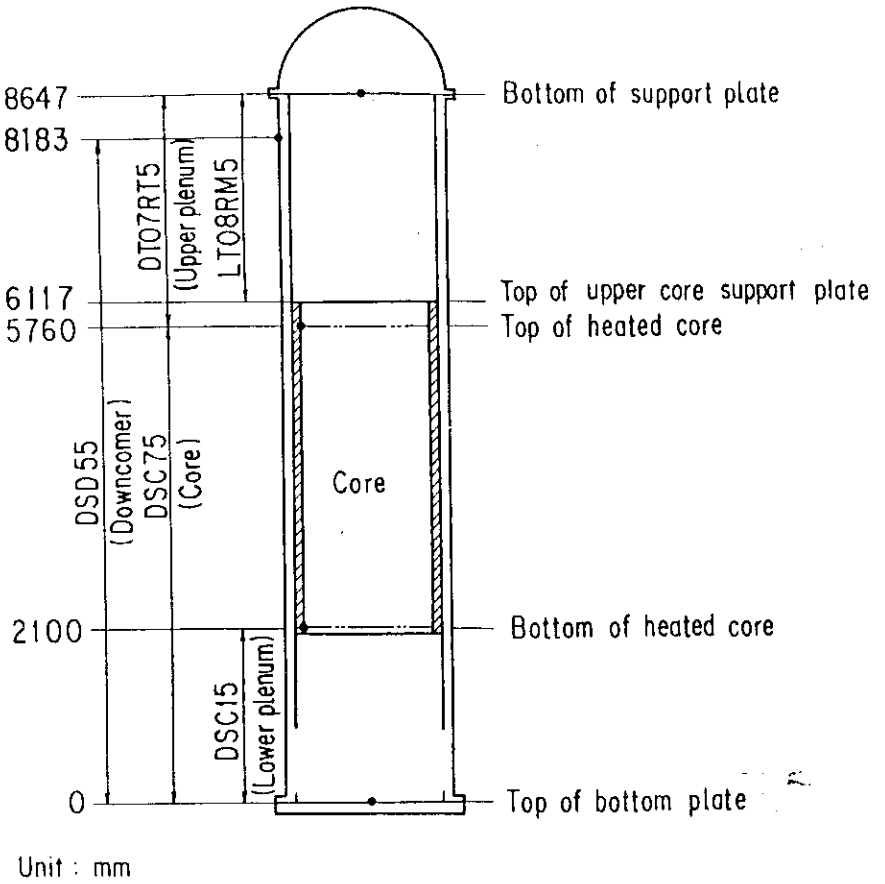

Fig. A-4 Definition of Tag. ID for differential pressure through downcomer, upper plenum, core, and lower plenum
(DSD55, DTO7RT5, LTO8RM5, DSC75, DSC15)

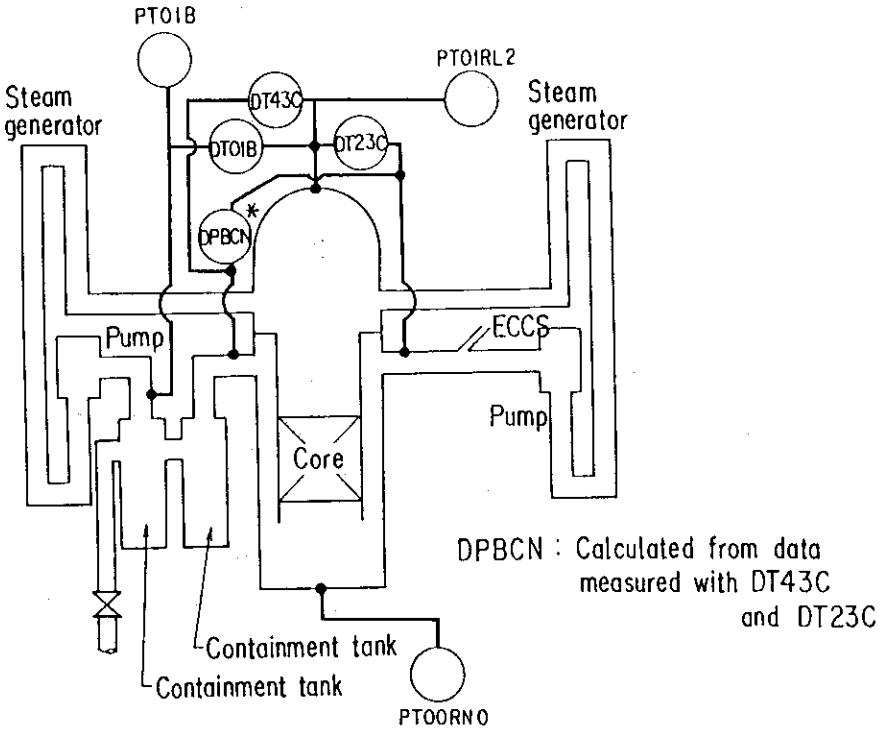

Fig. A-5 Definition of Tag. ID for pressures in upper and lower plena and containment tank 2 (PT01RL2, PT00RN0, PT01B) and for differential pressure through intact and broken loop and broken cold leg nozzle (DT23C, DT01B, DPBCN)

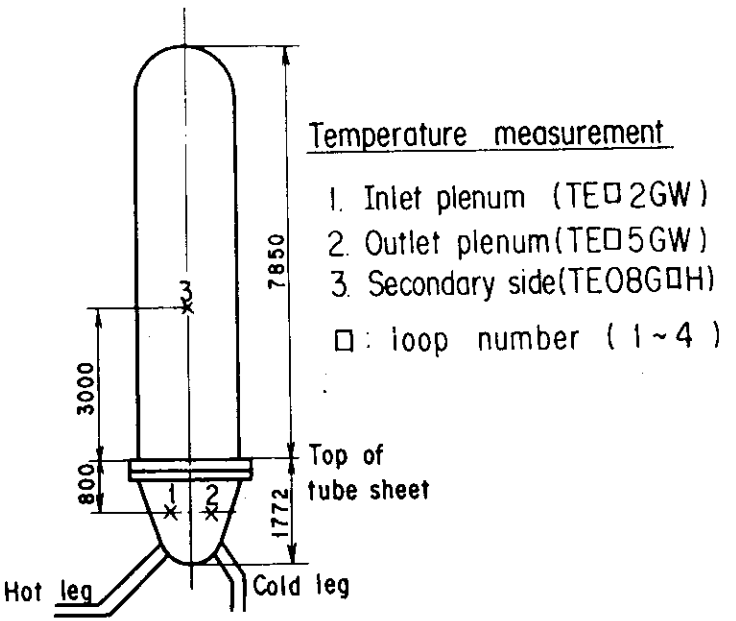

Fig. A-6 Definition of Tag. ID for fluid temperature in inlet and outlet plenum and secondary of steam generator (TE□2GW, TE□5GW, TE08G□H)

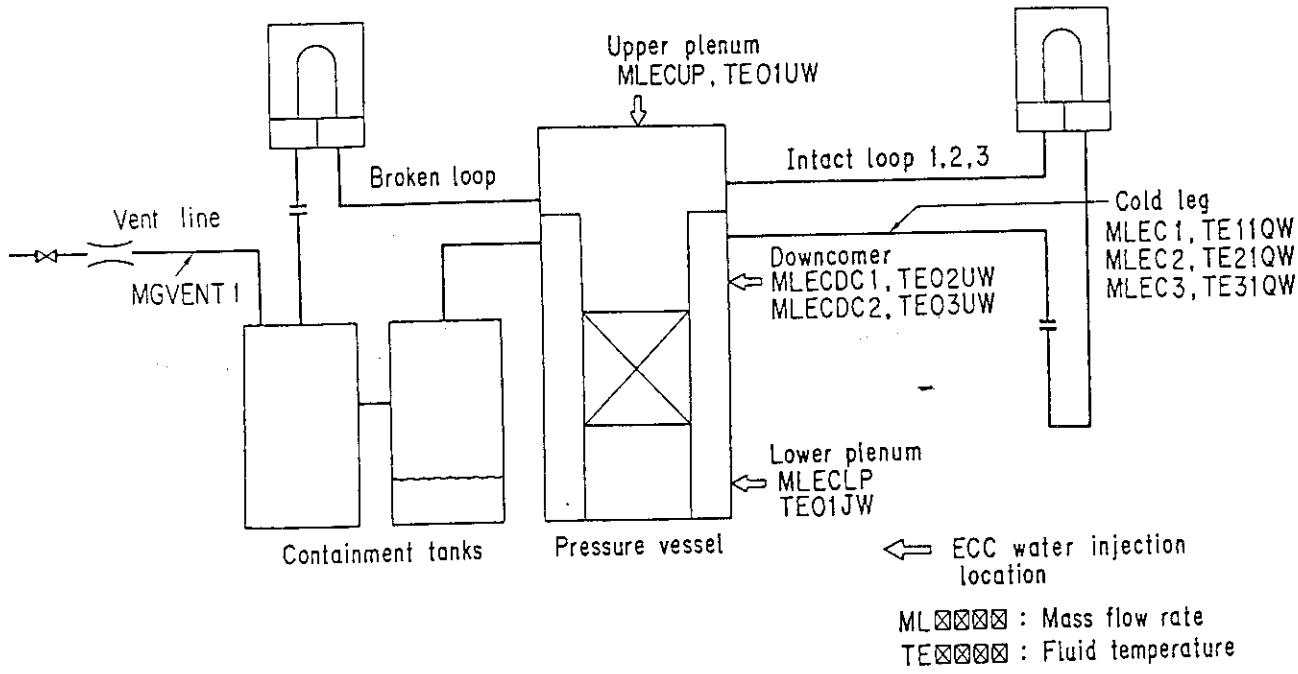

Fig. A-7 Definition of Tag. ID for ECC water injection rate, ECC water temperature and vented steam flow rate

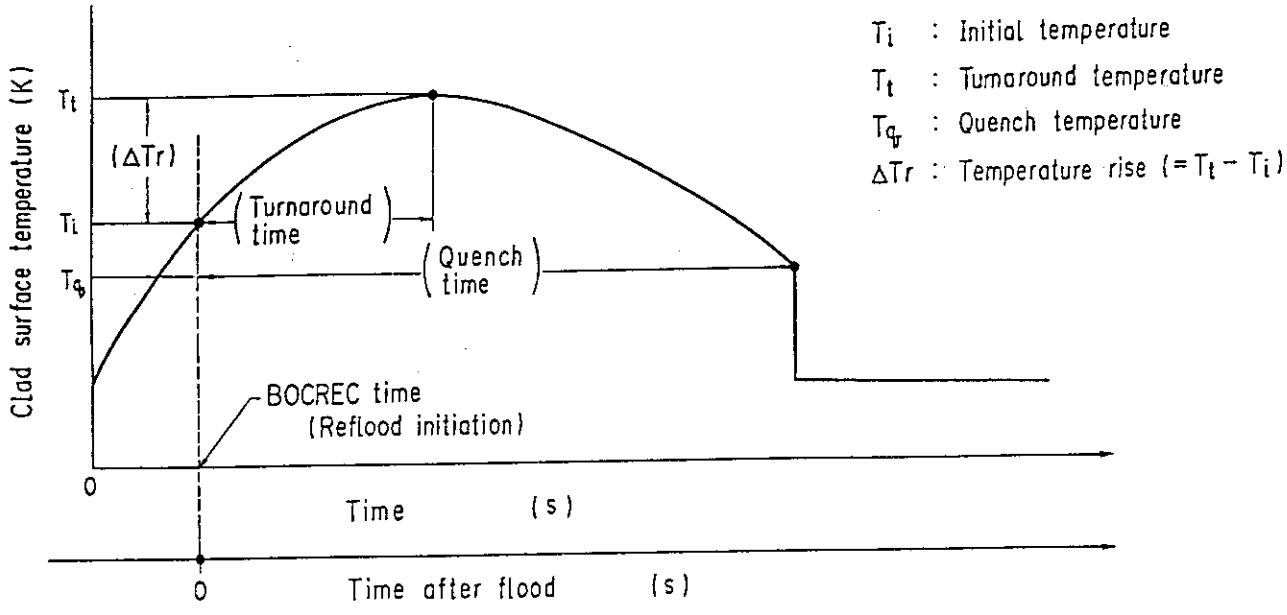

Fig. A-8 Definition of initial temperature, turnaround temperature, quench temperature, temperature rise, turnaround time and quench time

Appendix B

Selected data of CCTF Test C2-SH2 (Run 54)

Figure List

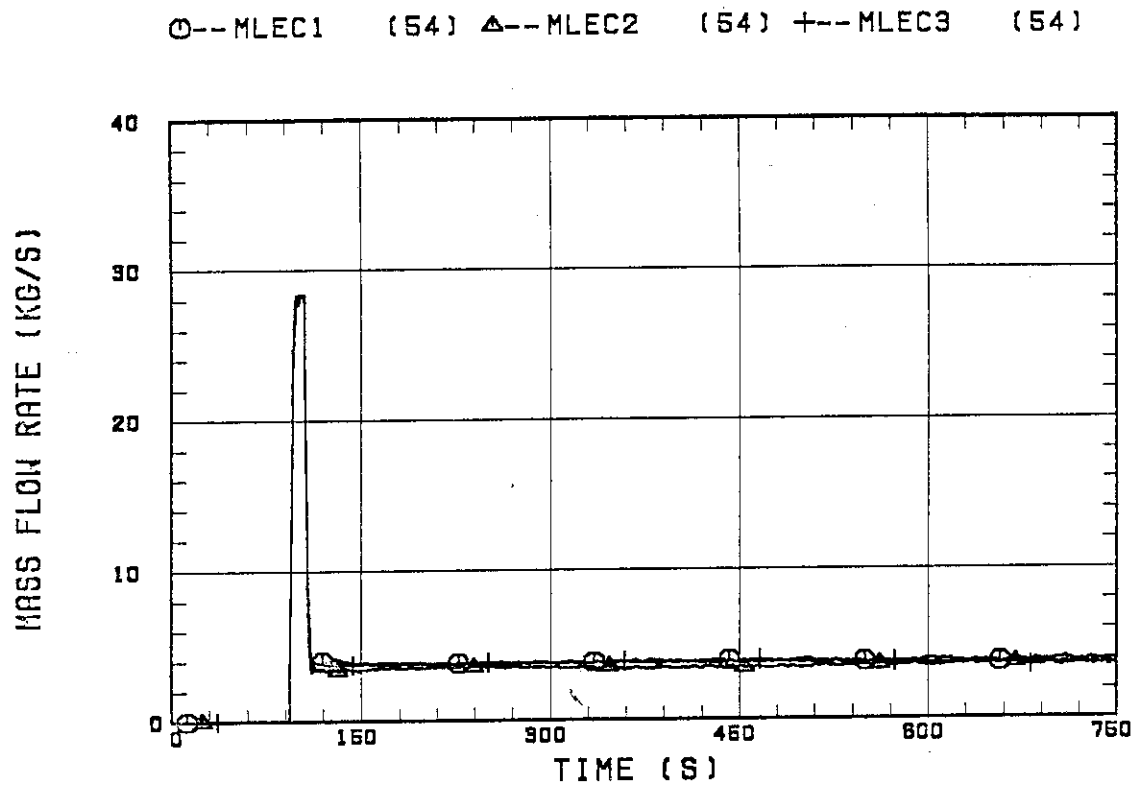

Fig. B.1 ECC water injection rates into the primary system.

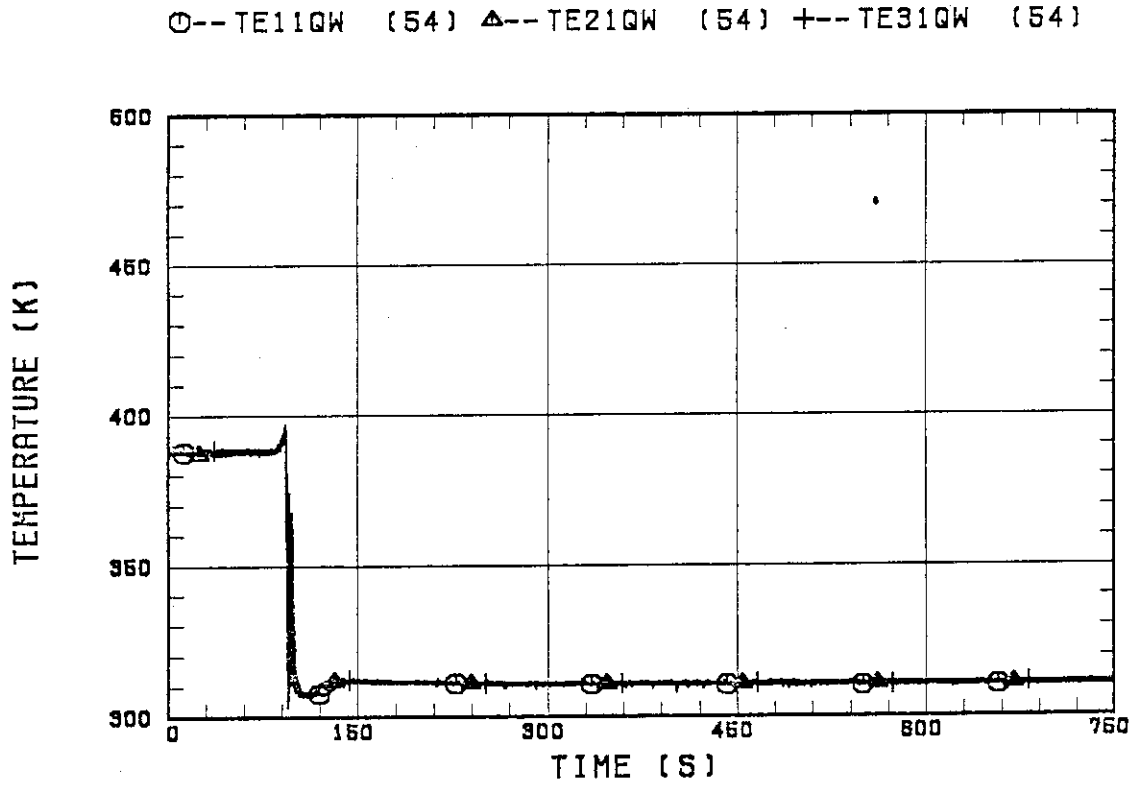

Fig. B.2 ECC water temperature.

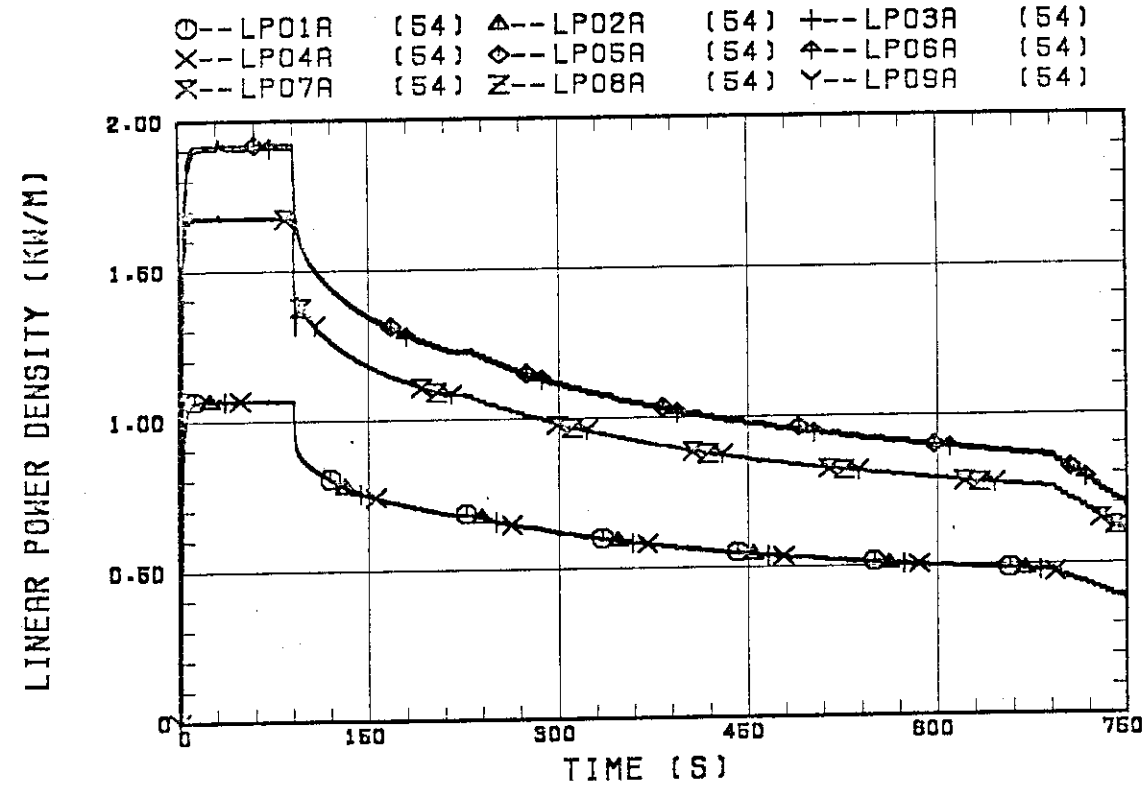

Fig. B.3 Average linear power of heater rod in each power unit zone.

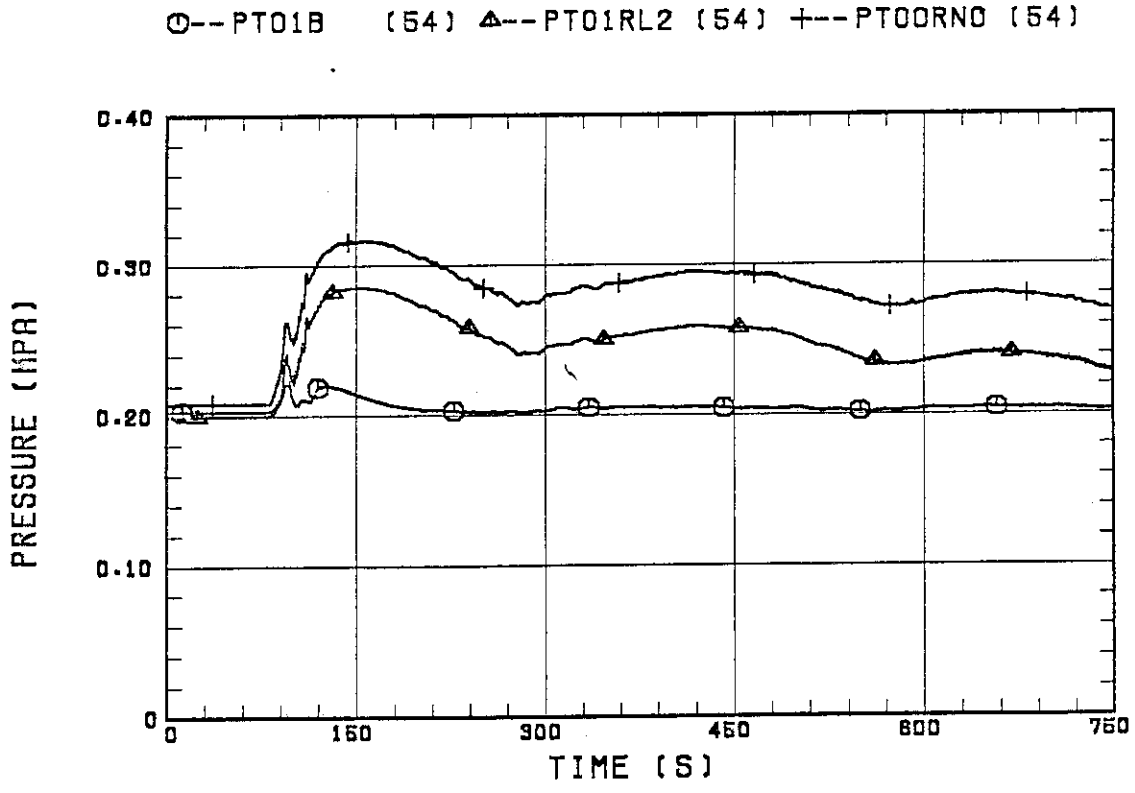

Fig. B.4 Pressure history in containment tank 2, upper plenum and lower plenum.

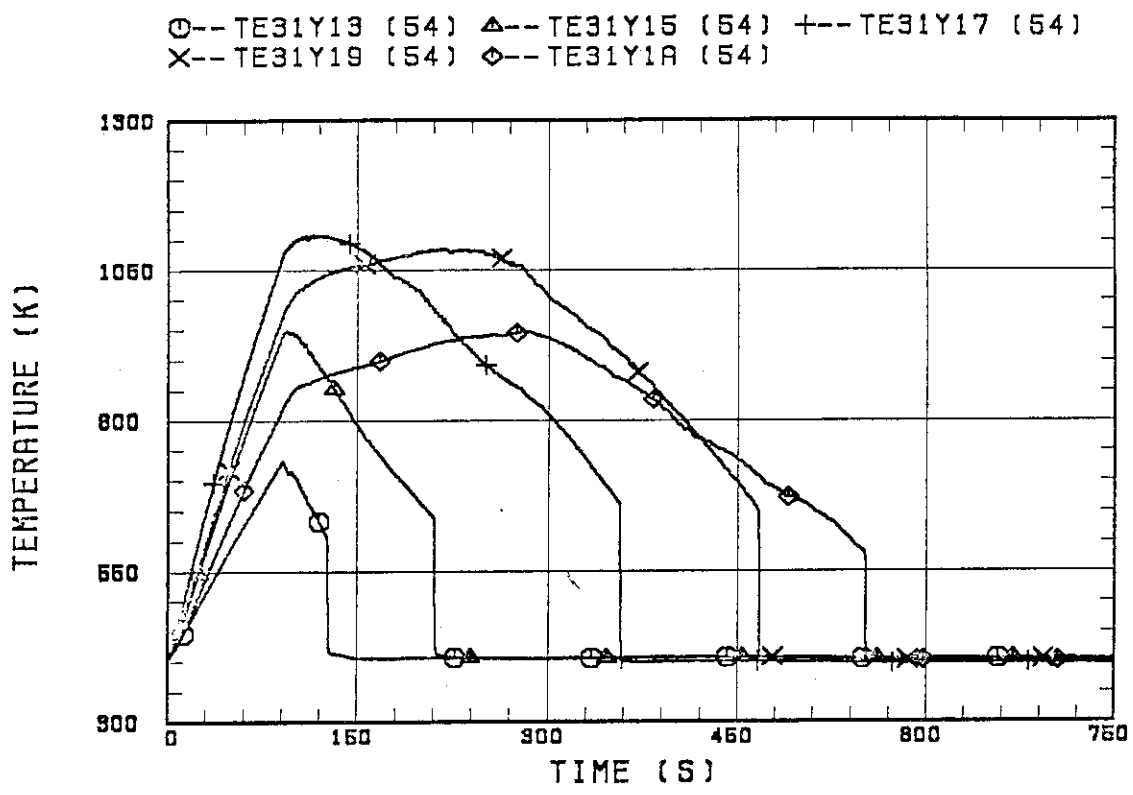

Fig. B.5 Clad surface temperature at various elevations along a heater rod in high power region (A region).

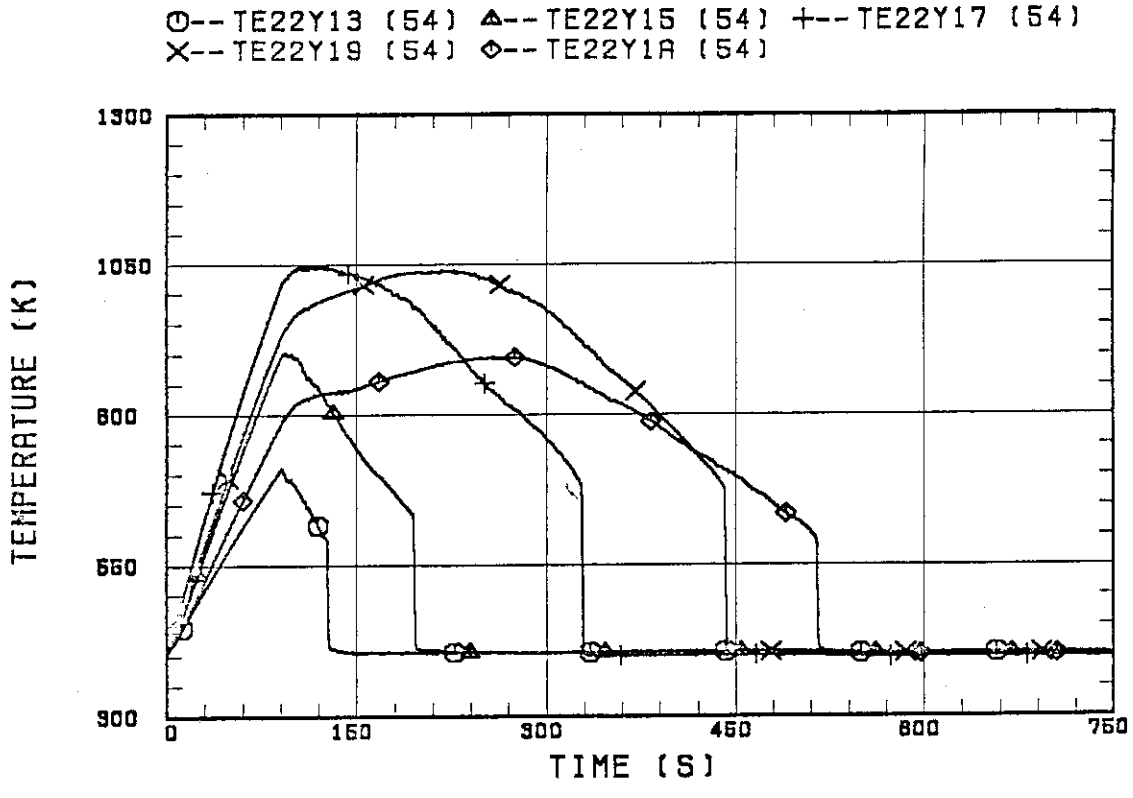

Fig. B.6 Clad surface temperature at various elevations along a heater rod in medium power region (B region).

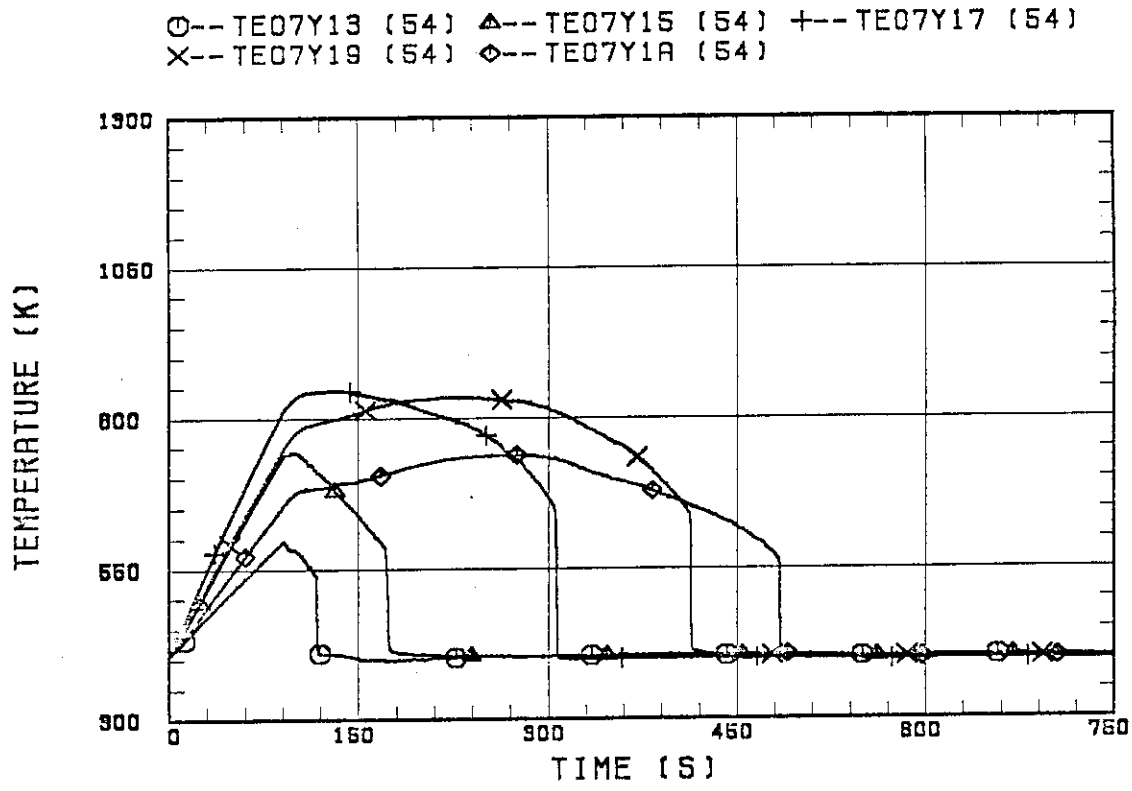

Fig. B.7 Clad surface temperature at various elevations along a heater rod in low power region (C region).

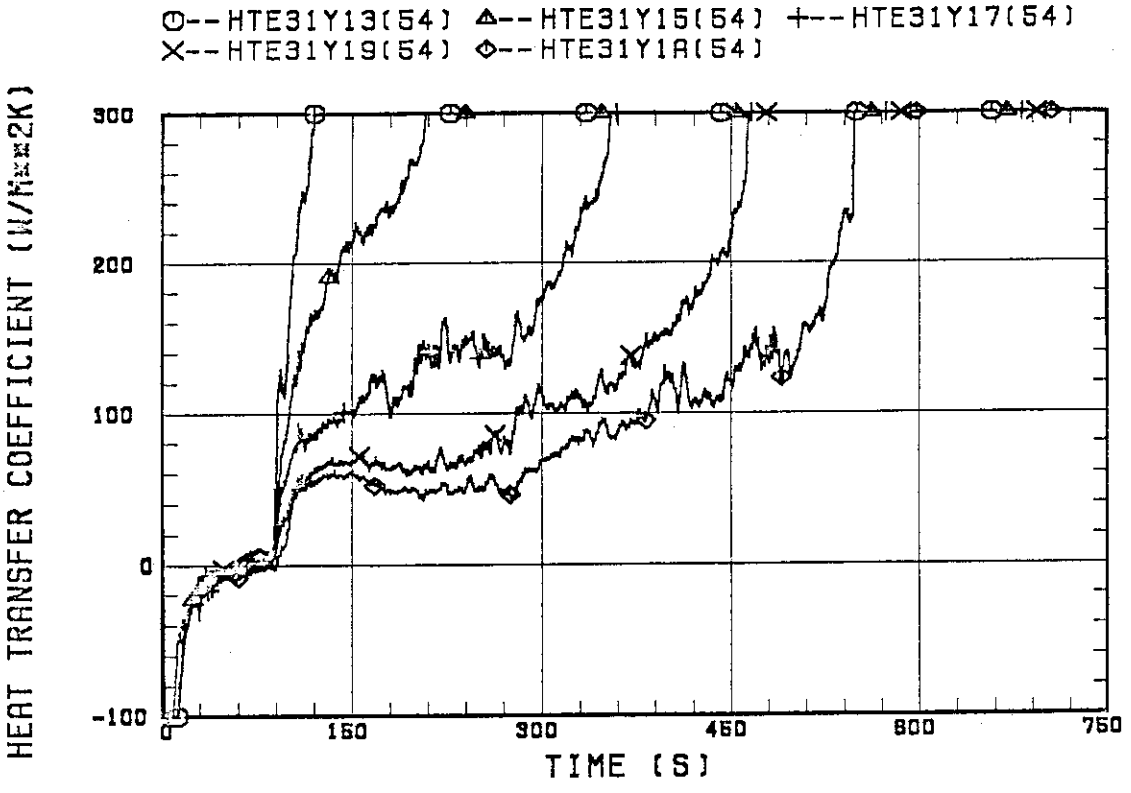

Fig. B.8 Heat transfer coefficient at various elevations along a heater rod in high power region (A region).

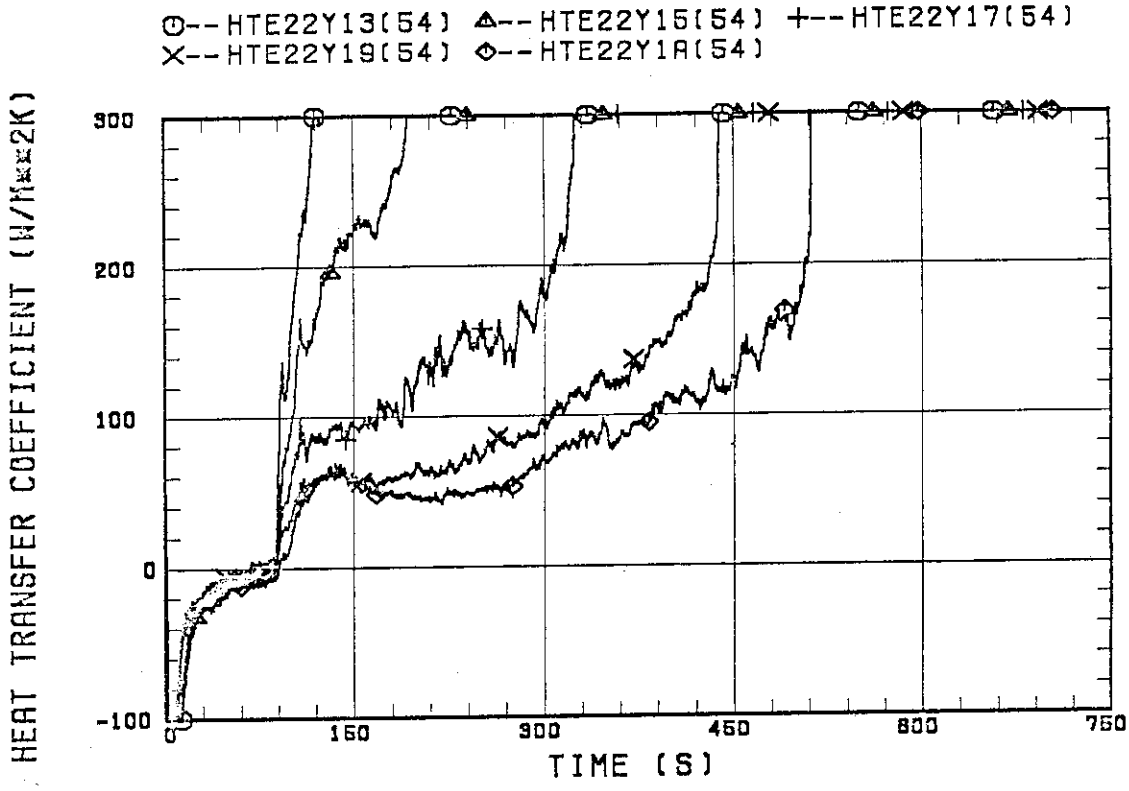

Fig. B.9 Heat transfer coefficient at various elevations along a heater rod in medium power region (B region).

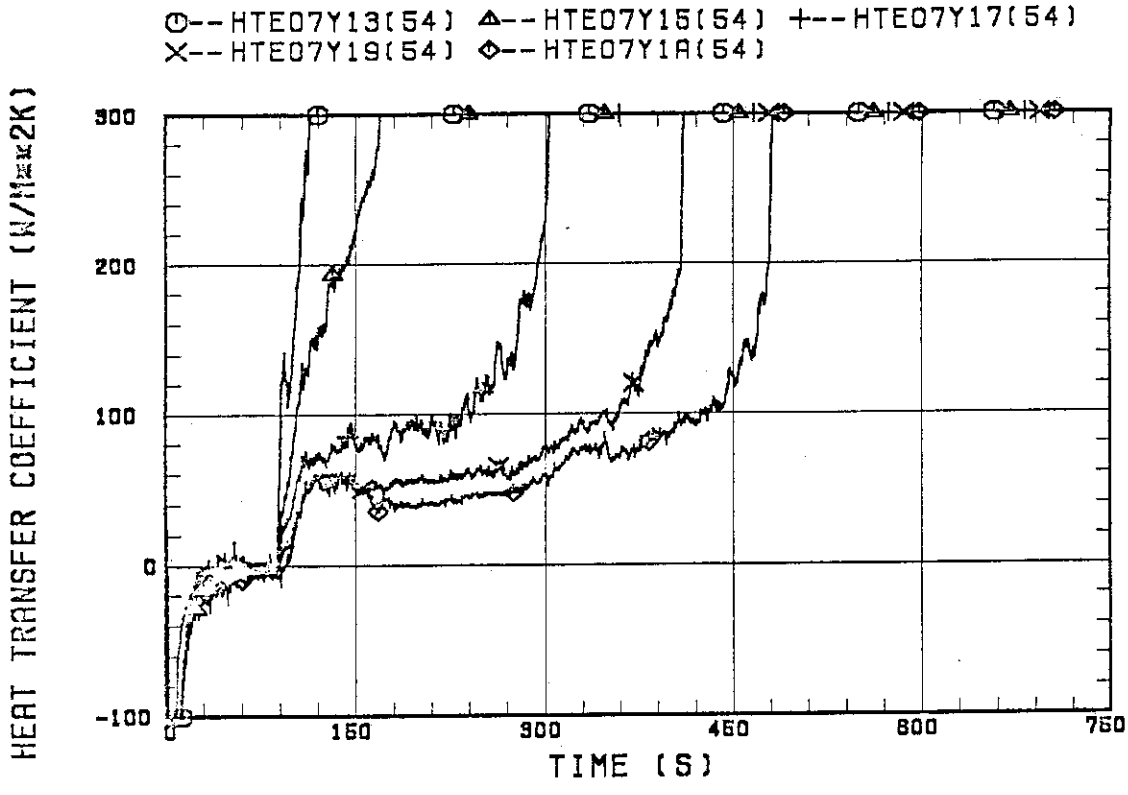

Fig. B.10 Heat transfer coefficient at various elevations along a heater rod in low power region (C region).

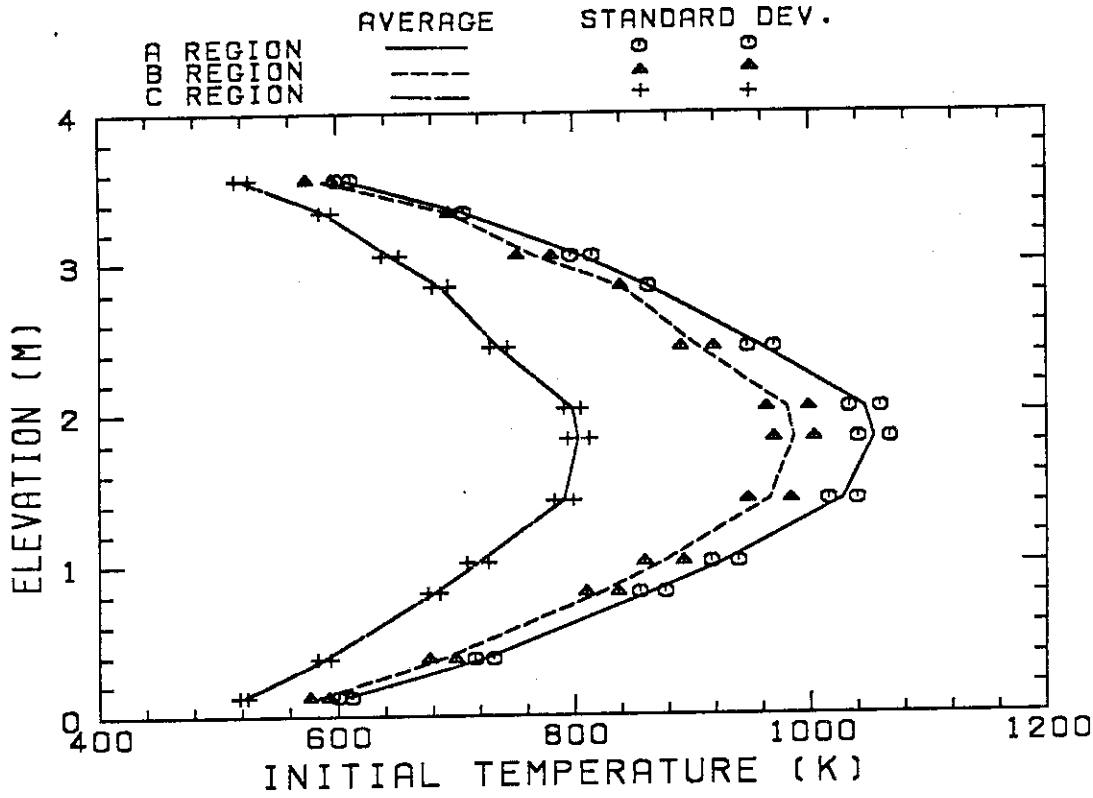

Fig. B.11 Initial clad surface temperature.

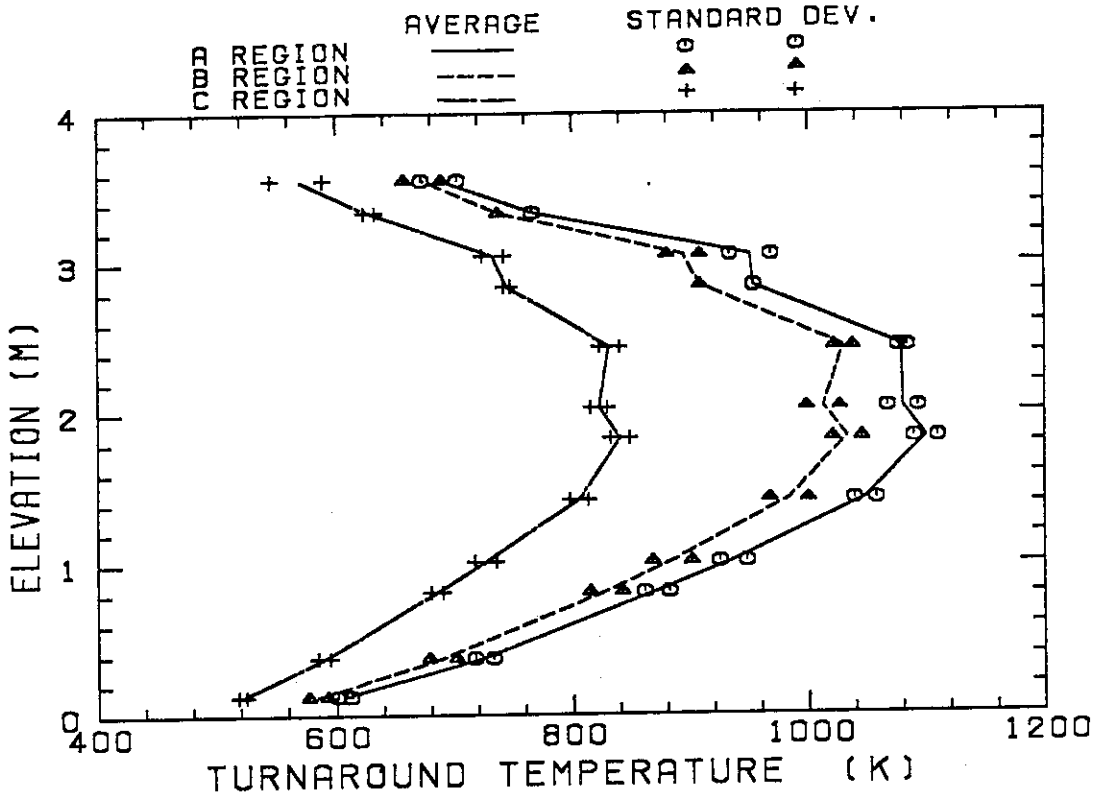

Fig. B.12 Temperature rise.

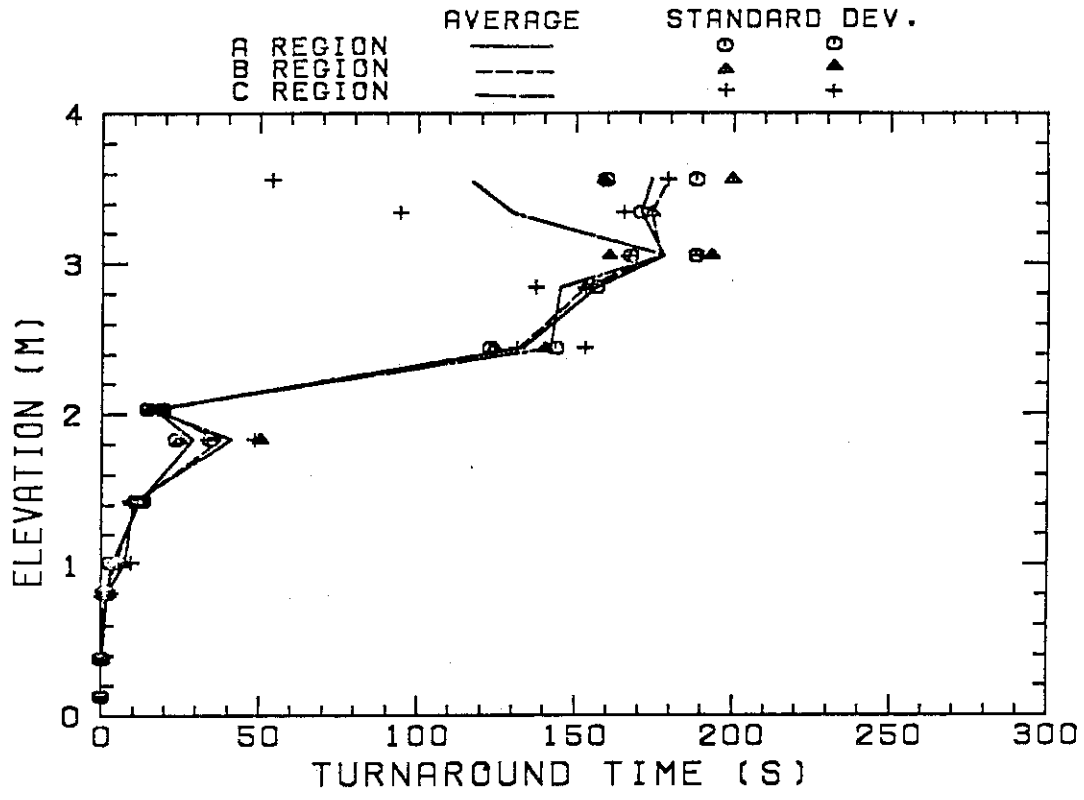

Fig. B.13 Turnaround temperature.

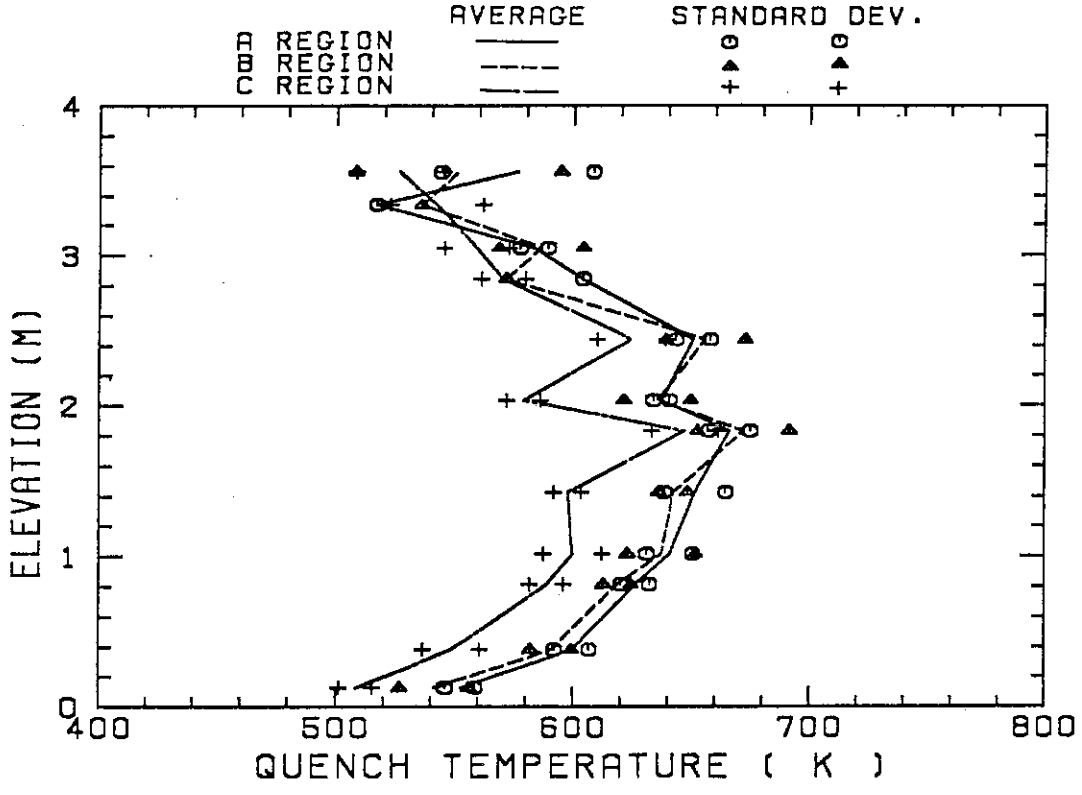

Fig. B.14 Turnaround time.

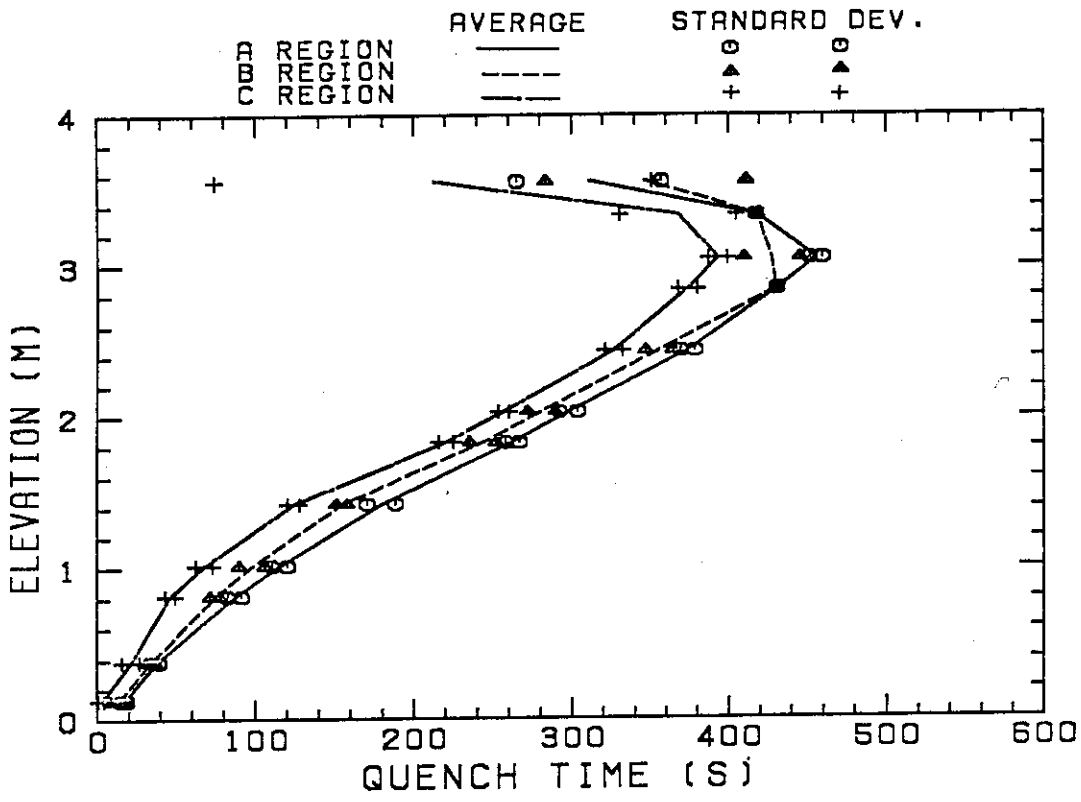

Fig. B.15 Quench temperature.

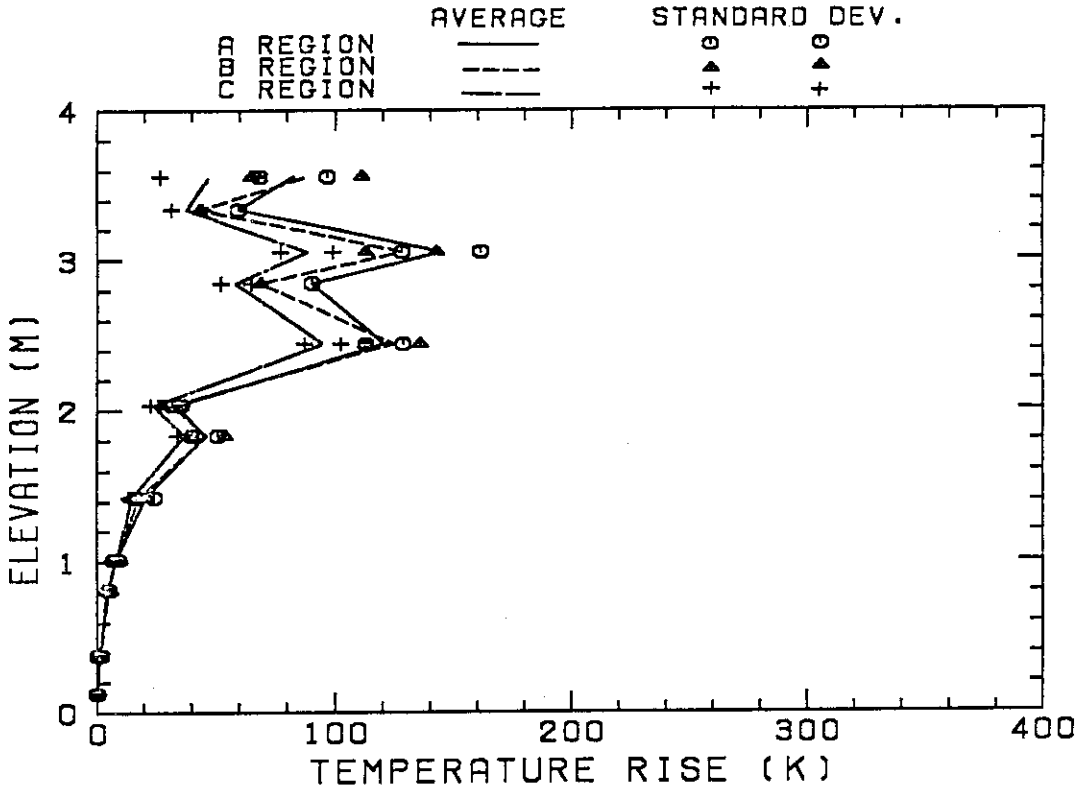

Fig. B.16 Quench time.

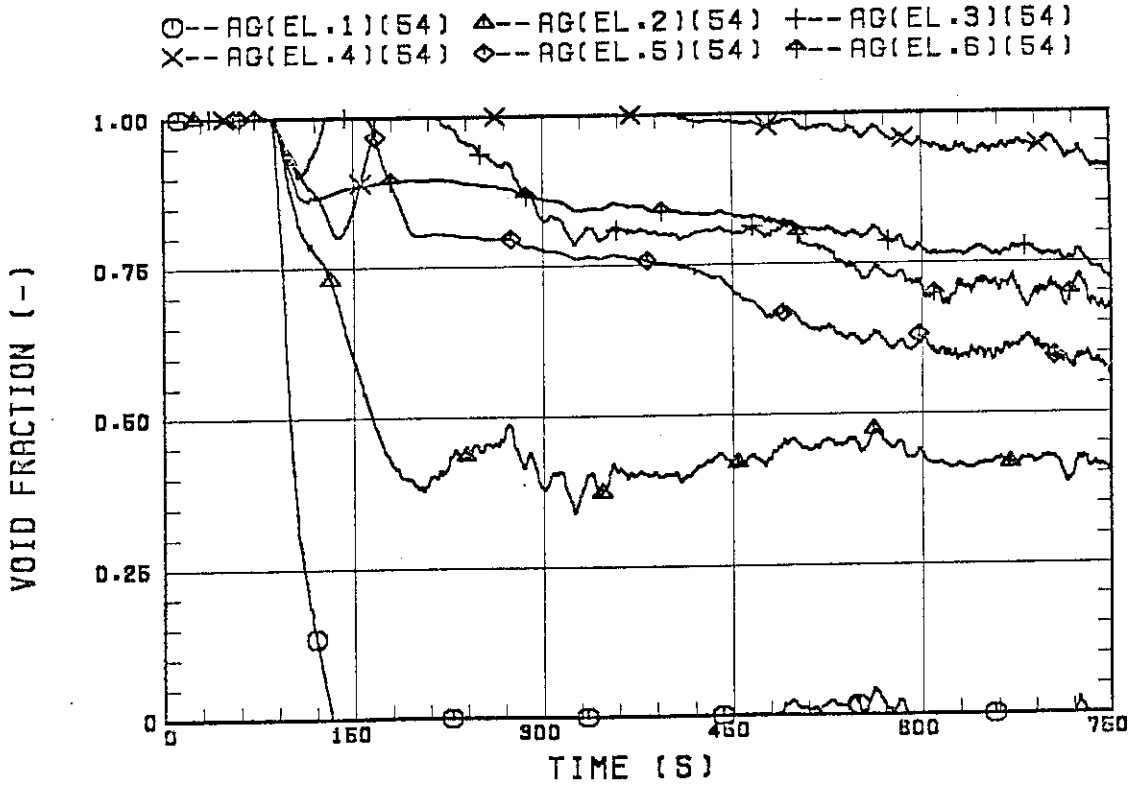

Fig. B.17 Void fraction in core.

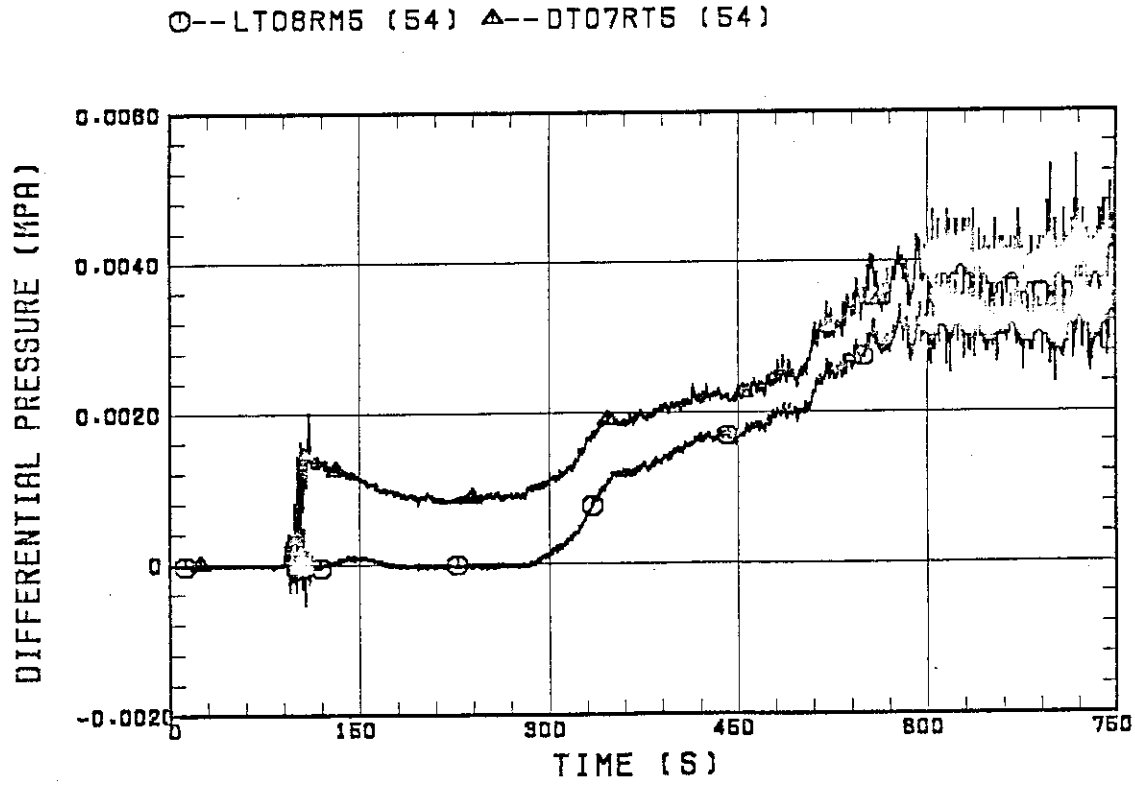

Fig. B.18 Differential pressure through upper plenum.

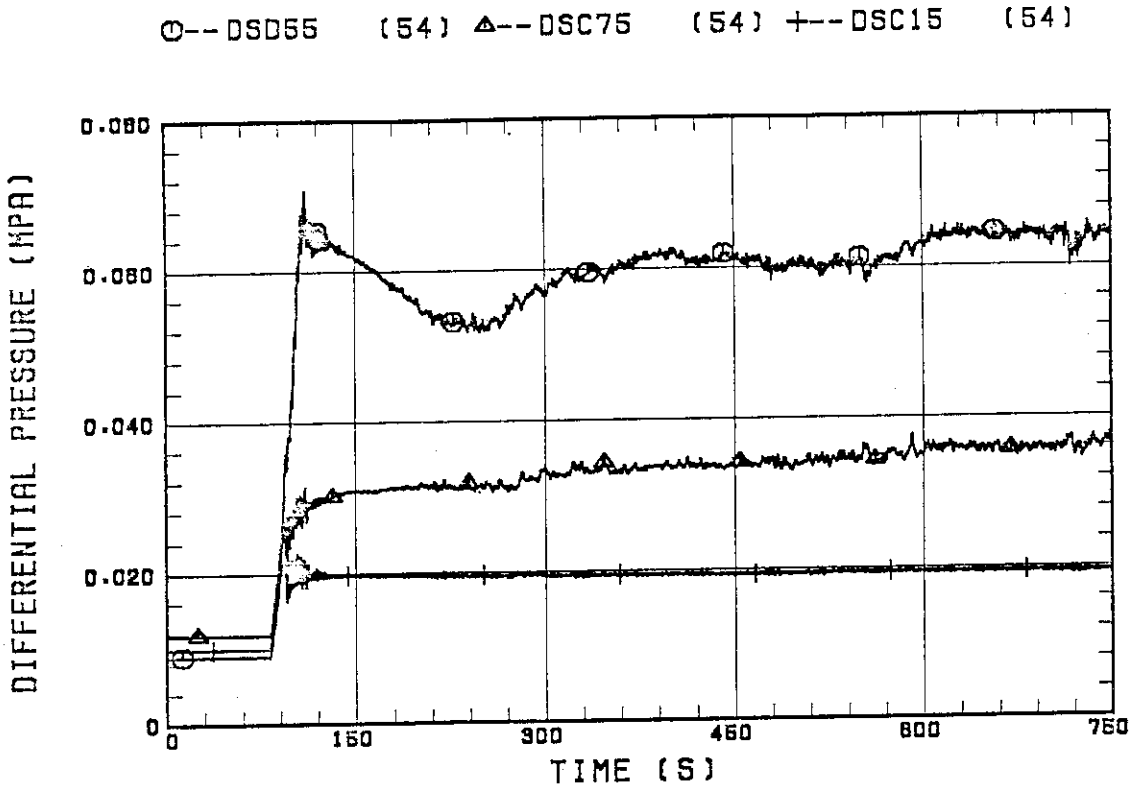

Fig. B.19 Differential pressure through downcomer, core, and lower plenum.

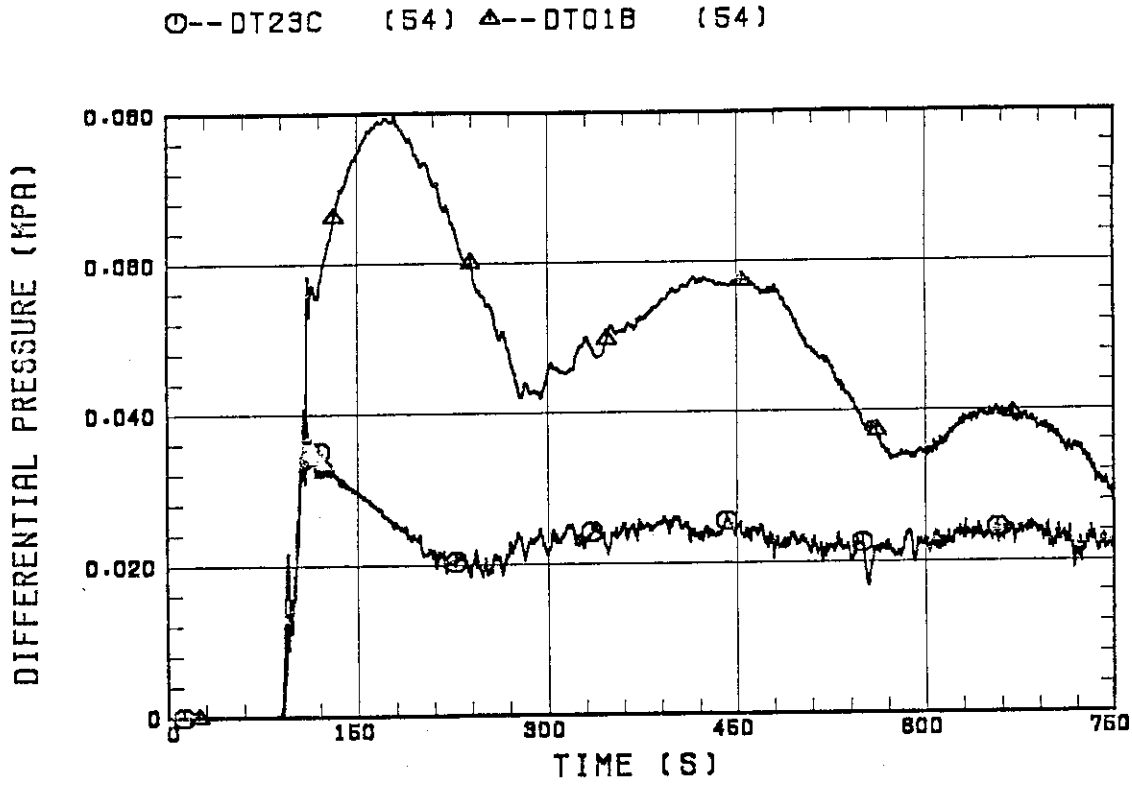

Fig. B.20 Differential pressure through intact and broken loops.

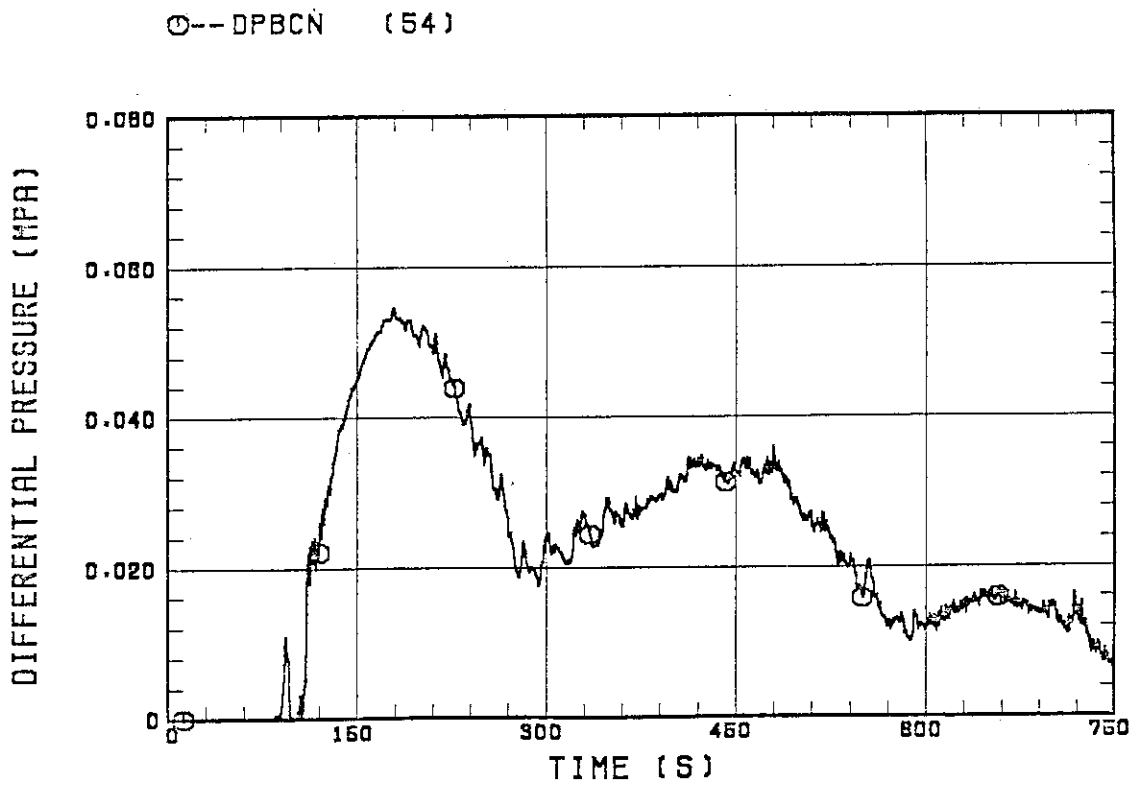

Fig. B.21 Differential pressure through broken cold leg nozzle.

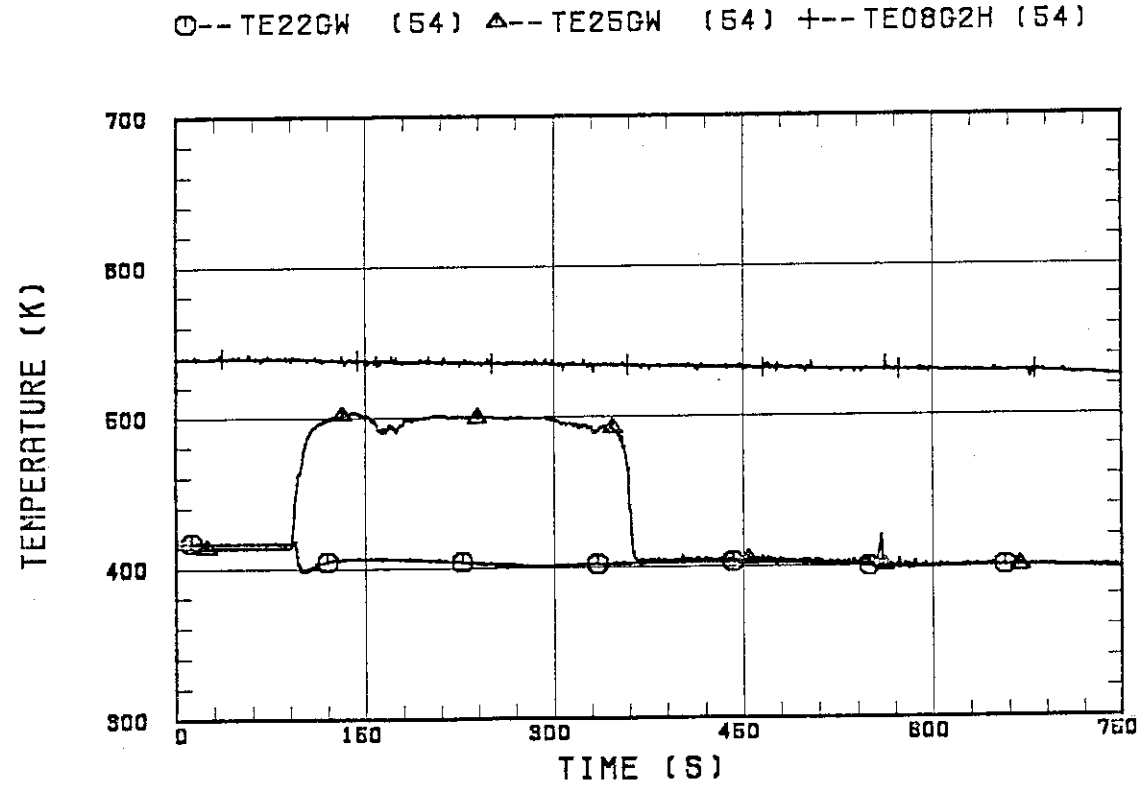

Fig. B.22 Fluid temperature in inlet plenum, outlet plenum, and secondary of steam generator 1.

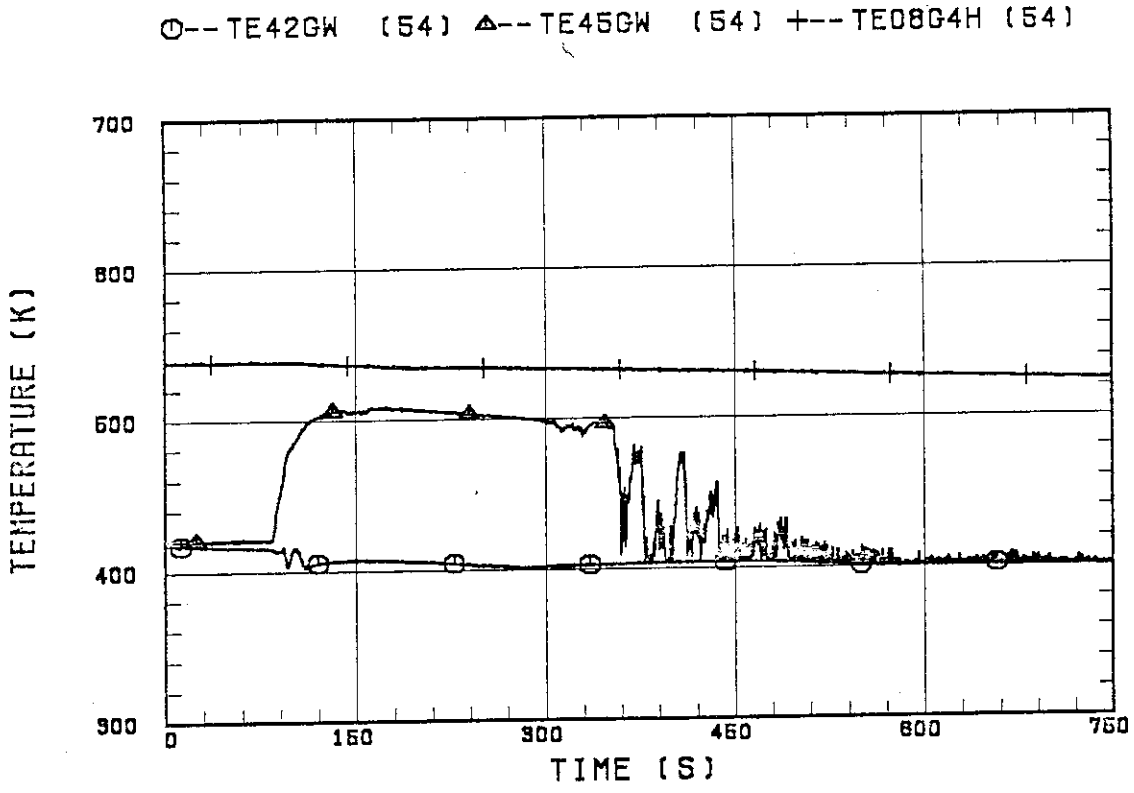

Fig. B.23 Fluid temperature in inlet plenum, outlet plenum, and secondary of steam generator 2.

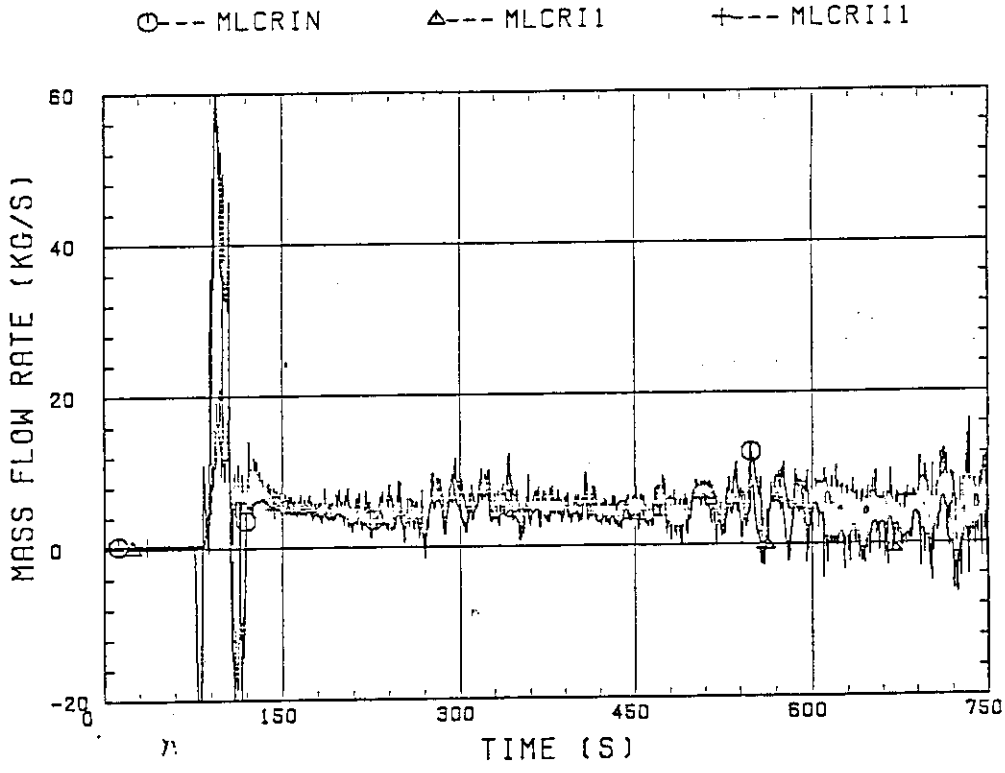

Fig. B.24 Core flooding mass flow rates evaluated with Eqs. (A.1) and (A.2)

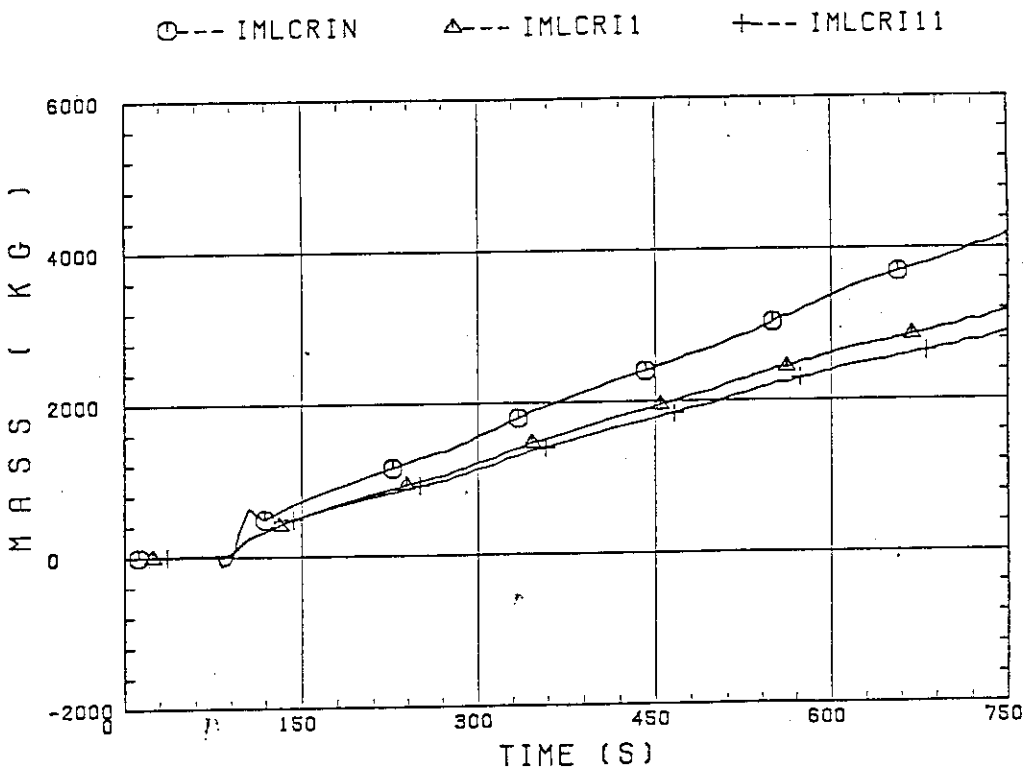

Fig. B.25 Time-integral mass flooded into core evaluated with Eqs. (A.1) and (A.2).

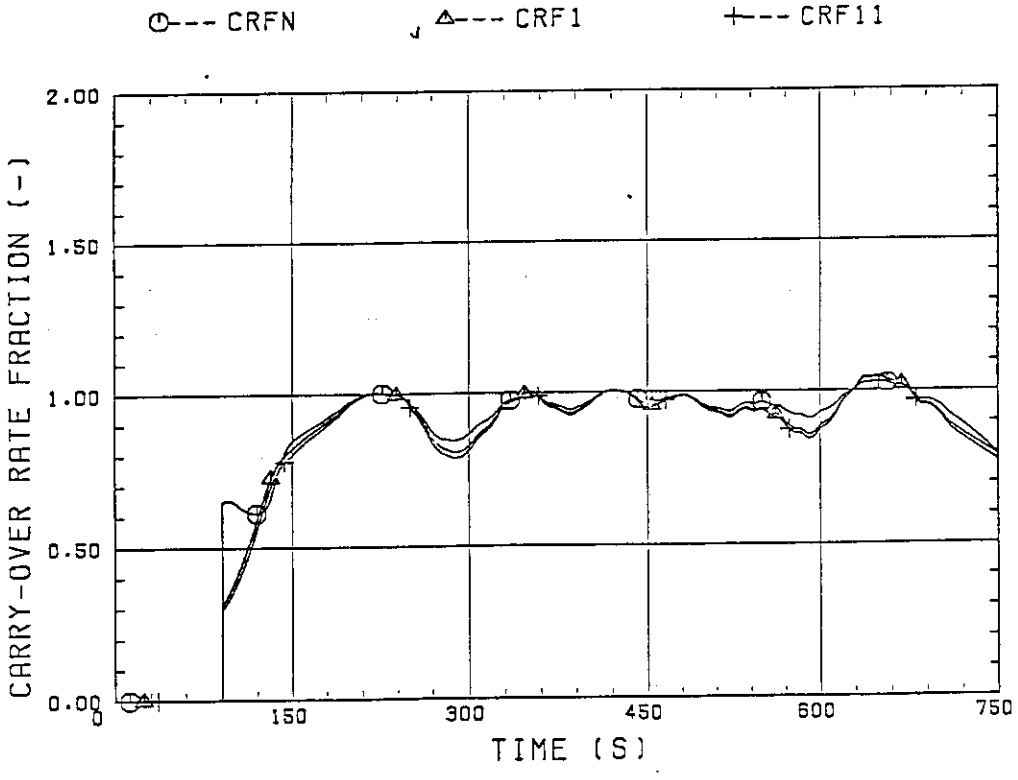

Fig. B.26 Carry-over rate fraction.

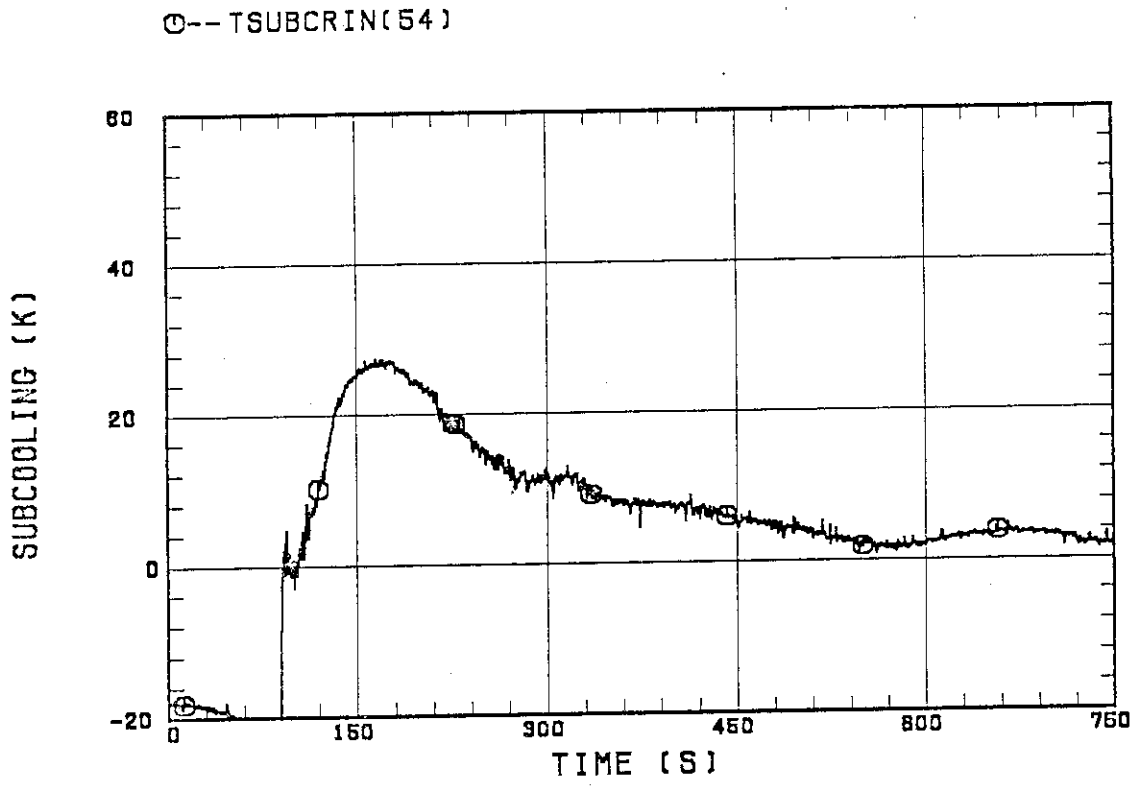

Fig. B.27 Core inlet subcooling.

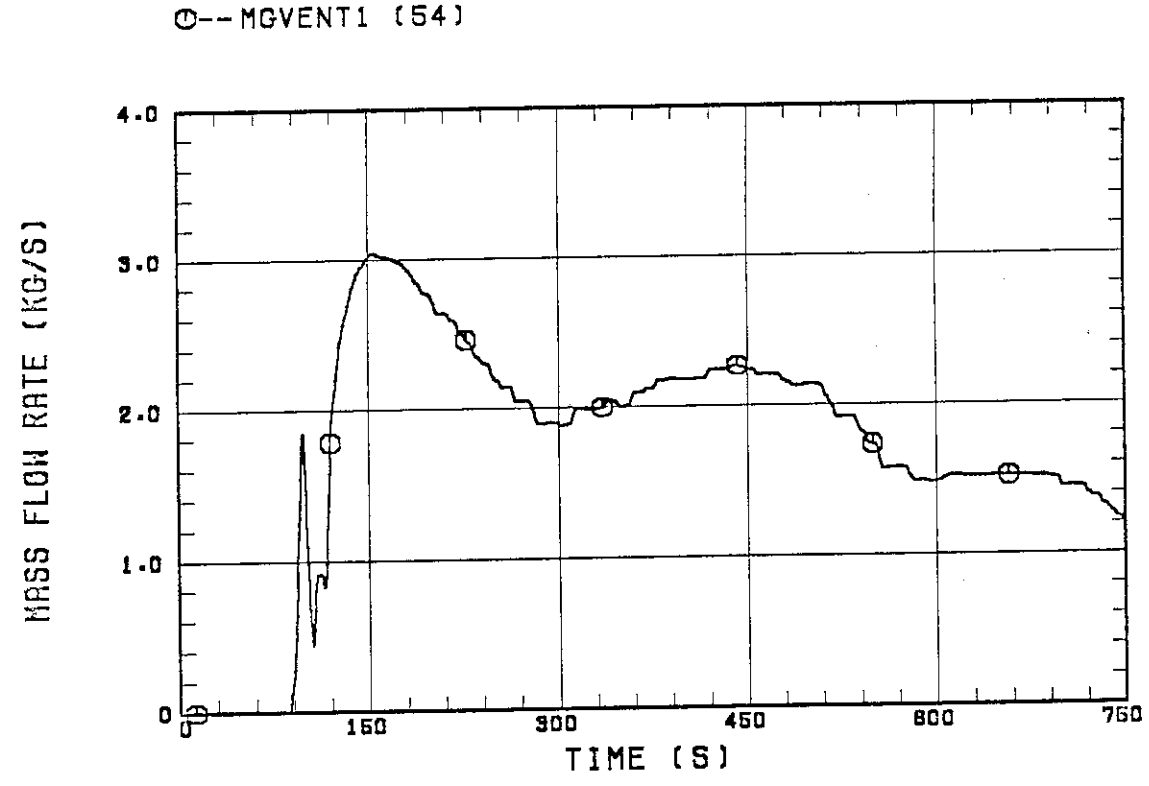

Fig. B.28 Exhausted mass flow rate from containment tank 2.